Computational Modelling of Brain Network Dynamics in Psychotic and Affective Disorders

Inaugural Dissertation

zur

Erlangung des Doktorgrades
philosophiae doctor (PhD) in Health Sciences
der Medizinischen Fakultät
der Universität zu Köln

vorgelegt von

Linnea Swantje Hoheisel

aus Hannover

Grafische Medien, Forschungszentrum Jülich GmbH, Jülich

2025

Betreuerin / Betreuer:	Prof. Dr. Joseph Kambeitz
Gutachterin / Gutachter:	Prof. Dr. Özgür Abdullah Onur
	Prof. Dr. Thilo van Eimeren
Datum der Mündlichen Prüfung:	08.04.2025

Acknowledgments

I am immensely grateful to my doctoral advisor, Prof Joseph Kambeitz, whose scientific guidance, support, and faith in my abilities were essential to my success in this project and my professional development. I am equally thankful to Prof Silvia Daun, my co-advisor, for many stimulating discussions and extensive advice, and Dr Lana Kambeitz-Ilankovic, for providing essential insights and helping me develop invaluable communication and teaching skills.

I also want to thank my thesis tutors, Prof Dr Özgür Onur and Dr Merle Hönig, for their constructive feedback and important suggestions within the framework of the Interdisciplinary Program Health Sciences (IPHS).

My deep appreciation goes to all of my current and former colleagues both at the Forschungszentrum Jülich and at the Uniklinik Köln. Their insight and advice shaped this work and helped me grow as a researcher, and their camaraderie made the last few years a joyful and enriching experience.

Finally, I want to thank my family and friends for their support and encouragement throughout this journey, especially my parents, who have been a continuous source of strength and motivation.

Table of Contents

List of abbreviations

AD	Alzheimer's disease
APS	attenuated psychosis syndrome
BLIP	brief limited intermittent psychosis
BOLD	blood oxygen level-dependent
BS	basic symptoms
CCA	canonical correlation analysis
CEN	central executive network
CHR	clinical high risk for psychosis
CSF	cerebrospinal fluid
CV	crossvalidation
DAN	dorsal attention network
DMN	default mode network
DTI	diffusion tensor imaging
EEG	electroencephalography
FC	functional connectivity
dFC	dynamic FC
sFC	static FC
FCV	functional connectivity variance
FD	framewise displacement
FDR	false discovery rate
GABA	gamma-aminobutyric acid
GAF	global assessment of functioning
GM	grey matter
GRD	genetic risk and deterioration syndrome
HC	healthy control
HCP	Human Connectome Project
MEG	magnetoencephalography
MRI	magnetic resonance imaging

fMRI	functional MRI
NC	node cohesion
PANSS	positive and negative symptom scale
PCA	principal component analysis
ROD	recent-onset depression
ROP	recent-onset psychosis
RSN	resting-state network
SC	structural connectivity
SMN	somatomotor network
SN	salience network
SSRI	selective serontonin reuptake inhibitor
TC	temporal correlation
VN	visual network
WM	white matter

List of figures

List of tables

1. Introduction

1.1 Psychotic and affective disorders

1.1.1 Prevalence and symptoms

Psychotic and affective disorders are among the most common psychiatric conditions, affecting 26.6 (Jongsma et al., 2019) and 35.3 (GBD 2021 Diseases and Injuries Collaborators, 2024) individuals per 1000 worldwide respectively. They severely limit patients' quality of life (Saarni et al., 2007), and represent a significant burden on their families and society as a whole (Jenkins & Schumacher, 1999). Psychotic disorders include schizophrenia, schizoaffective disorder, schizophreniform disorder, delusional disorder, brief psychotic disorder, and schizotypal personality disorder, while affective disorders encompass major depressive disorder, dysthymic disorder, and bipolar disorder, with major depression the most common (World Health Organization, 2004). Both psychotic and affective disorders can be treated with medication and behavioural therapy (Correll et al., 2022; Marwaha et al., 2023), but treatment options currently available are ineffective or insufficient for a large proportion of patients (McIntyre et al., 2014; Siskind et al., 2022). The lack of a comprehensive understanding of the mechanisms of these disorders (Kajumba et al., 2024; Tandon et al., 2024), as well as the heterogeneity in the clinical presentation (Kochunov et al., 2019; Koutsouleris & Fusar-Poli, 2024; Milaneschi et al., 2020) and frequent presence of comorbidities (Arnaud et al., 2022; Buckley et al., 2009) in patients complicate the development of effective, evidence-based treatment options.

Patients with psychotic disorders experience a range of symptoms which can be grouped into three categories (Kay et al., 1987; McCutcheon, Reis Marques, et al., 2020). Positive symptoms of psychosis include hallucinations, delusions, and suspiciousness, while negative symptoms include social and emotional withdrawal, motor retardation, and blunted affect, a failure to verbally or non-verbally express emotions. Cognitive symptoms, including impairments in memory, reasoning, information processing, verbal fluency, and social

cognition, often appear long before core symptoms, and are present even in patients in remission and spared relatives. Psychotic episodes most commonly occur for the first time in early adulthood (Solmi et al., 2022), and the further progression of the illness can take several forms. While some patients recover after a single psychotic episode, others will cycle between periods of remission and relapse, and a third group will experience symptoms throughout their lives (McGorry et al., 2010; Peralta et al., 2022). The duration between symptom onset and treatment has been shown to negatively affect functional outcomes (Fusar-Poli et al., 2017; Penttilä et al., 2014), suggesting that developing better mechanisms for early detection could improve care for psychotic disorders.

The majority of psychosis patients will go through a prodromal stage, during which they have a clinical high risk (CHR) for psychosis (Fusar-Poli et al., 2013). A patient is considered to be in a CHR state if they meet the criteria for one or more of four conditions based on their symptom severity and progression: genetic risk and deterioration syndrome (GRD), attenuated psychosis syndrome (APS), brief limited intermittent psychotic episode (BLIP), or basic symptoms (BS). Patients with GRD have a family history of psychosis or a schizotypal personality and exhibit a decline in psychosocial functioning. APS is characterised by the presence of mild psychotic symptoms which do not meet the threshold for diagnosis for a psychotic disorder. BLIPs refer to short periods of less than a week during which a patient experiences psychotic symptoms before spontaneous remission. BS are generally considered to occur in an earlier stage than the other conditions, and consist of subjectively experienced disturbances of processes including perception, language, attention and cognition. Approximately one third of patients in the CHR stage will transition to psychosis, while symptoms will persist in another third of patients, and the last third will experience full remission (Addington et al., 2011; Salazar de Pablo et al., 2021). Identifying pathological changes in this early stage could provide important insights into the mechanisms of psychosis, and improve early diagnosis and treatment options.

Symptoms of depression characteristically include low mood and anhedonia, an inability to feel pleasure, as well as rumination on feelings of worthlessness, hopelessness, and regret. Patients with depression also often display concentration and memory difficulties, irritability, and social withdrawal, as well as sleep disturbances, which can be marked by either insomnia or hypersomnia. Some patients with major depression additionally experience psychotic symptoms such as delusions or hallucinations (Dubovsky et al., 2021). Many patients with psychotic disorders also exhibit some depressive symptoms (Horan et al., 2008).

Patients with the same diagnosis can exhibit diverse symptom profiles, and many psychiatric patients experience symptoms consistent with more than one diagnosis (Lynch et al., 2020; Picardi et al., 2012; Upthegrove et al., 2017). Solely comparing abnormalities between diagnostic groups risks equating individuals with different pathologies and overlooking symptom-related changes that span diagnoses. To address this, it is crucial to account for individual differences in neurobiology and behaviour, and test associations of potential disease mechanisms with symptom profiles. Additionally, long-term patients may show not only primary disorder-related changes but also effects of prolonged medication use and chronic stress (B.-C. Ho et al., 2011; Kugaya et al., 2003; T. Li et al., 2017). In contrast, changes observed in early or prodromal stages are less influenced by these factors. Thus, studying patients who are recently diagnosed or exhibit early signs of a disorder offers more direct insights into disease mechanisms and potential markers for early intervention.

1.1.2 Causes and mechanisms

The mechanisms leading to the development of psychiatric disorders are still a major focus of research. The vulnerability-stress model is often used to explain risk and resilience in psychiatric illness (Colodro-Conde et al., 2018; Walder et al., 2014). It posits that individual risk is determined by the predisposition for a disorder, in the form of a genetic or environmental risk, and stress, a psychological burden caused by life events. If the combination of these two

factors exceeds a certain threshold, a person is likely to develop a psychiatric disorder. Thus, this model provides an explanation for the interaction between genetic, biological, environmental and psychological mechanisms contributing to mental ill health.

A range of risk factors have been identified for both depression and psychosis. For both disorders, there is evidence of a familial component, with family members of patients exhibiting an increased risk of developing the disorder (Rasic et al., 2014). Some rare genetic variants are directly associated with the development of schizophrenia in some patients (Marshall et al., 2017), while a polygenic risk score, which summarises the effect of a range of different genes previously linked with schizophrenia, explains some of the variance in individual psychosis risk (Purcell et al., 2009). The evidence for genetic risk in depression is less strong, although some polygenic variations have been shown to be slightly associated with depression (Howard et al., 2019; Wray et al., 2018). Another major risk factor for both conditions are adverse childhood experiences, including abuse and neglect during childhood (Misiak et al., 2017; Sahle et al., 2022). Individuals who have experienced multiple forms of adversity are particularly at risk, and more severe childhood trauma has been linked to worse clinical outcomes (Bentall et al., 2012; Muenzenmaier et al., 2015; Shevlin et al., 2008). The consumption of psychoactive drugs is also linked with a higher risk of psychiatric conditions (Fiorentini et al., 2021; Hjorthøj et al., 2021). In particular, frequent use of cannabis in adolescence increases the likelihood of developing a psychotic disorder (Gage et al., 2016; Godin & Shehata, 2022).

The biological mechanisms of depression and psychosis are less well understood. For years, the most commonly accepted hypothesis suggested that these conditions are caused by abnormalities in signalling pathways involving monoamine neurotransmitters (Coppen, 1967; Grace, 2016; Jauhar et al., 2023). These molecules are considered neuromodulators; in contrast to simple neurotransmitters, they not only regulate targeted, short-term synaptic transmission, but can also act as hormones, inducing longer-term changes across the brain (Marder, 2012). Depression has long been linked in particular to abnormalities in serotonin

signalling (Coppen, 1967), and most first-line antidepressants act as selective serotonin reuptake inhibitors (SSRIs), limiting reuptake of serotonin back into the synapse and thus keeping the serotonin concentration in the synaptic gap high (Artigas et al., 2002). The efficacy of these medications, as well as the association of depression with the depletion of serotonin precursor molecules (Almulla et al., 2022; Ruhé et al., 2007), and with a decrease in serotonin receptor binding (J. P. Kambeitz & Howes, 2015), have been taken as evidence for the importance of this mechanism. However, this hypothesis has become increasingly controversial since the evidence for it is somewhat inconclusive (Jauhar et al., 2023; Moncrieff et al., 2023). Many patients do not respond to this type of medication (Trivedi et al., 2006), indicating that the relationship between serotonin signalling and depression is not straightforward. Disruptions in signalling pathways involving other monoamine neurotransmitters, particularly norepinephrine (Moret & Briley, 2011) and dopamine (Grace, 2016), have also been linked to depression. In addition, depressed patients exhibit changes in the balance between excitatory and inhibitory neural activity (Hu et al., 2023), indicating abnormalities in these pathways. Disruption in the excitation-inhibition balance alters brain function and connectivity (Deco et al., 2014), potentially contributing to depression symptoms.

A leading theory for the development of psychosis implicates changes in dopamine signalling (McCutcheon, Krystal, et al., 2020; Tost et al., 2010). Patients with schizophrenia have been shown to exhibit higher dopamine levels than healthy controls (Howes et al., 2012) as well as increased concentration and sensitivity of dopamine receptors (Seeman, 2013). In addition, common antipsychotic medications act as dopamine receptor antagonists (Kaar et al., 2020), and drugs which increase dopamine levels, such as cocaine (Tang et al., 2014) or amphetamines (Moran et al., 2019), can induce or exacerbate symptoms of psychosis. Other evidence suggests a role of abnormal glutamate signalling in psychosis (McCutcheon, Krystal, et al., 2020). Patients with schizophrenia exhibit increased levels of glutamate metabolites in subcortical regions (Merritt et al., 2016), and administration of glutamate receptor antagonists produces psychosis-like symptoms (K. Beck et al., 2020). As the dopamine and glutamate

signalling pathways are linked, both of these mechanisms likely interact to produce the symptoms observed in psychotic disorders (McCutcheon, Krystal, et al., 2020). In addition, some evidence also suggests abnormalities in inhibitory signalling mediated by gamma-aminobutyric acid (GABA) (Orhan et al., 2018). Together, glutamatergic and GABAergic signalling govern the excitation-inhibition balance (X.-J. Wang, 2020). Disturbances in this characteristic have been shown to affect FC (Driesen et al., 2013; Nasrallah et al., 2017), and thus represents a potential mechanism for the development of FC alterations in patients with psychotic disorders. Recent research has also suggested a range of wider biological processes which could contribute to the development of both depression and psychosis, including immune system dysregulation leading to neuroinflammation (Najjar & Pearlman, 2015; Troubat et al., 2021), and abnormalities in the gut microbiome which can affect neurobiology via the gut-brain axis (Cryan & Dinan, 2012; Nemani et al., 2015).

Despite the wealth of evidence for the role of neuromodulation and excitation-inhibition balance in these disorders, inconsistent findings and high individual variability (Beijers et al., 2019; Hu et al., 2023; Merritt et al., 2023; van Hooijdonk et al., 2022), as well as heterogeneity in the response to medications targeting these systems (Kaar et al., 2020; Phillips et al., 2015) and in the clinical presentation (Lynch et al., 2020; Picardi et al., 2012), indicate that there could be some heterogeneity in disease mechanisms between patients with the same diagnosis. On the other hand, some of the underlying physiological changes and symptom profiles appear to overlap between psychotic and depressed patients (Goodkind et al., 2015; Upthegrove et al., 2017). Together, these findings highlight the importance of studying the variability of neurobiological and psychological processes across individuals, using methods such as subgroup and correlational analyses, in order to improve our understanding of these disorders and develop appropriate treatment options for all patients.

1.2 Resting-state functional connectivity

1.2.1 General principles

In order to gain a comprehensive understanding of psychiatric disorders, neurobiological mechanisms need to be linked to clinical and behavioural outcomes via brain activity. One important measure of brain function in health and disease is functional connectivity (FC), the statistical association in activity between different brain regions (Woodward & Cascio, 2015; J. Zhang et al., 2021). While communication between brain regions is clearly essential during task performance, distributed patterns of brain connectivity also arise at rest, in the absence of a particular task or stimulus (Biswal et al., 1995; B. T. T. Yeo et al., 2011). Imaging FC in the resting state, as opposed to during a task, presents both practical advantages and provides an opportunity to gain important insights. The use of resting-state FC facilitates the comparison of connectivity patterns across studies and eliminates the work of developing and administering a suitable task paradigm. It also limits the impact of specific task demands on overall FC patterns and allows us to study common cognitive processes, such as mind wandering, which occur in this condition (van den Heuvel & Hulshoff Pol, 2010). Differences in resting-state FC have been shown to relate to age (Geerligs et al., 2015), personality (Nostro et al., 2018), and cognitive ability (Ooi et al., 2022), and mark brain disorders including schizophrenia (Dong et al., 2018), depression (Mulders et al., 2015), anxiety (Xu et al., 2019), autism (Hull et al., 2017), and Alzheimer's disease (Sheline & Raichle, 2013).

The biological mechanisms producing FC patterns are still actively studied. Evidence suggests that FC is constrained by the anatomical connections between regions, the structural connectivity (SC) (Honey et al., 2007, 2009). However, the relationship between FC and SC is complex (Bullmore & Sporns, 2009), and multiple other processes have been shown to influence FC networks. Neuromodulators such as serotonin, dopamine, and catecholamine can temporarily change the excitability of neurons, but also produce long-term remodelling of the architecture and physiology of neural networks (Marder, 2012). Differences in the

architecture of signalling pathways, such as receptor expression profiles, contribute to variations in brain connectivity (Brink et al., 2016; Hansen et al., 2022), and disruption of neuromodulatory processes leads to alterations in FC (Luppi et al., 2021; Olsen et al., 2022). In addition, FC is shaped by physiological processes within brain regions, particularly those governing excitatory and inhibitory synaptic signalling (Gu et al., 2019; Levar et al., 2019). The balance between excitation and inhibition is essential for maintaining normal brain function (Anticevic & Lisman, 2017; Deco et al., 2014; Sohal & Rubenstein, 2019), and manipulation of this process affects global brain connectivity (Anticevic et al., 2015; Driesen et al., 2013).

Exploration of connectivity patterns in the resting state has revealed consistent principles of FC architecture. Networks consist of a small number of highly-connected hub nodes, and a large number of nodes exhibiting weak connectivity (Bullmore & Sporns, 2009; Fransson & Thompson, 2020; Zamani Esfahlani et al., 2020). Disruption of hub nodes has been suggested as a factor in several brain disorders (Crossley et al., 2014; Royer et al., 2022; Rubinov & Bullmore, 2013), and simulations show that lesions in certain regions have an outsized impact on FC patterns (Aerts et al., 2016; Alstott et al., 2009). In addition, the overall connectivity pattern can be decomposed to reveal a number of resting-state networks (RSNs) of regions that are highly connected between each other (B. T. T. Yeo et al., 2011). While there is still some debate on the exact number and topography of these networks, the majority of frameworks include a set of six networks, each of which is linked to a specific set of brain functions (Uddin et al., 2019).

The visual network (VN) or occipital network, which consists of regions in the occipital lobe, is primarily related to visual processing, while the somatomotor network (SMN), made up of regions around the central sulcus, is responsible for somatosensory information processing and movement execution. The dorsal attention network (DAN) or dorsal frontoparietal network, which is linked to visuospatial attention, consists mainly of the intraparietal sulcus, middle temporal complex, and frontal eye fields. The remaining three networks are known to interact to support higher cognitive functions. The default mode network (DMN) is considered to

contribute to functions such as remembering, planning, social judgments and introspection, and shows particularly strong activity at rest, which has led to suggestions of its involvement in daydreaming and mind-wandering. Regions assigned to the DMN are distributed across the brain, with the medial prefrontal cortex, posterior cingulate cortex and the posterior part of the inferior parietal lobule thought to be particularly important. The central executive network (CEN), or frontoparietal network, has been linked to executive functions, working memory, and goal-directed behaviour, and consists of regions including parts of the lateral prefrontal and the anterior inferior parietal lobule. The salience network (SN), cingulo-opercular network, or ventral attention network, is implicated in functions such as the detection and integration of stimuli, and is thought to govern the engagement of other functional networks, in particular the switch between the internally oriented DMN and the externally oriented CEN (Sridharan et al., 2008). The SN encompasses the anterior insula and the anterior cingulate cortex.

Networks that have been suggested in addition to these five include the limbic network (B. T. T. Yeo et al., 2011), which includes subcortical and associated cortical regions but is sometimes considered to be part of the DMN (Uddin et al., 2019), and the cerebellar network, which encompasses the cerebellum (Dosenbach et al., 2010).

1.2.2 Dynamic characteristics

Traditionally, FC has been assumed to remain stable over the course of a resting-state functional magnetic resonance imaging (fMRI), electroencephalography (EEG), or magnetoencephalography (MEG) scan. Most research quantifies FC by computing the correlation of the brain activity of different regions across the time of the scan, yielding a measure of static FC (sFC). Over the last decade, however, increasing amounts of evidence of temporal fluctuations in FC have led to an expansion in the interest in the temporal characteristics of FC (Hutchison et al., 2013; Lurie et al., 2020). This time-varying or dynamic FC (dFC) has been observed across neuroimaging modalities (Lurie et al., 2020), and has

been investigated as a marker of behavioural states such as task-induced arousal (Gonzalez-Castillo & Bandettini, 2018), sleep (El-Baba et al., 2019), and anaesthesia (Miao et al., 2023), cognitive performance (Cohen, 2018; Liégeois et al., 2019), and brain disorders including depression (Demirtaş et al., 2016), psychosis (Y. Du et al., 2018), dementia (Schumacher et al., 2019), and autism (Y. Li et al., 2020).

The most widely accepted model for this phenomenon states that at rest, the brain cycles between a number of recurrent connectivity patterns, or states (Lurie et al., 2020). A range of studies have since identified such connectivity states in resting participants (Cabral et al., 2017; Shappell et al., 2019; Wu et al., 2019). Evidence suggests that the repertoire of recurrent states is largely unchanged in patients with brain disorders (Damaraju et al., 2014; Zhi et al., 2018), although the lack of methodological consistency, and particularly the disagreement over the number of identifiable states (Barber et al., 2018; Snyder et al., 2021; Wu et al., 2019; Yao et al., 2019), makes a comparison across studies difficult. Differences in the dynamic characteristics of these states have been identified across patient groups and behavioural states (M. Du et al., 2021; C. Wang et al., 2016; Yao et al., 2019).

The relevance of recurrent FC states is still a matter of debate. Research has linked dynamic fluctuations in FC to changes in cognitive states and arousal (Shine et al., 2016; C. Wang et al., 2016). Thus, switches between FC states during rest might also coincide with cognitive processes such as mind wandering, or fluctuations in attention. However, different FC states have also been identified during sleep and anaesthesia (Barttfeld et al., 2015; El-Baba et al., 2019), suggesting that at least some of the dynamic behaviour of FC is independent of conscious thought. dFC might therefore also result from physiological processes, or be a natural product of neural activity within a brain network.

1.2.3 Methods for dynamic functional connectivity analysis

There are a multitude of techniques which can be used to study FC dynamics, and a consensus on the optimal metric is still lacking (Lurie et al., 2020). Most analysis approaches begin with the application of the sliding window method (Hutchison et al., 2013). For this, the FC is computed within a window, a small subsection of the scan of a specific length. This window is then moved along the time course by a specific offset which is generally a small fraction of the window length, resulting in large overlap between successive windows, and a new FC matrix is computed. This procedure is repeated until the end of the scan is reached, yielding a time course of FC matrices which capture the evolution of the connectivity over time.

Based on this FC time course, several metrics capturing different aspects of dFC can be calculated (Lurie et al., 2020). The simplest of these is the FC variance, which quantifies the change in FC over time, and is calculated by determining the variance in the connectivity between each pair of regions across all windows. While the FC variance reflects how strongly the connections vary over time and provides spatial resolution, it cannot capture other aspects such as recurrence of FC patterns or temporal order. Another strategy involves considering the time course of FC matrices as a dynamic graph, with edges between region nodes changing over time. From this graph, it is then possible to calculate dynamic graph parameters (Sizemore & Bassett, 2018). The temporal correlation quantifies the consistency of the neighbours, the regions which exhibit strong connections, of a region over time. This is calculated by taking the average over the correlation between a region's connectivity to all other regions at time point t and the connectivity at the subsequent time point t+1 across all time points. This metric indicates whether a region's connectivity tends to change gradually or abruptly and thus captures some of the temporal organisation of dFC patterns. However, it only reflects the overall connectivity of a particular region and does not account for differences in the variability of individual connections. Another set of graph-based metrics involves grouping nodes into dynamic communities, which exhibit high connectivities between nodes within the group and low connectivities to nodes outside the group. The node cohesion, which

represents the number of times two nodes switch communities together, indicates whether nodes tend to be part of the same communities, and thus whether they are likely to be involved in similar processes. While this measure cannot capture the overall level of dynamic variability in the brain, it provides information about the meso-scale network integration of each region pair over time. Many other classical graph metrics can also be extended to the dynamic case, but are either redundant or computationally expensive to calculate, making them unsuitable for the analysis of large-scale data sets.

State-level measures are based on the underlying model of the FC dynamics as an alternation between states, and aim to identify recurring connectivity patterns (Calhoun et al., 2014). FC matrices are clustered into a set of recurrent patterns across time points, and their dynamic parameters determined. These can include the lifetime or dwell time, the duration for which a state is active before switching to another state, the frequency, the total duration spent in a particular state as a fraction of the scan time, and the transition frequencies, the likelihood that a certain state converts to each of the other states (Lurie et al., 2020). These parameters can then be compared across subject groups or conditions. State-based measures provide a comprehensive characterisation of dFC patterns and are thus highly useful in comparing dFC across groups. However, the clustering algorithm requires a considerable amount of data to generate reliable states, making these metrics unsuitable for small sample sizes. The approach also relies on the identification of corresponding states across study groups. If the connectivity patterns differ strongly between groups, the comparison of state-level dFC features becomes impossible.

1.2.4 Functional connectivity alterations in brain disorders

FC has been extensively investigated as a marker of psychiatric disorders. Changes in the connectivity of the DMN, CEN, and SN are observed across diagnoses, and have led to the development of the triple network model of psychopathology, which states that alterations in

the interaction of these networks are related to psychiatric symptoms (Menon, 2011). In depression, the disruption in this triple network system is mainly associated with altered connectivity in the DMN (Yan et al., 2019). As this network is involved in cognitive processes during wakeful rest and self-referential processes, these changes have been linked to symptoms such as rumination and negative self-reflection (H.-X. Zhou et al., 2020). Research on triple network abnormalities in psychosis has largely focused on the salience network (Palaniyappan & Liddle, 2012). This network facilitates context-dependent recruitment of the DMN, which is involved in internally oriented, and the CEN, which is involved in externally oriented thought processes (Sridharan et al., 2008; Uddin et al., 2019). Altered connectivity in the SN observed in schizophrenia is thought to contribute to symptoms including hallucinations, which could be explained in the context of aberrations in the assessment of the salience of internal and external stimuli (Mallikarjun et al., 2018). This observation has also been linked to dysfunction in dopaminergic signalling, which is involved in salience attribution (Howes et al., 2020) and modulates FC in the SN (McCutcheon et al., 2019).

A more detailed analysis of the evidence (Mulders et al., 2015) shows that patients with depression exhibit decreased connectivity of the anterior cingulate cortex and the prefrontal cortex with a number of other regions, as well as an increase in the connectivity between cortical areas and the thalamus and striatum, and a decrease in connectivity between the hypothalamus and cortex. These changes were associated with affective symptoms, while cognitive symptoms showed distinct FC correlates, including increased FC between the CEN and SN, increased connectivity within the DMN, and aberrant connectivity between the precuneus, posterior cingulate cortex, and orbitofrontal cortex. Treatment in the form of medication, behavioural therapy or brain stimulation reverses some of these aberrant connectivity patterns.

Patients with psychosis, on the other hand, show reductions in FC between seeds in the DMN and regions in the DMN, SN and CEN, including the anterior cingulate cortex, insula, and medial and dorsolateral prefrontal cortex (Dong et al., 2018). In addition, disruptions in the FC

of the SMN and auditory network have been observed in psychosis, potentially contributing to symptoms of impaired language processing and production. Further FC abnormalities in psychosis patients include reduced connectivity within a thalamic network, and between this network and areas including the middle cingulate cortex and the cerebellum, as well as decreased connectivity between the SN and a range of regions distributed across the brain. CHR individuals already exhibit some of the changes in FC which are observed in psychosis patients, including decreased connectivity in the SN compared to healthy controls (Del Fabro et al., 2021).

Alterations in dynamic FC in psychotic and affective disorders have not been studied as widely, and findings are less consistent due to the variety of methodological approaches employed (Cattarinussi et al., 2023; Sun et al., 2024). Patients with depression exhibit lower temporal variability (Demirtaş et al., 2016), and spend more time in a weakly connected FC state (Yao et al., 2019). In psychosis patients, both increases and decreases in dFC have been observed across the brain on different spatial scales (Deng et al., 2019, 2021; Dong et al., 2019). They spend less time in a globally integrated state (Damaraju et al., 2014; Espinoza et al., 2019; Sanfratello et al., 2019), and more time in states with strong FC in the DMN (Weber et al., 2020), but overall showed more variable and less stable dynamic behaviour (Fu et al., 2021). Individuals with CHR exhibit some common changes with psychosis patients in the recurrent FC patterns, but also unique abnormalities specific to the CHR stage (Y. Du et al., 2018).

While FC features were initially employed with some success for the prediction of depression and psychosis (J. Kambeitz et al., 2015, 2017), newer studies in large cohorts indicate that the predictive value of FC alterations for the diagnosis of these disorders is limited (Gallo et al., 2023; Schnack & Kahn, 2016). Research has instead turned towards the identification of subgroups and the prediction of clinical outcomes and treatment response (Drysdale et al., 2017; Mehta et al., 2021). These approaches consider both the clinical and the neurobiological

heterogeneity of patients, and endeavour to link the two to identify clinically relevant biomarkers.

1.3 Brain network modelling

1.3.1 General principles

Computational modelling provides the opportunity to study causal mechanisms of brain activity and examine individual neurobiology, making it a powerful tool for research in both basic and clinical neuroscience (Bansal et al., 2018; Schirner et al., 2018). The models mathematically describe neurobiological processes and simulate brain activity (Breakspear, 2017; Schirner et al., 2018; Shine et al., 2021). Using this technique, researchers are able to analyse the effect of perturbations, such as brain stimulation (Kunze et al., 2016; Meier et al., 2022), administration of psychoactive drugs (Herzog et al., 2023), or stroke (Adhikari et al., 2017; Rocha et al., 2022), on human brain function, complementing correlational analyses and studies in animal models. In addition, model parameters can be adjusted to optimally reproduce the brain activity of a particular individual. The identified optimal parameter values then allow for inferences about the neurobiology of that person, and could potentially serve as markers of brain disorders, clinical outcomes, and treatment response (H. E. Wang et al., 2024).

Recent years have seen the advent of a number of different approaches to modelling brain activity (Deco et al., 2008). Due to the complexity of neural networks, all models rely on some simplification of brain processes, with complementary approaches using different levels of abstraction to investigate different facets of brain activity. Some model families replicate the activity of individual, interconnected neurons, but only consider a fraction of the number of neurons present in all but the simplest of organisms (He et al., 2019; Yu et al., 2014). These models elucidate the communication and activity dynamics of connected cells, as well as mechanisms of low-level information processing and memory, but cannot be used to explore

whole-brain connectivity. Other approaches use small subsets of connected neurons to represent brain areas, which are then integrated to form a whole-brain model (Pronold et al., 2024).

Brain network models represent the brain as a network of regions linked via anatomical connections. The activity of each region is described by a set of equations replicating the behaviour of one or more populations of neurons rather than individual cells. The models rely on a structural connectome extracted from diffusion tensor imaging (DTI) data. The weights of the structural connections, which are proportional to the number of fibres between each pair of regions, scale the signal that is transferred from each brain region to the others. The lengths of the connections provide a measure of time delay with which the signal arrives at its destination (Sanz-Leon et al., 2015).

Currently, the majority of studies working with brain network models of individual subjects optimise them to reproduce empirical functional connectivity. Generally, they calculate FC matrices for both the simulated and the empirical data, and determine their correlation or the overlap in their distributions across region pairs to quantify the fit (Klein et al., 2021; Zimmermann et al., 2018). As a result, those models reflect the static FC well, but it is not clear to what extent they are able to replicate dynamic fluctuations in FC. Some recent studies have tried to address this by optimising models for both the static FC and the FC dynamics, the correlation in the FC between each pair of sliding windows across all regions (Deco et al., 2021; S. Zhang et al., 2024). While this approach allows for the replication of the extent of FC fluctuations within a particular scan, it does not reflect the temporal progression or the spatial distribution of these connectivity changes. Optimising the model parameters for both static and more comprehensive dynamic FC metrics would produce more accurate models, and allow for the identification of neurobiological processes shaping both static and dynamic FC.

1.3.2 Models of regional brain activity

A number of different models varying in their complexity and biological relevance have been developed to describe the neural activity within a brain region (Sanz-Leon et al., 2015). Phenomenological models replicate abstract behaviours of neuronal populations without relating directly to neurophysiological mechanisms. Generic oscillator models, for example, consider regional activity to be produced by a system consisting of a single population, which exhibits dynamic behaviour based on external currents, membrane potential and recovery. Despite their simplicity, oscillator models are able to reproduce a range of behaviours exhibited by neuronal populations, including multistability and dynamic activity on multiple time scales. More physiological models describe regional activity using parameters corresponding to physiological characteristics which can be empirically observed. These models tend to be more complex, and often consist of two or more populations of different types of neurons, which interact with each other according to biologically realistic rules.

The reduced Wong-Wang model introduced by Deco et al. (Deco et al., 2014) strikes a balance between complexity and explainability. It considers two populations within each region, one of excitatory and one of inhibitory neurons. Regional activity is determined by a set of coupled equations which reflect three types of input. The excitatory population receives long-range excitatory information from connected regions. Each signal is first scaled by the strength of the SC between the transmitting and the receiving region, and then all inputs are combined and scaled by a global coupling parameter G and an excitatory synaptic coupling parameter J_N. Input into the excitatory population from the inhibitory population of the same region is scaled by an inhibitory synaptic coupling parameter J_i, and is added with a negative sign. Additionally, the excitatory population receives input from itself via recurrent excitation, which is scaled by an excitatory recurrence parameter w_p and J_N. The inhibitory population is excited by the excitatory population, but self-inhibitory.

If the parameter values are selected from an appropriate range, the reduced Wong-Wang model replicates multistable behaviour observed in empirical neuronal populations. In the

absence of noise, the activity of the model converges to one of two states, depending on the initial condition. If the model is initialised with an activity pattern that exceeds a certain threshold, it will reach a high-activity regime. If the initial condition is one of low activity, the model will eventually reach a low-activity regime. Without external input, the model will remain in a stable state, and consistently output either high or low activity. When noise is added to the model specification, the activity fluctuates between these two stable states, producing a biologically realistic oscillation in activity.

While the four relevant parameters of the reduced Wong-Wang model each represent a specific physiological quantity, they capture information about a wealth of biological processes. The synaptic coupling parameters J_N and J_i indicate the efficiency of excitatory and inhibitory signalling respectively, which represent the computational implications of mechanisms related to the provision, release, reception, and reuptake of neurotransmitters (Choquet & Triller, 2013; V. M. Ho et al., 2011). The excitatory recurrence parameter w_p denotes the level of self-excitation, which is affected by the neuronal architecture of each regional network (Douglas et al., 1995). Together, these three parameters determine the balance between excitatory and inhibitory signalling, which is an important factor in maintaining healthy brain connectivity (Hu et al., 2023; Sohal & Rubenstein, 2019). The global coupling parameter G describes the strength of external input into each region, which reflects both neuromodulatory processes (Marder, 2012) and the characteristics of global fibre tracts (Huntenburg et al., 2017; Yang et al., 2021).

1.3.3 Brain network modelling in clinical research

In recent years, brain network modelling approaches have been used to reveal a number of key insights into brain activity and connectivity in psychiatric disorders. Several studies have investigated biological mechanisms of Alzheimer's disease (AD) using this methodology. Zimmermann et al. (Zimmermann et al., 2018) identified individualised optimal model

parameters of participants with mild cognitive impairment, AD patients and healthy older adults based on their resting-state FC, and found a correlation of these parameters with cognitive performance. Demirtaş et al. (Demirtaş et al., 2017) modelled resting-state FC of participants with preclinical AD, mild cognitive impairment due to AD, and mild dementia due to AD, and healthy control individuals. They identified differences in the optimal effective connectivity between the groups, and were able to replicate the empirical FC of the AD patients from models optimised for healthy controls by systematically changing the dynamic behaviour of the regional models to disturb synchronisation, providing evidence for altered regional dynamics as a mechanism of functional abnormalities in AD.

Computational modelling has also been employed to explore links between SC, FC and neurophysiology in schizophrenia. Zhang et al. (X. Zhang et al., 2021) investigated models of healthy controls, schizophrenia patients, and first-degree relatives of patients, and found that patients and relatives exhibited a reduction in optimal parameters relating to spatial constraint and topological neighbourhood structure which was associated with polygenic risk score and cognitive performance. In addition, Cabral et al. (Cabral et al., 2013) simulated rs-fMRI data based on the SC of schizophrenia patients and healthy control participants, and determined that characteristic alterations in FC in schizophrenia were not produced by differences in the structural connectome, but by changes in global coupling. Klein et al. (Klein et al., 2021) studied healthy individuals with different polymorphisms in a gene purported to contribute to disturbances in the excitation-inhibition balance in schizophrenia, and concluded that carriers of one allele exhibited higher excitatory and inhibitory synaptic coupling, and lower recurrent excitation and global coupling, providing additional evidence for a role of this gene in determining excitation-inhibition balance.

Together, the highlighted studies show that brain network modelling allows for the investigation of causal relationships between neuroanatomy, neurophysiology, and brain function, as well as the analysis of individual variability in these processes, contributing important findings on the mechanisms of neuropsychiatric disorders.

1.4 Thesis rationale and objectives

The objective of this PhD thesis is to contribute to the current understanding of alterations in FC in patients with psychiatric disorders and the underlying neurobiological mechanisms shaping FC. Specifically, this thesis seeks to characterise dynamic FC in psychotic and affective disorders, and uncover computational processes contributing to static and dynamic FC patterns. In addition, the work of this thesis aims to reveal relationships between individual variability in neurobiology, FC, and clinical and behavioural characteristics to provide insights into the heterogeneity of these processes in health and disease. While the research presented here is not primarily translational, it is intended to inform future clinical studies by identifying differences in dFC and model-derived neurophysiological characteristics which might be suitable as biomarkers, and uncovering pathological mechanisms in psychiatric disorders which could serve as targets for novel therapeutic strategies.

In the context of these aims, this thesis will present and explore findings from three experimental studies in both healthy individuals and patients with recent-onset psychosis (ROP), recent-onset depression (ROD), and clinical high risk for psychosis (CHR). These three studies employed different but complementary methodological approaches to investigate the association of static and dynamic FC with clinical, behavioural and neurobiological variables. By integrating the joint findings of these three studies and discussing them in the context of available literature and future research goals, this thesis aims to elucidate the role of dFC in linking neurobiology and behaviour in healthy individuals and psychiatric patients.

The first study (see Section 2) compared dFC in patients with psychotic and affective disorders with healthy controls, with the aim of providing a characterisation of disorder-specific and transdiagnostic changes to dFC in these conditions. Resting-state fMRI data was obtained from ROP, ROD, and CHR patients, and healthy individuals. Using a sliding window technique and k-means-based clustering approach, recurrent connectivity patterns, or brain states, were

identified and their dynamic characteristics determined. These dFC profiles were compared between the four subject groups, and their association with clinical, cognitive and demographic variables was assessed in the patient groups.

The second study (see Section 3) investigated the relationship between neurobiology and functional connectivity using computational modelling, aiming to identify neurobiological contributions to individual variability in FC patterns. Based on empirical group-average diffusion tensor imaging data and four model parameters, simulated resting-state fMRI time courses were produced and their static and dynamic FC compared with that of 200 healthy individuals. The set of parameters which best described the brain of each participant, and the fit of the static and dynamic FC produced by that model, were associated with whole-brain static and dynamic FC patterns. In addition, the study assessed the effect of altering regional model parameters on static and dynamic FC. The strength of the global input into each region was systematically manipulated, and the resulting changes to static and dynamic FC analysed and related to graph parameters and gene expression maps.

The third study (see Section 4) aimed to analyse the biological underpinnings of the alterations in dFC in psychiatric patients identified in Study I by using the computational modelling approach developed and applied to healthy controls in Study II to determine the individual neurophysiological characteristics of patients and controls. The biologically derived model parameters optimally reproducing static and dynamic FC were compared between the ROP, CHR, ROD and HC groups to reveal common and unique alterations in neurobiology across the patient groups.

The three studies together advance the overall objective of the thesis, contributing insights into different facets of the relationship between alterations in neurobiology and psychiatric illness via the intermediate phenotype of dynamic functional connectivity.

2. Study I

This study investigated changes in dFC in patients with recent-onset psychosis, patients with recent-onset depression, and individuals with a clinical high risk for psychosis relative to healthy control individuals (HC). The analysis of dFC allows for a detailed characterisation of complex abnormalities of brain function (Hutchison et al., 2013), providing insight into the biological processes underlying these disorders. Given that psychotic patients and affective patients overlap in their clinical presentation (Conley et al., 2007; Ohayon & Schatzberg, 2002; Upthegrove et al., 2017), comparing dFC between these groups could provide evidence of common and unique mechanisms contributing to their symptoms. In addition, CHR individuals have shown abnormalities resembling those of psychosis patients in both static and dynamic FC (Del Fabro et al., 2021; Y. Du et al., 2018), which could relate to either psychosis symptoms, or to affective symptoms or general impairment which occur across psychiatric conditions. By comparing the dFC of the three patient groups, we aimed to distinguish diagnosis-specific from transdiagnostic patterns of dFC. We further studied the association of dFC and clinical features in order to identify dFC patterns related to symptoms or risk factors across patient groups.

Previous studies of dFC in psychotic and affective disorders have been conducted in small samples and provided heterogeneous findings. In addition, assessments of dFC patterns across patient groups have previously been limited by the lack of a consistent methodology for the quantification of dFC (Cattarinussi et al., 2023; Sun et al., 2024). The analysis framework used in this study, consisting of the estimation of time-varying FC with the sliding window method and a consensus clustering algorithm for the identification of recurrent connectivity states, was devised to reflect well-established and robust approaches used in previous studies. Its application to a large sample of patients and controls is likely to provide a detailed and reliable characterisation of dFC patterns in patients and controls.

Given these considerations, this study investigated the following hypotheses:

(a) Patients with psychiatric disorders exhibit alterations in dFC compared to healthy individuals.
(b) Patients with affective and psychotic disorders exhibit overlapping but distinct patterns of dFC alterations
(c) Patients with recent-onset psychosis exhibit more severe alterations than individuals in a prodromal stage
(d) Alterations in dFC are associated with psychiatric symptoms, demographic characteristics and cognitive performance

Please note that the methods and results presented here are related to the following published experimental study:

Linnea Hoheisel, Lana Kambeitz-Ilankovic, Julian Wenzel, Shalaila S. Haas, Linda A. Antonucci, Anne Ruef, Nora Penzel, Frauke Schultze-Lutter, Theresa Lichtenstein, Marlene Rosen, Dominic B. Dwyer, Raimo K.R. Salokangas, Rebekka Lencer, Paolo Brambilla, Stephan Borgwardt, Stephen J. Wood, Rachel Upthegrove, Alessandro Bertolino, Stephan Ruhrmann, Eva Meisenzahl, Nikolaos Koutsouleris, Gereon R. Fink, Silvia Daun, Joseph Kambeitz, and the PRONIA Consortium (2024). **Alterations of Functional Connectivity Dynamics in Affective and Psychotic Disorders,** Biological Psychiatry: Cognitive Neuroscience and Neuroimaging, 9 (8), 765-776, doi: 10.1016/j.bpsc.2024.02.013.

2.1 Methods

2.1.1 Participants

The data used in this investigation was a subset of the data acquired during the PRONIA study (www.pronia.eu) (Koutsouleris et al., 2018, 2021), a naturalistic longitudinal study conducted at seven European institutions. The study included ROP patients, ROD patients, CHR individuals and HC individuals. Participants underwent extensive clinical characterisation, cognitive assessment, blood sampling, and a multimodal neuroimaging protocol including structural MRI, resting-state functional MRI, and diffusion tensor imaging. Informed consent was provided in writing by all adult study participants, and by the guardians of minor participants (below 18 years of age) who assented to participation. The study was approved by the local research ethics committees in each study centre and registered at the German Clinical Trials Register (DRKS00005042). Participants of all study groups had to fulfil the following general inclusion criteria: age between 15 and 40 years, language skills that were adequate for study participation, and the capacity to provide informed consent. Participants were excluded from the study if they exhibited an IQ below 70, current or past head trauma with loss of consciousness for more than 5 minutes, a current or past neurological or somatic disorder that might affect brain structure or functioning, current or past alcohol dependence or polysubstance dependence during the last six months, or any contraindications for MRI scanning. Patients were included in the ROD and ROP groups if they met diagnostic criteria for depression or psychosis respectively in the past three months as assessed by the Structured Clinical Interview for DSM-IV-TR (SCID) (First et al., 2002), as long as symptoms had occurred for the first time within the past 24 months. Inclusion criteria for the CHR group were cognitive disturbances (COGDIS) according to the Schizophrenia Proneness Instrument (SPI-A) (Schultze-Lutter et al., 2007), or the fulfillment of ultra-high-risk (UHR) criteria for psychosis according to the Structured Interview for Psychosis-Risk Syndromes (SIPS) (McGlashan et al., 2010). In addition, ROP patients were excluded if they had received antipsychotic medication at a daily dose above the minimum dosage of S3-guidelines of the

German Society for Psychiatry, Psychotherapy and Psychosomatics (Deutsche Gesellschaft für Psychiatrie, Psychotherapie, Psychosomatik und Nervenheilkunde, DGPPN) (DGPPN e.V., 2019) for longer than 90 days to minimise long-term effects of medication on this study group. HC participants were excluded if they exhibited any current or past DSM-IV axis disorder, had a first-degree relative diagnosed with an affective or non-affective psychosis, or had received psychotropic medications or drugs more than five times per year and in the month before inclusion in the study.

2.1.2 Clinical and neuropsychological assessment

Participants completed a range of clinical assessments including the Beck Depression Inventory-II (BDI-II) (A. T. Beck et al., 1996), the Positive and Negative Syndrome Scale (PANSS) (Kay et al., 1987), the Global Functioning: Role Scale (GF Role) (Niendam et al., 2006) and Global Functioning: Social Scale (GF Social) (Auther et al., 2006), measuring global role and social functioning, and the global assessment of functioning (GAF) (Pedersen et al., 2007). Information on types and dosages of psychiatric medications was also gathered. In addition, participants were assessed with a range of cognitive tests covering five domains of the MATRICS Consensus Cognitive Battery (Kern et al., 2008; Nuechterlein et al., 2008). The Diagnostic Analysis of Nonverbal Accuracy (Nowicki & Duke, 1994) was used as a measure of social cognition, the verbal fluency test (Ruff et al., 1996) and the Trail Making Test part A (Tombaugh, 2004) to measure speed of processing, the auditory digit span (Wechsler, 1955) and self-ordered pointing tasks (Petrides & Milner, 1982) to measure working memory, the Rey Auditory Verbal Learning Test (Schmidt, 1996) to measure verbal learning and memory, and the Continuous Performance Test - Identical Pairs (Eliason & Richman, 1987) to measure attention. An average of the five domain scores was computed to obtain a total cognition score.

2.1.3 MRI Acquisition and Preprocessing

T1-weighted structural and resting-state functional MRI scans were acquired of each participant. A multi-echo MPRAGE sequence with 190 contiguous sagittal slices was used to acquire T1 reference images. For the acquisition of the functional blood oxygen level dependent (BOLD) images, an echo planar imaging (EPI) sequence with 53 ascending slices was employed, using the intercommissural line (AC-PC) as a reference. Resting-state fMRI scans produced 200 volumes, with the total scan having a duration of 603 s. Participants were instructed to keep their eyes open during the scan. Further details of the MRI acquisition parameters are presented in Table 1.

scan session	repetition time (TR)	echo time	flip angle	field of view	matrix size	slice thickness	slice gap	voxel size
T1	9.5 ms	5.5 ms	8 °	250 x 250 mm^2	256 x 256	1 mm	1 mm	0.97 x 0.97 x 1 mm^3
BOLD	3000 ms	30 ms	90 °	230 x 230 mm^2	80 x 80	3 mm	3 mm	2.875 x 2.875 x 3 mm^3

Table 1: Acquisition parameters for structural T1 and functional BOLD sequences.

The CAT12 pipeline (Gaser et al., 2024) was used to preprocess the structural T1 images (Koutsouleris et al., 2018). The data was first denoised by Spatially Adaptive Non-Local Means (SANLM) filtering (Manjón et al., 2008). Segmentation was performed with an Adaptive Maximum A Posteriori (AMAP) technique, which produces a homogeneous segmentation across cortical and subcortical regions. The AMAP-generated initial segmentation was further refined by adding spatial prior information of adjacent voxels using a Markov Random Field approach (Rajapakse et al., 1997). White matter (WM) inhomogeneities and varying grey matter (GM) intensities were accounted for by employing Local Adaptive Segmentation (LAS).

Subsequently, a final AMAP segmentation was produced. The images were further processed by the application of a partial volume segmentation algorithm, which improved segmentation by adding tissues with intensities between GM and WM, as well as GM and cerebrospinal fluid (CSF) to the model. The images were registered to an MNI template produced from the MRI data of 555 healthy controls in the IXI database (http://www.braindevelopment.org) using a high-dimensional DARTEL.

The preprocessing of the resting-state fMRI images was modelled on that employed by Patel et al. (Patel et al., 2014), and has been previously described by Haas et al. (Haas et al., 2021). It consisted of two parts, the initial preprocessing and denoising steps. Statistical Parametric Mapping, version 12 (SPM12) (https://www.fil.ion.ucl.ac.uk/spm/software/spm12/) was employed to complete core preprocessing tasks. First, the initial 8 volumes were removed, and the 192 residual images were slice-time corrected, unwarped and corrected for head motion by realignment to the first volume. Six parameters, denoting translation in each direction and rotation around each axis, were computed to assess head motion of each subject. In addition, framewise displacement (FD) was calculated by adding the absolute temporal derivatives of the six motion parameters, with FD for the first volume set to 0 (Power et al., 2012). Subjects with excessive head motion, defined as those for which 38.5 % of volumes exhibited a mean FD of more than 0.50 mm, were excluded from further analyses (Power et al., 2014).

Resting-state fMRI images were then co-registered to the structural T1 images by an affine algorithm and resliced via 4th-degree B-Spline interpolation. The CAT12 template was then converted from DARTEL space to MNI space, and the resulting image applied as a deformation field to normalise co-registered images to MNI space. Grey matter, white matter and CSF masks were produced with SPM12 image calculator, using the thresholds of 0.20, 0.20, and 0.50 respectively. Then, the 24 Friston motion parameters (Satterthwaite et al., 2013) were determined, including the six basic motion estimates, six temporal derivatives, six quadratic terms and six quadratic expressions of the derivatives of motion estimates. The

signal variance detected in the WM and CSF was regressed out to produce individual estimates of GM signal. Using the GM mask, functional volumes were then extracted and spatially smoothed using a Gaussian kernel of 6 mm full width at half-maximum.

In the second step of the preprocessing pipeline, the resting-state fMRI data was denoised via further motion correction and filtering. Time series were despiked using the BrainWavelet Toolbox (Patel et al., 2014). The effects of the 24 Friston motion parameters and the residuals of WM and CSF signal were removed using confound regression. Filtering consisted of background and temporal band-pass filtering in a range of 0.01 - 0.08 Hz. By removing the highest and lowest frequency fluctuations, the effects of low-frequency drift and high-frequency noise were minimised (Song et al., 2011). These steps were performed according to the Resting-State fMRI Data Analysis Toolkit (REST version 1.8; http://www.restfmri.net/). Lastly, the data was parcellated by calculating the average BOLD signal over all voxels in each of the 160 cortical and subcortical regions of the Dosenbach atlas (Dosenbach et al., 2010).

2.1.4 Dynamic functional connectivity analysis

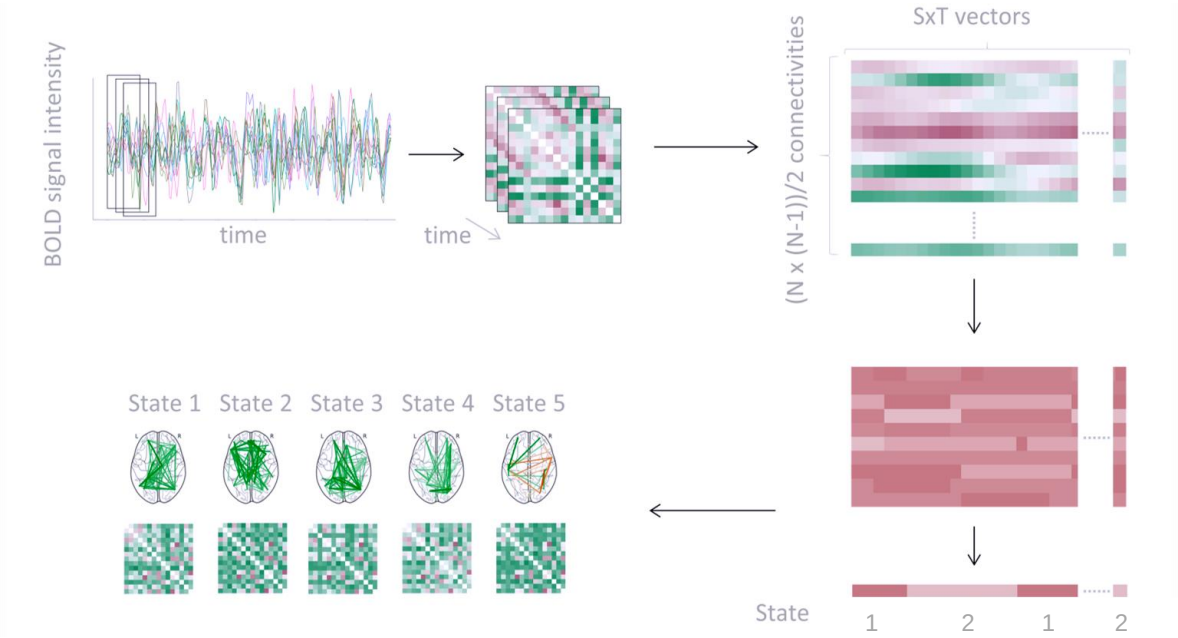

Figure 1: Methodology for generating time-resolved FC.

We computed functional connectivity matrices representing pairwise correlations between brain regions for each time window using a sliding-window approach, and aggregated the upper triangular portions of these matrices across time windows for each subject into a single matrix. We then repeatedly applied k-means clustering, and obtained a clustering consensus. Using this approach, we identified and characterised distinct FC states.

Figure 1 shows a graphical overview of the analysis workflow. For each subject, moment-by-moment FC was determined using sliding windows (Hutchison et al., 2012). The Pearson correlation (Pearson, 1895) of the fMRI time courses in each pair of regions was calculated within a window encompassing 90 seconds of scan time, or 30 volumes, yielding an FC matrix of 160 x 160. The window was then shifted by one frame, and a new FC matrix computed. The window length was chosen in accordance with previous recommendations for dFC analysis (Leonardi & Van De Ville, 2015). The correlations were calculated using the Pearson correlation coefficient weighted with a Gaussian kernel of $\sigma = 3$. Due to the weighting, the

influence of specific data points gradually increases and later decreases with each subsequent window. As a result, changes in FC produced by outliers in regional or global brain activity are less abrupt than in conventional sliding window analysis (Allen et al., 2014). The entire scan was split into a series of 162 overlapping sliding windows, with an FC matrix computed for each one. FCs were transformed to a normal distribution using the Fisher z-transformation (Hotelling, 1953). Given that FC matrices are symmetrical, only the upper triangular vectors were considered for further analysis. The sliding window FC consisted of a 162x12720 matrix, with FC in 12720 pairs of regions computed at 162 timepoints.

We employed a consensus clustering approach to identify recurrent FC patterns in each of the four study groups. The FC vectors of all time points and all subjects were clustered using a k-means algorithm (Lloyd, 1982), and the clustering repeated 10 times. For each pair of FC vectors, the number of times which they were assigned to separate clusters was determined, producing a distance matrix. An agglomerative hierarchical algorithm (Ward Jr., 1963) was then applied to produce a consensus cluster assignment based on this matrix. The consensus approach provides a more robust clustering solution than k-means clustering alone. The k-means algorithm initially receives a set of random cluster centroids, which are then iteratively improved. Depending on the choice of initial centroids, the algorithm can converge to local optima, potentially resulting in an unsuitable cluster assignment. By combining several clustering solutions based on different initial centroids, the influence of this initial selection is reduced. As there is still some debate on the optimal number of FC states, with studies reporting anything from two (Yao et al., 2019) to five (Snyder et al., 2021) states, nine partition models consisting of between two and ten clusters were considered. For each partition model, a number of measures of clustering performance were calculated, including the Davies-Bouldin score, which represents the average similarity between clusters (Davies & Bouldin, 1979), and the Calinski-Harabasz score, the ratio of the mean between-cluster dispersion and the within-cluster dispersion (Caliński & Harabasz, 1974). In addition, a split-half analysis was conducted. The first and second halves of each scan in the HC group were assigned to two

separate sets, and the clustering performed for each set separately. To estimate the agreement in clustering performance, the FC patterns representing the states identified in the first half and those of the corresponding states identified in the second half were then correlated.

2.1.5 Differences in dynamic functional connectivity in CHR, ROD and ROP patients

Brain states identified separately in each subject group were matched to enable the comparison of their dynamic characteristics across the groups. The most similar states, as measured by the correlation between the means over all FC vectors assigned to the states, were considered to correspond. Each state identified in each of the patient groups (CHR, ROD, ROP) was assigned a corresponding HC-derived state. For each group, a similarity matrix was computed, representing the correlation between each HC-derived and each patient-derived state. The pair of HC-derived and patient-derived states with the highest correlation was first selected as a corresponding set. For both states, the correlation to all other states, represented by the row and column of the similarity matrix in which the highest correlation was contained, were set to 0, ensuring that each HC-derived state was assigned to one patient-derived state and vice versa. This step was repeated until a matching HC-derived state was identified for each patient-derived state. In order to compare the corresponding states of the four subject groups, the correlation of the mean FC of the state was computed between each pair of groups. To further characterise each state, the mean FC within and between the seven RSNs characterised by Dosenbach et al. (Dosenbach et al., 2010), and the mean FC within cortical, subcortical and cortico-subcortical links, were determined for the HC-derived FC means.

Three dynamic FC metrics were calculated for each subject: i) the lifetime of each state, the mean duration for which a state persists before a transition into another state, ii) the frequency of each state, the fraction of the entire scan which an individual spends in the state, iii) the transition frequency between each pair of states, the number of times an individual transitions

from exhibiting one state to exhibiting a second state, and iv) the in-degree of each state, the total number of times the subject transitions into the state (Hutchison et al., 2013). The variables were transformed to a normal distribution with a Yeo-Johnson transform (I. Yeo & Johnson, 2000) in order to allow for the application of parametric statistical methods. Confound regression was applied to control for effects of gender, age, site, and motion, represented by the mean framewise displacement. For each variable, a linear model was fitted which included the four confounds as predictors, and the residuals used for further analysis. The dFC parameters of each state, or pair of states, were then compared between the four subject groups using Mann-Whitney U-tests (Mann & Whitney, 1947), and the resulting p-values corrected for multiple comparison by Bonferroni correction (Dunn, 1961).

2.1.6 Association with clinical variables

In addition to the group-wise comparison of dFC parameters, we attempted to identify relationships between individual variation in dFC and clinical variables in the patient groups, particularly potential transdiagnostic associations between brain and behavioural features. To that extent, canonical correlation analysis (CCA) (Hotelling, 1936; H.-T. Wang et al., 2020) was applied to a set of dFC features, consisting of lifetimes, frequencies and transition frequencies for each state or pair of states, and a set of clinical features, including symptom severity scores, demographic variables and cognitive scores. Missing values in the clinical variables were filled in with a group-wise median in subjects which only exhibited one missing value. Subjects which were missing data in more than one feature were removed from further analysis. CCA is a method of finding associated patterns in two separate datasets. It identifies pairs of canonical variables, linear combinations of features in each of the two datasets, which maximally correlate with each other. The association of individual features with the new canonical variable can be expressed by the feature loadings, the correlation between each feature and the canonical variable. The statistical significance of the correlations of canonical variable pairs and feature loadings was determined via permutation testing. The feature values

in the dFC and clinical sets were shuffled 1000 times across the subjects. CCA was then performed on each permutation, and the correlation between canonical variable pairs and feature loadings calculated to produce null distributions for each.

2.1.7 Validation analyses

Several additional analyses were performed in order to establish the validity of the results. While the removal of potential artefacts via confound regression is a standard technique, it risks removing potentially salient information, or missing some confound-related variation. To evaluate the effect of confound removal procedures on the results, several were compared. The standard procedure included age, sex, site and mean FD as covariates. Analyses were repeated without confound correction, providing results based on the raw dFC parameters. The effect of motion- and medication-related artefact removal were tested specifically by removing mean FD and adding medication dose respectively as covariates. These two variables are particularly important to appropriately control for as they represent artificial noise which could confound the outcomes in unexpected ways.

In addition, the clustering of states and subsequent analyses of dFC were repeated with the second best partition model. As the there is no consensus on a ground truth for the number of states the brain alternates between, with different studies yielding different results, the comparison of initial findings with those obtained with a different number of clusters ensures the robustness of conclusions even in the case that the selected partition model is not the optimal one.

2.2 Results

2.2.1 Sample description

							HC v CHR		HC v ROP		HC v ROD		CHR v ROP		CHR v ROD		ROP v ROD	
	HC	CHR	ROP	ROD	χ^2/t-value	p-value	χ^2	p-value	χ^2	p-value	χ^2	p-value	χ^2	p-value	χ^2	p-value	χ^2	p-value
Subjects, n	261	130	143	136	–	–	–	–	–	–	–	–	–	–	–	–	–	–
Gender, male/female	105/156	67/63	87/56	59/77	χ^2 = 17.511	0.001	4.057	0.044	14.919	< 0.001	0.248	0.618	2.032	0.154	1.461	0.227	7.830	0.005
Age, mean (sd)	28.9 (6.4)	27.1 (5.0)	28.6 (5.4)	29.1 (6.4)	t = 9.055	0.029	19673.5	0.010	18746.5	0.940	17357.5	0.719	7688.0	0.013	7251.0	0.011	9481.5	0.719
Medication (daily dose in CPZE), mean (sd)	0.0 (0.0)	20.2 (56.1)	374.4 (932.7)	23.1 (108.8)	t = 285.336	< 0.001	13702.5	< 0.001	5742.0	< 0.001	14877.0	< 0.001	3883.0	< 0.001	9125.0	0.495	15550.0	< 0.001
PANSS positive scale, mean (sd)	–	11.4 (3.4)	19.0 (5.9)	8.3 (1.7)	t = 231.306	< 0.001	–	–	–	–	–	–	2344.0	< 0.001	13528.0	< 0.001	17350.5	< 0.001
PANSS negative scale, mean (sd)	–	12.4 (6.9)	16.2 (10.7)	12.4 (6.7)	t = 24.166	< 0.001	–	–	–	–	–	–	6107.5	< 0.001	8011.5	0.468	11530.0	< 0.001
PANSS general scale, mean (sd)	–	27.8 (5.8)	35.5 (7.8)	27.3 (4.8)	t = 58.662	< 0.001	–	–	–	–	–	–	4848.5	< 0.001	8597.0	0.724	13332.5	< 0.001
BDI-II, mean (sd)	3.5 (5.0)	25.9 (12.5)	21.2 (12.4)	26.2 (13.9)	t = 351.716	< 0.001	1445.5	< 0.001	2579.5	< 0.001	1379.0	< 0.001	9064.5	0.002	7369.0	0.753	6087.5	0.011
GAF Disability/ Impairment, mean (sd)	85.2 (6.4)	56.2 (13.7)	45.2 (12.1)	56.4 (14.7)	t = 462.127	< 0.001	32740.5	< 0.001	36500.0	< 0.001	34112.0	< 0.001	13520.0	< 0.001	8673.5	0.871	5227.5	< 0.001
GAF Symptoms, mean (sd)	86.7 (6.4)	55.0 (11.0)	40.9 (13.1)	55.6 (11.9)	t = 499.402	< 0.001	33528.0	< 0.001	36630.0	< 0.001	34548.0	< 0.001	14641.0	< 0.001	8505.0	0.665	3780.5	< 0.001
EHI, mean (sd)	75.8 (45.6)	66.7 (57.6)	70.4 (53.8)	75.6 (45.5)	t = 1.538	0.464	–	–	–	–	–	–	–	–	–	–	–	–

Table 2: Sample description.

CPZE: chlorpromazine equivalent units, PANSS: Positive and Negative Symptom Scale, BDI-II: Beck Depression Inventory-II, GAF: Global Assessment of Functioning, EHI: Edinburgh Handedness Inventory

Out of the 688 participants originally included in the sample, four were excluded due to missing data, and an additional 14 participants were excluded because of excessive motion during the fMRI scan. The final sample for the current analysis comprised 261 HC participants, 130 CHR patients, 143 ROP patients, and 136 ROD patients (Table 2). Age and sex distributions differed significantly between some of the groups. The ROP group included a higher proportion of male participants than the ROD group (p(ROP-ROD) = 0.005). Similarly, the CHR and ROP groups both included a higher percentage of male participants than the HC group (p(HC-CHR) = 0.044, p(HC-ROP) < 0.001). The CHR group showed a significantly lower mean age than all other groups (p(HC-CHR) = 0.010, p(CHR-ROP) = 0.013, p(CHR-ROD) = 0.011). The CHR and ROD groups only showed significant differences in the positive symptom subscale of the

PANSS, while the other groups differed significantly on most clinical scales and the medication dosage.

Study participants were recruited at seven different research centres, with the largest cohorts included in Munich (n=179) and Cologne (n=123). Additional participants were enrolled in Basel (n=92), Udine (n=88), Birmingham (n=69), Turku (n=78), and Milan (n=41). The number of participants included in each study group varied significantly between some research sites (Table 3).

					Turku		Birmingham		Milan		Udine		Basel		Cologne	
	HC	CHR	ROP	ROD	χ^2	p-value	χ^2	p-value	χ^2	p-value	χ^2	p-value	χ^2	p-value	χ^2	p-value
Munich	57	39	38	45	3.683	0.298	9.489	0.023	3.628	0.305	3.648	0.302	4.640	0.200	7.848	0.049
Cologne	58	19	24	22	8.135	0.043	2.202	0.532	4.600	0.204	2.968	0.397	1.622	0.654		
Basel	38	18	22	14	3.481	0.323	4.351	0.226	1.934	0.586	4.268	0.234				
Udine	37	18	12	21	8.929	0.030	1.802	0.615	7.368	0.061						
Milan	13	7	14	7	0.380	0.944	9.004	0.029								
Birmingham	36	13	8	12	12.276	0.006										
Turku	22	16	25	15												

Table 3: Distribution of participants across sites.

Effect sizes and p-values were estimated using a chi-square test.

2.2.2 Identification of functional connectivity brain states

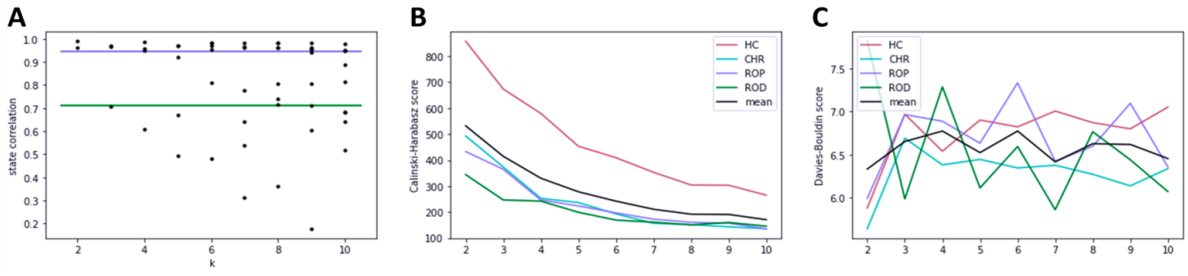

Figure 2: Assessment of different partition models to determine optimal number of clusters.

A Overlap of matching states in split-half analysis. Each pair of states is represented by a dot. The purple line represents the maximal correlation of separate states identified in the same

subset. The green line symbolises the mean correlation of different states identified in the same subset. Clusters are likely to be conserved between halves if their correlations are above the green line. B Calinski-Harabasz score for each partition model. Better clustering performance is indicated by higher values. C Davies-Bouldin score for each partition model. Better clustering performance is indicated by lower values.

To assess the stability of the clustering procedure and identify the number of clusters producing the most consistent FC patterns, we applied it separately to the first and second halves of the fMRI time series from HC participants and analysed several partition models. In the split-half analysis, multiple clusters exhibited strong correlations between the two halves, regardless of the number of clusters k considered (Figure 2A). We determined the average and the maximal correlation between distinct clusters identified in the same subset of the data to use as benchmarks for evaluation. Matching clusters identified in the two different halves using partition models with fewer than four clusters consistently exhibited higher correlations than the maximum distinct-cluster correlation threshold, suggesting that matching clusters can be reliably considered to represent the same brain state. Partition models with more clusters produced some which were less similar to their counterparts in the other half of the data, although several clusters still exhibited above-threshold correlations. A k value of five proved to be a good clustering solution, as only one cluster showed below-threshold consistency. The between-half correlation of this cluster was nonetheless higher than that of several clusters identified with other partition models. The results of the split-half analysis complement those of the clustering score evaluation with regards to the optimal number of states. The Davies-Bouldin score was particularly low for clustering solutions with 5, 6 and 10 clusters, whereas there were no partition models which achieved a particularly high or low Calinski-Harabasz score (Figure 2B-C). Given that the five-cluster model performed well in terms of both split-half consistency and clustering scores, it was selected for further analysis.

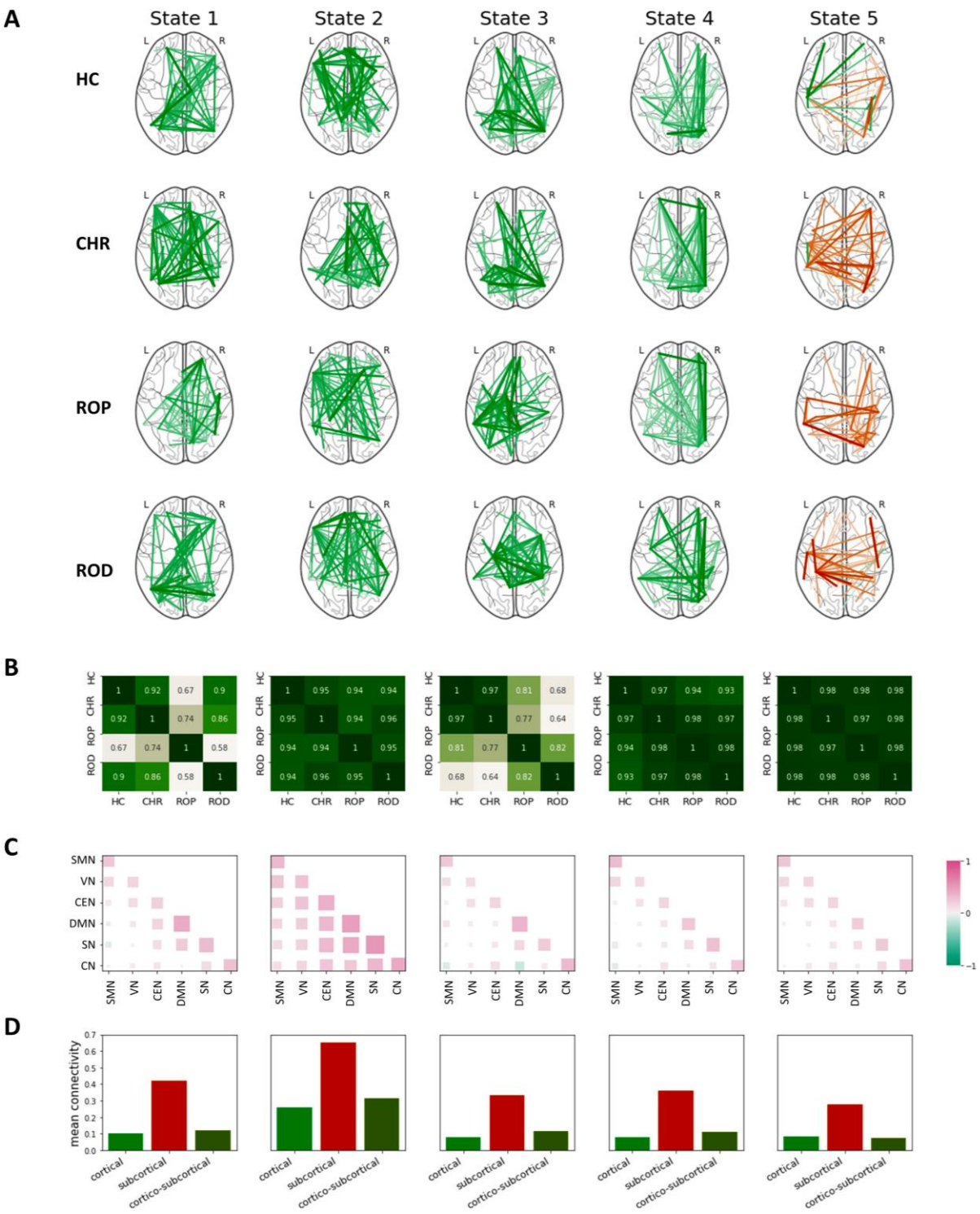

Figure 3: Five distinct states identified by dFC analysis (k=5).

A Network representation of FC states for each study group. Mann Whitney U-tests were used to identify uniquely high or low connectivities characteristic for each state compared to the other states. Only connections with the highest 5% of effect sizes are presented. Positive

connectivities are represented by green lines, negative connectivities by red lines. B Correlation of state FC patterns between groups. C Average connectivities within and between resting state networks. Absolute values are represented by the size of each square. D Average FC of cortical, subcortical, and cortico-subcortical connections.

Five brain states, each represented by a distinct FC pattern, were identified in each diagnostic group (Figure 3A). Figure 3B shows the correlations between the states obtained from the HC groups and the corresponding states in each patient group determined by the matching procedure, as well as the correlations between patient-derived states assigned to the same HC-derived state. States 2, 4, and 5 exhibited high correlations between all study groups, suggesting that they were conserved and robustly identifiable in patients as well as in HC participants. The FC pattern of state 1 obtained in the ROP group deviated from those of the other groups, and the HC, CHR, and ROD groups showed lower correlations between each other. For state 3, only the FC patterns of the HC and CHR groups were similar, with the other correlations between groups weaker.

Average connectivities within and between canonical resting-state networks, as well as within and between cortical and subcortical regions, were computed for the HC state in order to enhance interpretability of the FC patterns (Figure 3C). State 1 displayed negative FC values in connections between the SMN and the SN as well as the DMN, while the FC within the DMN and SN was high. State 2 showed consistently high within- and between-network connectivites. State 3 exhibited strong FC in the cerebellum and the DMN, but negative FC between the cerebellar and the SMN as well as the DMN. State 4 was characterised by higher FC in the SN and SMN, and negative FC between the SMN and cerebellar areas compared to state 5, although both states showed consistently low within- and between-network FC. Figure 3D shows the connections in each FC pattern which are distinctive for that particular state compared to other states identified in the same group, highlighting the distributed nature

of characteristic connections across the states and the importance of negative connections in state 5.

2.2.3 Group-level differences in dynamic parameters of FC states

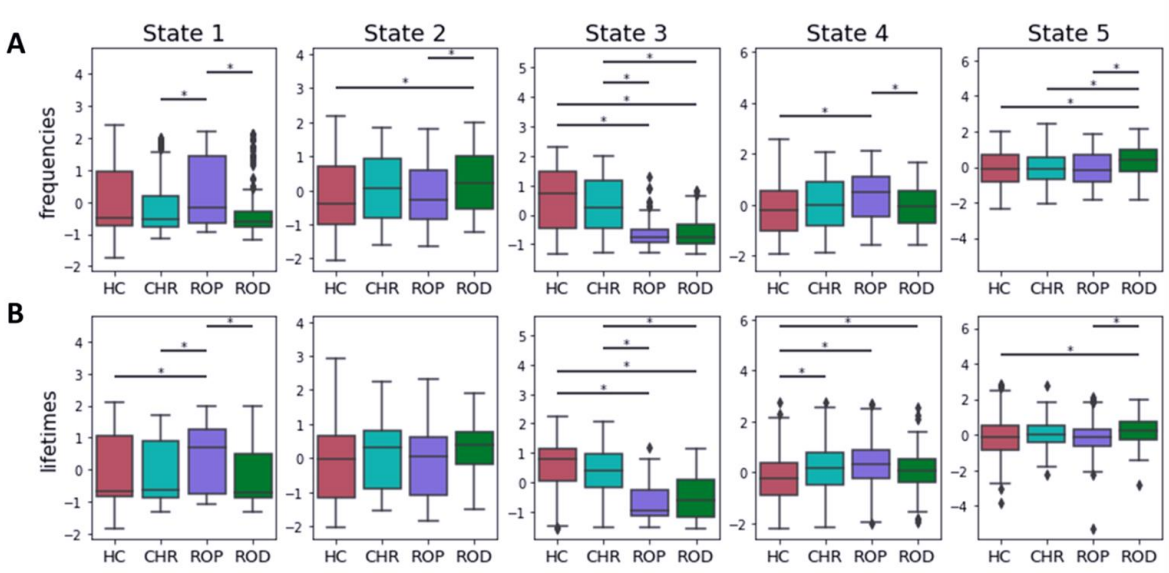

Figure 4: Comparison of dFC parameters between study groups.

A Frequencies and B lifetimes of each state for each group after normalisation and confound correction. Stars represent significant differences after Bonferroni correction ($p < 0.0016$). Effect sizes and p-values are supplied in Supplementary Table 1 and Supplementary Table 2.

For each state, lifetimes and frequencies of each group were transformed to a Gaussian distribution and underwent confound regression to allow for comparison of their means (Figure 4). Participants in each group exhibited states 4 and 5, which also displayed the most consistent FC patterns across the study groups, most often. State 5 occurred with a frequency of approximately 50%, state 4 with a frequency of 18-30% depending on the group. On average, less than 20% of the scan time was spent in the three remaining states. The average lifetime of state 5 was also the highest in each group, with the average lifetime of state 4 not

much lower (Supplementary Table 2). All states exhibited significant differences in their frequencies, and most in their lifetimes, between at least some of the study groups. The frequency of state 2 was lower in ROD patients than either HC or ROP individuals. ROD patients additionally experienced higher frequencies of state 5 than all other groups, and longer lifetimes than HC and ROP individuals. State 1 displayed a higher frequency in ROP patients than in CHR and ROD patients, and longer lifetimes than all other groups. HC participants exhibited significantly shorter lifetimes of state 4 than the study groups, although both HC and ROD groups exhibited higher frequencies of this state than the ROP group. The distributions of lifetimes and frequencies were particularly large in state 3, suggesting strong individual variability in these parameters. Group comparisons reveal small but significant differences in all parameters and between all groups other than between HC and CHR.

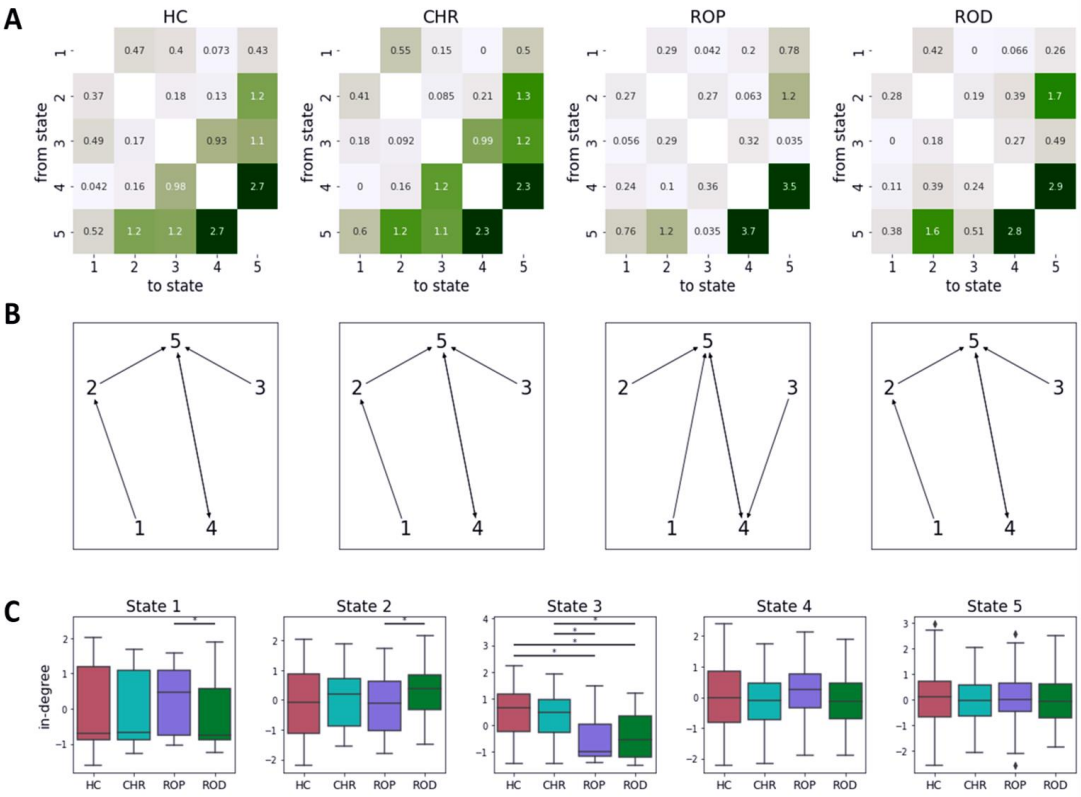

Figure 5: Comparison of transition behaviour between subject groups.

A Average number of switches between each pair of states. B Graph representation of the most frequent transition from each state. C In-degree of each state. Stars represent significant differences after Bonferroni correction ($p < 0.0016$). Effect sizes and p-values are supplied in Supplementary Table 3.

Investigation of state transition behaviour revealed both common and unique characteristics among the different study groups (Figure 5). The transition matrices showed a symmetric pattern, with transitions between states close to equally common in both directions. State 5, which showed the highest frequencies and lifetimes in all groups, was also the state most other states switched to with the highest frequency. Transitions from this state most commonly reached state 4 in all groups, with ROP patients exhibiting the highest frequency in this transition. Across the groups, transitions from state 5 to state 2 were next most common, while transitions into state 3 occurred similarly frequently in HC and CHR individuals, but not ROP or ROD patients. From state 4, state 3 was reached second most frequently after state 5 in the HC and CHR groups. This transition was less common in ROD patients, and rare in ROP patients. The overall structure of frequent transitions was the same in the HC, CHR and ROD groups, with the ROP group showing differences relating to transitions from state 1 and state 3. The comparison of state in-degree, the total number of transitions into each state, between groups revealed only a few significant differences. Transitions into state 1 were less common in ROD than in ROP patients, transitions into state 2 more common. The in-degree of state 3 was similar between HC and CHR individuals, as well as between ROP and ROD patients, but exhibited significant differences in all comparisons between those two sets of groups.

2.2.4 Association between dynamic functional connectivity and clinical characteristics

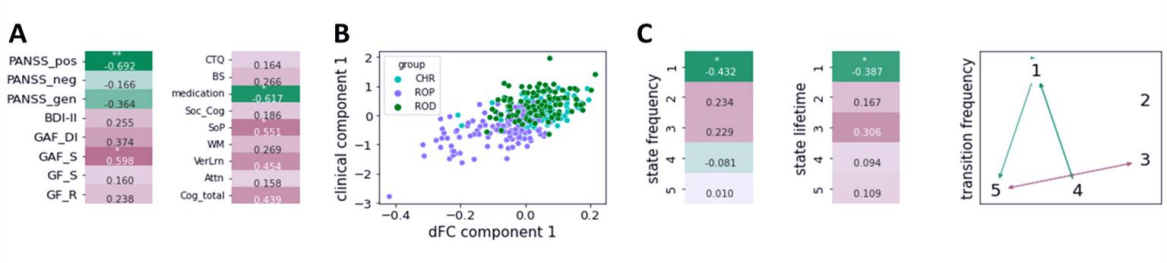

Figure 6: CCA component with significantly correlating canonical variables.

A Loadings of clinical features. B Clinical and dFC variables of the first component. C Loadings of dFC features. Stars represent significant loadings before and after Bonferroni correction for multiple comparisons (- p < 0.05, ** - p < 0.0029). The transitions displayed passed the significance threshold (p < 0.05). Colours indicate loadings, with positive loadings displayed in red and negative loadings in green.*

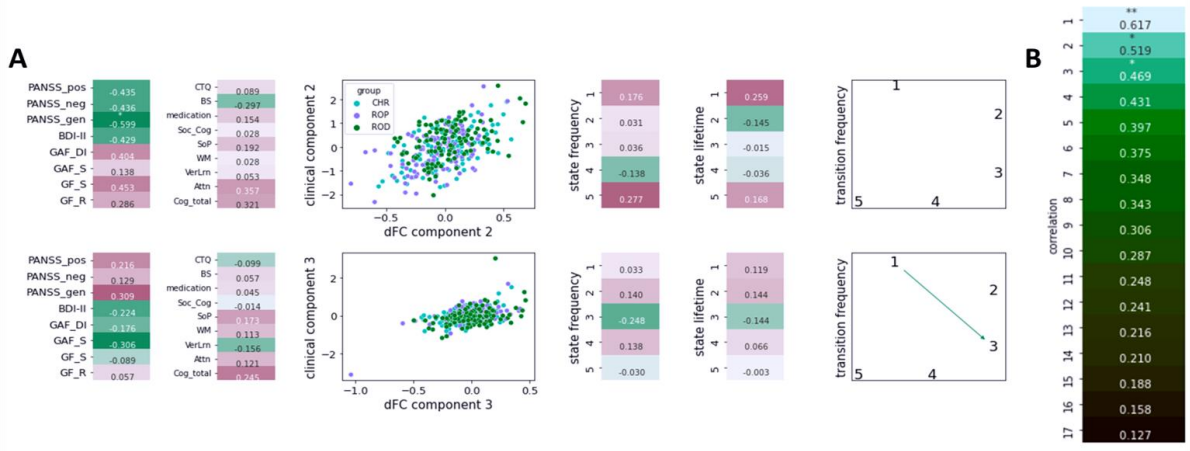

Figure 7: Exploration of additional CCA components.

A Loadings and variable values of CCA components with significantly correlating canonical variables before but not after correction for multiple comparisons. B Correlation of dFC and clinical variables for all components. Stars represent significant loadings before and after Bonferroni correction for multiple comparisons (- p < 0.05, ** - p < 0.0029). The transitions*

displayed passed the significance threshold ($p < 0.05$). Colours indicate loadings, with positive loadings displayed in red and negative loadings in green.

A single set of significantly associated canonical variables was identified by CCA (Figure 6). The clinical variable, the linear combination of features including demographic, clinical and cognitive characteristics, showed a significant loading of positive symptom severity, as well as significant loadings of medication dose, GAF Symptom score, and speed of processing, which did not survive correction for multiple comparisons. The dFC variable, combining state lifetimes, frequencies and transition frequencies, exhibited high loadings of the lifetime and frequency of state 1, as well as several state transitions. CHR and ROD patients overlap along the two dimensions, but ROP patients display lower values on both canonical variables. This distribution indicates that while the pattern of association is transdiagnostic, the identified dFC pattern reflects clinical differences between the diagnostic groups. The CCA revealed two additional sets of canonical variables which initially correlated significantly, but did not survive correction for multiple comparisons (Figure 7). For the first of these components, the PANSS general score loaded significantly on the clinical variable, while the dFC variable had no significant loadings. The second component exhibited no significant associations with its clinical variable, but the transition from state 1 to state 3 loaded significantly on the dFC variable. No distinctions between diagnostic groups were visible along either dimensions of either component.

2.2.5 Validation analyses

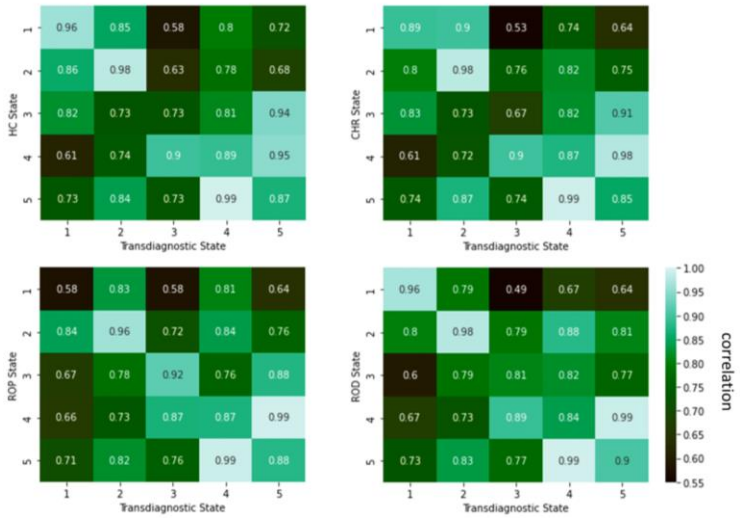

Figure 8: Overlap of states extracted via transdiagnostic and group-specific clustering.

Transdiagnostic states were identified by clustering FC features across all time points and all subjects in order to confirm which states were universal for all groups (Figure 8). Transdiagnostic states 2, 4, and 5 correlated highly with their corresponding group-derived state for each group. These states also showed high correlations between the group-derived FC patterns, indicating that they reflect recurrent FC patterns in health and disease. States 1 and 3 do not have a consistent corresponding state in all groups. Transdiagnostic state 1 exhibits high correlations with HC-, CHR-, and ROD-derived state 1, but does not have an equivalent ROP-derived state, suggesting that this FC pattern does not occur in that group. State 3, on the other hand, shows strong correlations with HC-, CHR-, and ROD-derived state 4, and ROP-derived state 3, which indicates that this state takes on a divergent form in the ROP group.

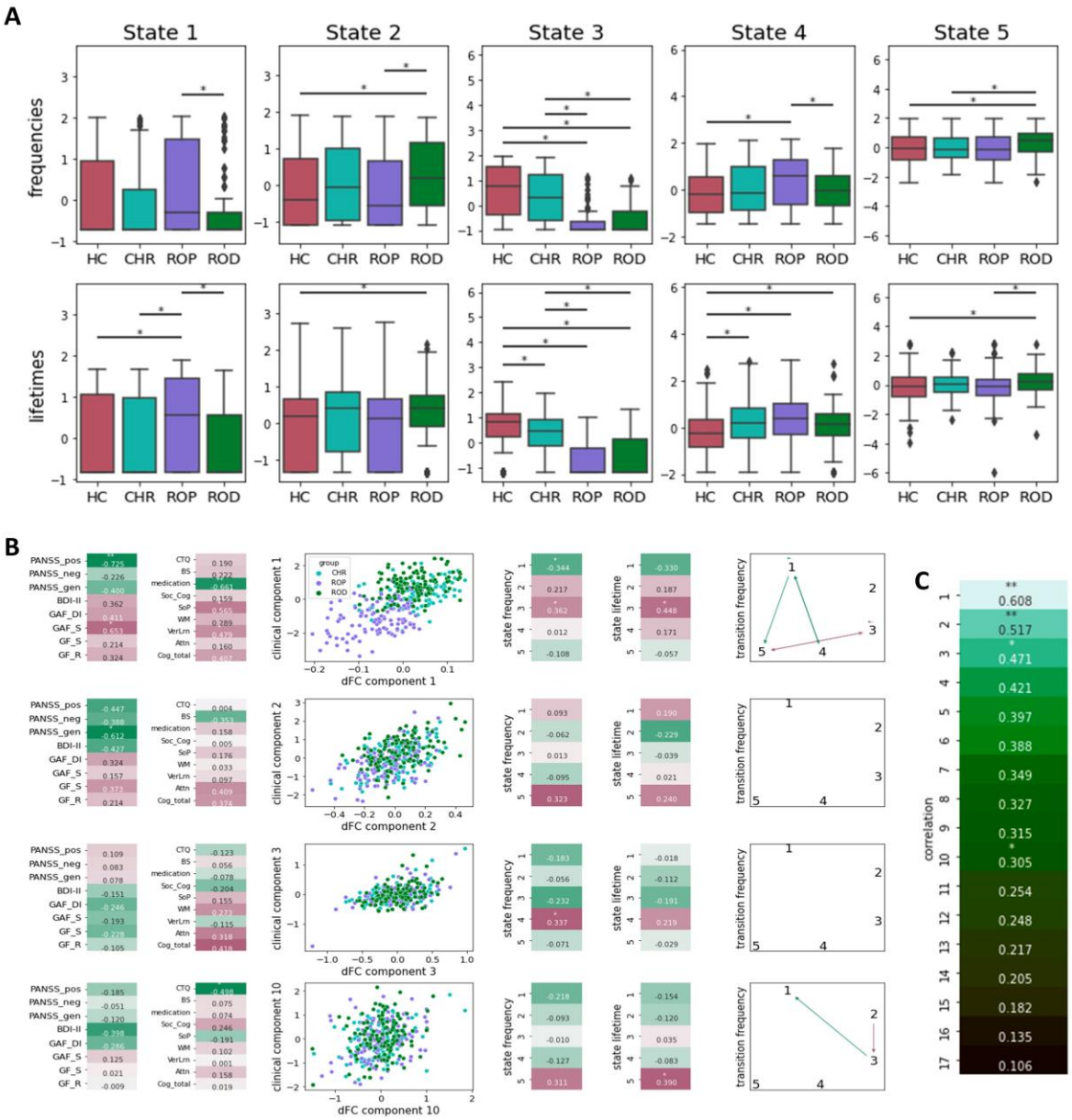

Figure 9: Repetition of the analysis without confound correction.

A Comparison of dFC parameters between study groups. Stars represent significant differences after Bonferroni correction ($p < 0.0016$). B CCA components with significantly correlating canonical variables. Stars represent significant loadings before and after Bonferroni correction for multiple comparisons (- $p < 0.05$, ** - $p < 0.0029$). The transitions displayed passed the significance threshold ($p < 0.05$). Colours indicate loadings, with positive loadings displayed in red and negative loadings in green. C Correlation of dFC and clinical*

variables for all components. Stars represent significant loadings or correlations before and after Bonferroni correction for multiple comparisons (- p < 0.05, ** - p < 0.0029).*

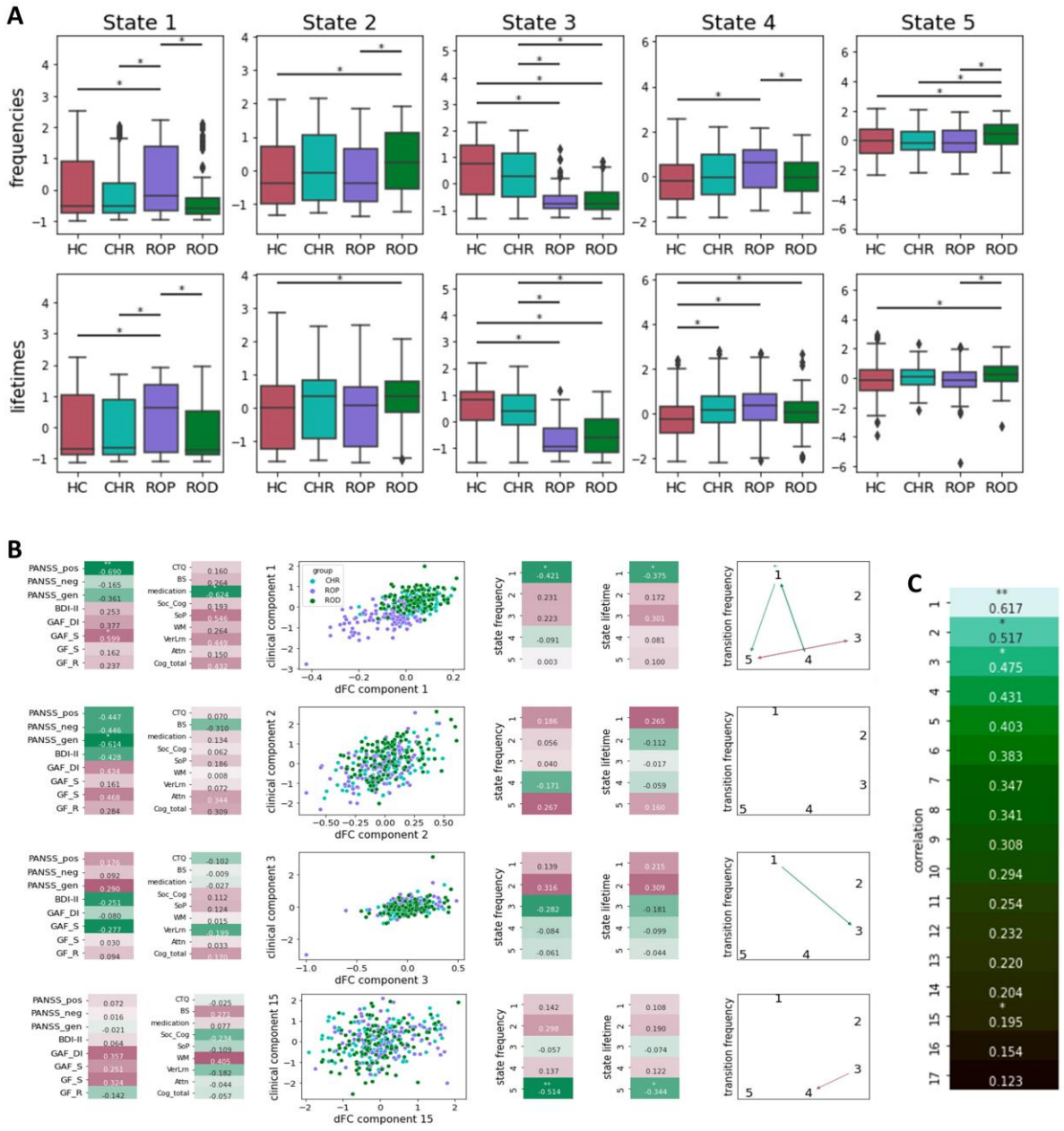

Figure 10: Repetition of the analysis without correction for motion effects.

A Comparison of dFC parameters between study groups. Stars represent significant differences after Bonferroni correction (p < 0.0016). B CCA components with significantly correlating canonical variables. The transitions displayed passed the significance threshold (p

< 0.05). Colours indicate loadings, with positive loadings displayed in red and negative loadings in green. C Correlation of dFC and clinical variables for all components. Stars represent significant loadings or correlations before and after Bonferroni correction for multiple comparisons (- p < 0.05, ** - p < 0.0029).*

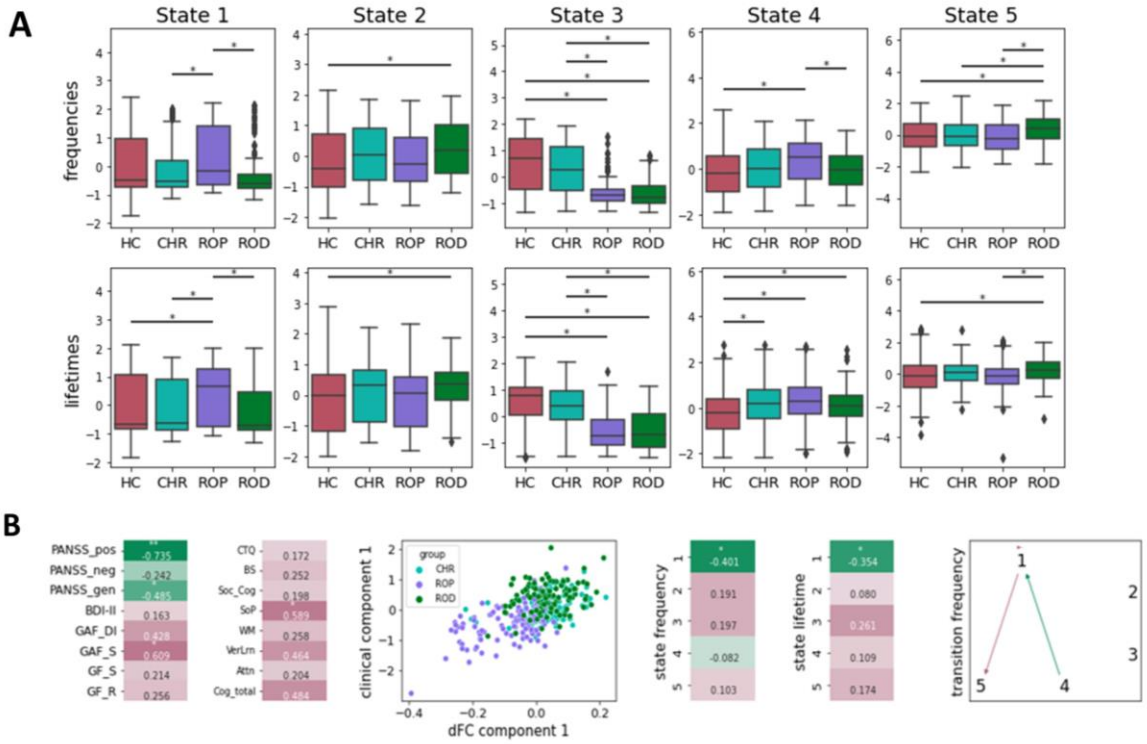

Figure 11: Repetition of the analysis without correction for medication effects.

A Comparison of dFC parameters between study groups. Stars represent significant differences after Bonferroni correction (p < 0.0016). B First component identified by CCA. Stars represent significant loadings before and after Bonferroni correction for multiple comparisons (- p < 0.05, ** - p < 0.0029). The transitions displayed passed the significance threshold (p < 0.05). Colours indicate loadings, with positive loadings displayed in red and negative loadings in green.*

Results largely remained the same across the four different preprocessing procedures, suggesting that they are reliable and not strongly influenced by confounds. Without accounting for confounds altogether, additional differences appear significant in the comparison of the lifetime of state 2 between the HC and ROD groups, and in the frequency of state 5 between the ROP and ROD groups (Figure 9A). On the other hand, the difference in the frequency of state 1 between ROP and ROD groups was only significant when confounds were removed. When motion effects were not accounted for during confound removal, the difference in the frequency of state 1 between the HC and ROP groups and the difference in the lifetime of state 2 between the HC and ROD groups were additionally significant (Figure 10A). The correction for medication effect resulted in the difference in the frequency of state 2 between the ROP and ROD groups no longer appearing significant, while the difference in the lifetime of state 2 between the HC and ROD groups achieved significance (Figure 11A). These findings indicate that the difference in the lifetime of state 2 between the HC and ROD groups should be carefully considered even though it was not significant following the standard preprocessing procedure.

The CCA also produced largely the same results regardless of preprocessing. When omitting all confound correction, the first component exhibited additional significant loadings (Figure 9B). The verbal learning score was newly associated with the clinical variable, and the dFC parameters of state 3 with the dFC variable, with the loadings appearing otherwise unchanged. The second component, which displayed a significant loading of the PANSS general score before correction for multiple comparisons, also achieved significance (Figure 9C). Removing motion as a confound did not alter the significance of the CCA components or clinical loadings (Figure 10B-C), while fewer transition frequencies load significantly on the first dFC variable when removing medication effects (Figure 11B).

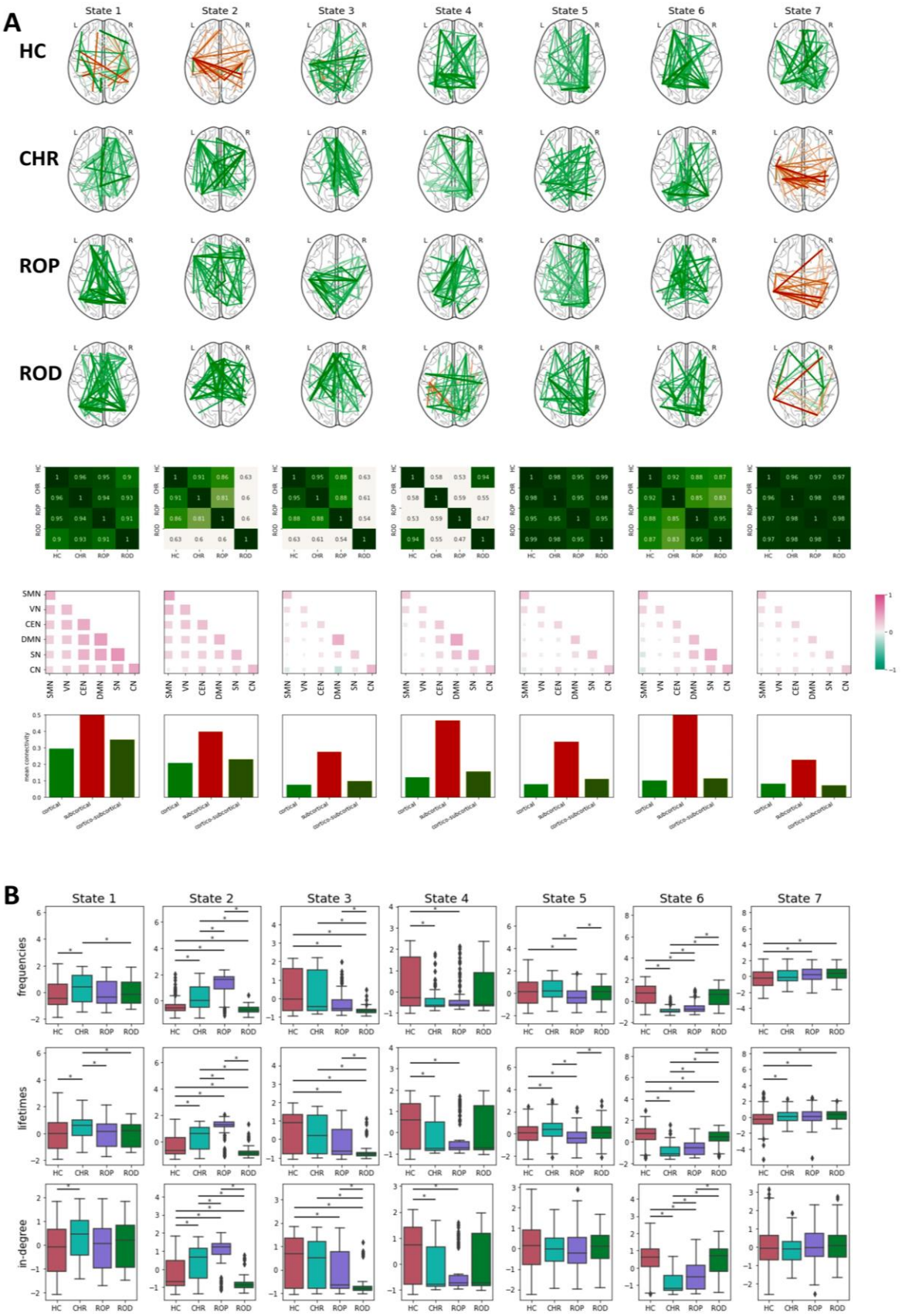

Figure 12: Repetition of dFC analysis for k=7 states.

A Connectivity patterns of seven distinct states identified by dFC analysis. Stars represent significant differences after Bonferroni correction (p < 0.0013). B Comparison of dFC parameters between study groups.

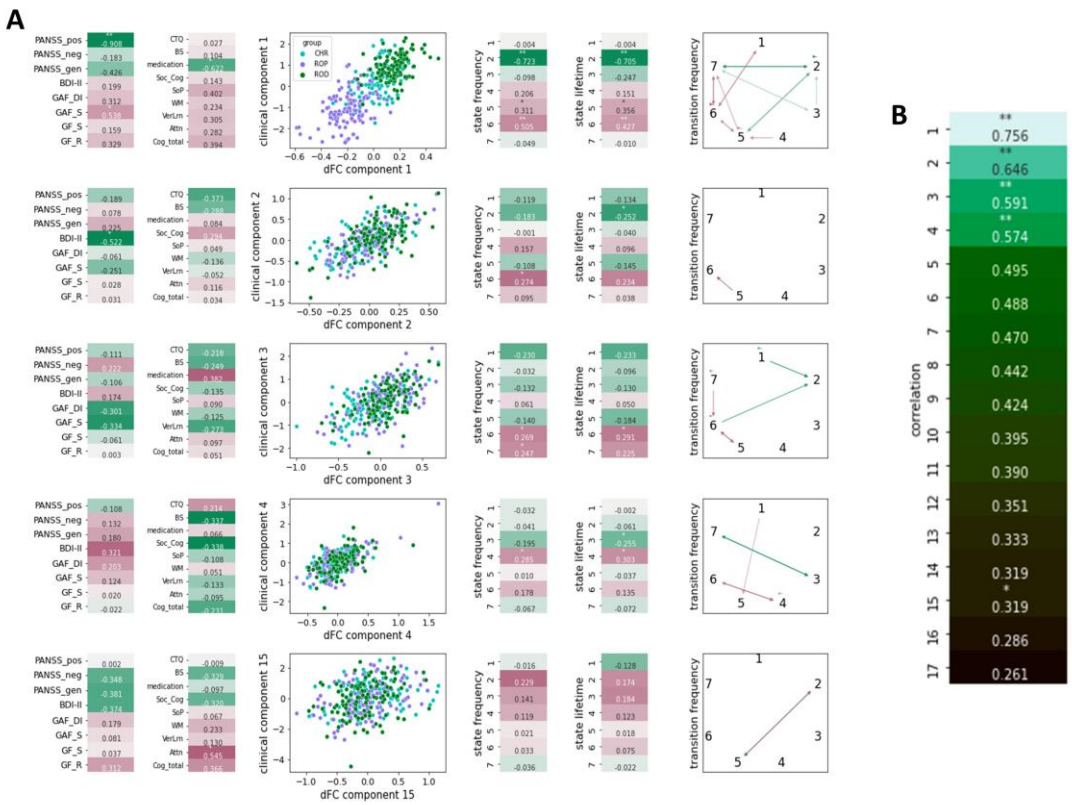

Figure 13: Repetition of CCA analysis for k=7 states.

A CCA components with significantly correlating canonical variables. The transitions displayed passed the significance threshold (p < 0.05). Colours indicate loadings, with positive loadings displayed in red and negative loadings in green. B Correlation of dFC and clinical variables for all components. Stars represent significant loadings or correlations before and after Bonferroni correction for multiple comparisons (- p < 0.05, ** - p < 0.0029).*

Five of the seven states of the k = 7 partition model matched one of the five states in the original partition model, but states 2 and 6 could not be assigned to a corresponding state in the five-state clustering solution (Figure 12). The seven-state equivalents of states 2, 4 and 5 exhibited high consistencies between the groups, just as the five-state FC patterns did. While both clustering solutions exhibit some specific differences that are not present or not significant in the other solution, particularly relating to the CHR and ROP groups, several significant differences, particularly between the HC and ROD groups, were consistent across the partition models. The CCA revealed a significantly correlated set of variables, with the PANSS positive scale and medication dose loading significantly on the clinical variable, matching the five-state results (Figure 13). Several dFC features exhibited significant loadings on the dFC variable which were not present in the five-state model. In addition, three further significant components were detected. While all of them showed some significant dFC loadings before correction, only the second component had a strong clinical loading, the depressive symptom severity, which did not survive correction for multiple comparisons.

3. Study II

This study investigated the contribution of neurobiological characteristics to individual variability in static and dynamic functional connectivity. Static FC has long been considered a useful phenotype for investigating brain function in health and disease (van den Heuvel & Hulshoff Pol, 2010), but increasing amounts of evidence show that dynamic FC is equally indicative of behavioural and clinical variables, and can capture variation between individuals that is not apparent from FC (Hutchison et al., 2013). However, the neurobiological mechanisms shaping both static and dynamic FC remain unclear. Studying the effect of disturbances in neurophysiological parameters on both measures could further elucidate causal relationships between neurobiology and FC, and provide insights into potential origins of FC alterations in brain disorders.

Brain network modelling allows for the inference of neurocomputational mechanisms from MRI data by optimising biologically relevant model parameters to replicate empirical FC as accurately as possible (Schirner et al., 2018). These optimal parameter values can be considered to describe physiological characteristics of an individual's brain. In particular, the modelling approach employed in this study enables us to extract information about the balance between excitatory and inhibitory signalling, and the global integration of activity of each participant (Sanz-Leon et al., 2015). Such models have proven to be powerful tools for the investigation of relationships between brain structure, physiology, and function (Meier et al., 2022; Proix et al., 2018; Schirner et al., 2018; Zimmermann et al., 2018). However, most current research focuses on static FC in model fitting and analysis. By optimising models for dynamic FC, and analysing the effect of both natural variation and targeted manipulation of neurophysiological parameters on dynamic as well as static FC, we can elucidate processes contributing to static and dynamic FC and differentiate between them.

Given these considerations, the study investigated the following hypotheses:

a) Heterogeneity in optimal model parameters and fits is related to individual variability in empirical static and dynamic FC patterns
b) Optimal model parameters and fits can be predicted from empirical static and dynamic FC patterns
c) Altering the coupling parameter of each region independently produces specific alterations in simulated static and dynamic FC patterns

Please note that the methods and results presented here are related to the following published experimental study:

Linnea Hoheisel, Hannah Hacker, Gereon R Fink, Silvia Daun, Joseph Kambeitz (2024). **Computational modelling reveals neurobiological contributions to static and dynamic functional connectivity patterns**, bioRxiv 2024.10.01.614888; doi: https://doi.org/10.1101/2024.10.01.614888

3.1 Methods

3.1.1 Data acquisition and preprocessing

The simulations were performed based on structural and resting-state functional MRI data of 200 healthy subjects from the Human Connectome Project (HCP) S1200 release (Van Essen et al., 2013). MRI scans were acquired on a 3T Siemens Magnetom Connectom (Siemens; Munich, Germany) scanner. The functional data consisted of four scans for each subject, with scans of two phase-encoding directions acquired on two separate days. Each scan consisted of 1200 volumes with a repetition time of 720 ms. In addition, a T1-weighted structural scan and a diffusion-weighted scan were provided for each subject. Scan parameters can be found in Table 4.

Scan	repetition time (TR)	echo time	flip angle	field of view	matrix size	slice thickness	voxel size
T1	2400 ms	2.14 ms	8 °	224 x 224 x 180 mm^3	320 x 320 x 256	0.7 mm	0.7 x 0.7 x 0.7 mm^3
BOLD	720 ms	33.1 ms	52 °	208 x 180 x 144 mm^3	104 x 90 x 72	2 mm	2 x 2 x 2 mm^3
dw	5520 ms	89.5 ms	78 °	210 x 180 x 139 mm^3	168 x 144 x 111	1.25 mm	1.25 x 1.25 x 1.25 mm^3

Table 4: Scan parameters of MRI images included in the HCP data set (Glasser et al., 2013; Smith et al., 2013; Sotiropoulos et al., 2013).

Preprocessing was performed by Domhof et al. (Domhof et al., 2021, 2022b, 2022a). SC matrices were extracted from diffusion-weighted images in four steps. Initial preprocessing included bias field correction, motion correction, eddy current distortion correction, registration to T1 images, and tissue segmentation. Whole-brain tractography was computed with a multi-

shell-multi-tissue constrained algorithm for spherical deconvolution. The images were then transformed from standard space into the native space of each subject, and the number of connections and their average length for each pair of regions determined.

Preprocessed and denoised fMRI volumes were obtained from the HCP and parcellated time courses extracted by Domhof et al. (Domhof et al., 2021, 2022a). The HCP preprocessing pipelines consisted of removal of spatial distortions, realignment of volumes to account for head motion, registration of the fMRI to structural images, bias field reduction, normalisation of the 4D image to a global mean, masking of the images, smoothing and transformation to a standard space (Glasser et al., 2013). The denoising step was performed using the ICA-FIX pipeline (Griffanti et al., 2014; Salimi-Khorshidi et al., 2014), which performs independent component analysis (ICA) decomposition of the fMRI signal into a set of components, which were then classified as noise or relevant signal by a machine learning algorithm. The components determined to be noise were then removed, providing an effective removal of artifacts despite minimal loss of signal.

We selected the SC and fMRI time courses provided in the Desikan-Killiany parcellation (Desikan et al., 2006) for our analyses. This atlas delineates 70 cortical regions of interest based on anatomical landmarks.

3.1.2 Brain Network Modelling

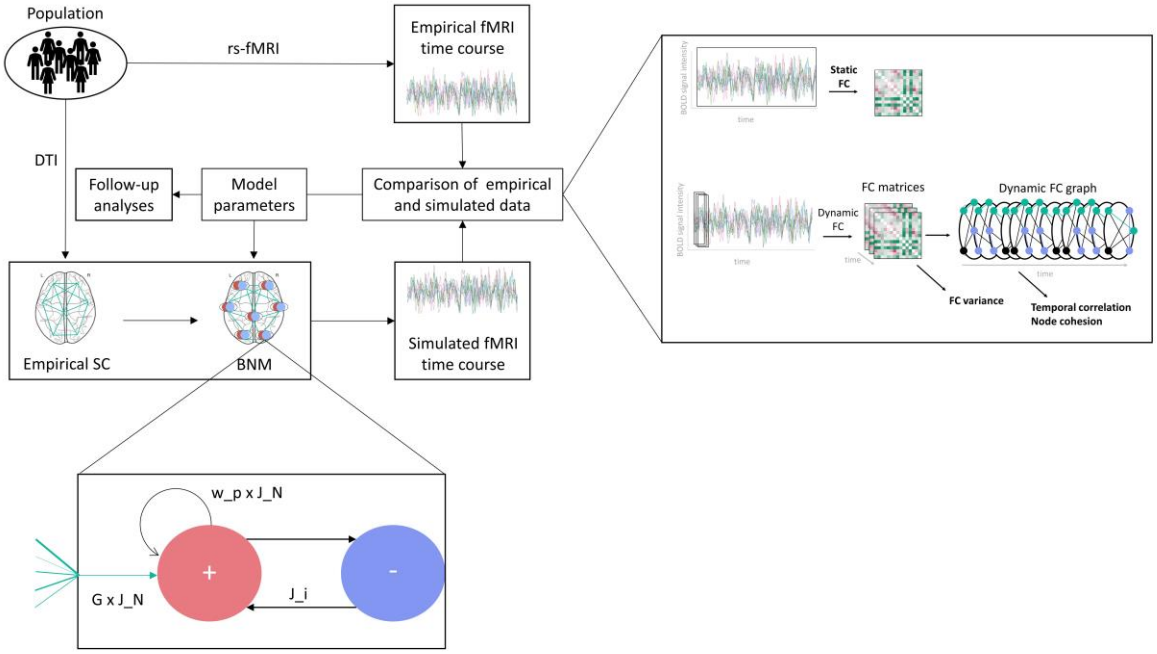

Figure 14: Schematic representation of computational modelling workflow.

Figure 14 shows an overview of the modelling approach. Models reproducing whole-brain activity rely on the underlying empirical SC, which connects regions that each exhibit specific activity patterns (Sanz-Leon et al., 2015). A set of parameters govern the balance between different populations of neurons that make up each region. The neuronal activity in each region is then translated into a simulated fMRI time course. Here, a dynamic mean field model, the reduced Wong-Wang model with excitatory and inhibitory components (Deco et al., 2014), was used to simulate regional activity based on the interaction of an excitatory and an inhibitory neuronal population in each region. A set of nonlinear differential equations describe the behaviour of these populations and produce a time course of each area's average synaptic activity and firing rates. Model equations are detailed in the appendix. The evolution of regional activity over time is driven by three types of input: i) long-range excitatory inputs from regions across the brain, controlled by the SC, the global coupling parameter G, and the local excitatory synaptic coupling J_N, ii) regional inhibitory currents, controlled by the local feedback inhibitory synaptic coupling J_i, and iii) recurrent excitation, controlled by the local

excitatory recurrence w_p and the local excitatory synaptic coupling J_N. Simulations were produced using a parameter space consisting of values for G, J_N, J_i and w_p.

All simulations were performed based on the mean white matter tract weights and lengths across all subjects in the HCP sample, constituting an average SC. The two matrices underwent a transformation consisting of removal of the median and scaling to the interquartile range, which is more robust to outliers than regular normalisation based on mean and standard deviation. Matrix entries were additionally rounded to integers. The implementation of the model supplied by the Virtual Brain toolbox (Sanz Leon et al., 2013) was used to perform the simulations. Table 5 shows all simulation settings.

Before simulating data that matched experimental conditions, an exploratory analysis was conducted to limit the parameters space. For each 101 coupling values distributed equally between 0 and 10, an interval was identified for the parameters J_N, J_i and w_p which produced models demonstrating bistable behaviour. In this range, the model can attain two states, or patterns of synaptic excitability, which are both stable, meaning the model can remain in either state, but can also alternate between them. In the absence of noise, a bistable model converges to a high state if the initial conditions are closer to that pattern, and a low state if they tend in the other direction. When we add noise to the model, the model visits both stable states, oscillating between them over time. This represents biologically plausible behaviour. As a result, only the parameters under which the model achieves bistability can produce simulated data that is reasonably close to empirical fMRI data. By restricting our further parameter exploration to this range, we can limit the amount of computing time necessary.

For each value of G, deterministic, i.e. noise-free, simulations were produced based on initial conditions close to either the high state, consisting of strong activity across all regions, or close to the low state, consisting of low activity. Simulations were set to last 10 seconds. Deco et al. (Deco et al., 2014) identified biologically reasonable ranges for J_N, J_i and w_p, from which

five equally distributed values were selected for each parameter, yielding a total of 250 simulations. The simulations produced a time course of the state variable S_i, which represents the average synaptic gating, or excitability, in each region. For both high and low initial conditions, the highest S_i value at the end of the simulation was identified, and the difference between maximal S_i reached for the two conditions was determined for each combination of parameters. Parameter sets exhibiting as S_i difference larger than 0.2, suggesting that the model converges to different states based on the initial conditions, and therefore exhibiting bistable behaviour, were selected for further analysis. An absence of such sets in the initial test interval indicated that the sampling rate of the parameters was too low, and the relevant range of parameters was smaller than the difference between the values used for the simulations. In these cases, models with parameter values below a certain threshold would converge to a low state, while those with higher values would converge to a high state, regardless of initial conditions. The relevant parameters range could be found in the interval between parameters in which the models switched from low-state convergence to high-state convergence.

For the next iteration, we thus selected the largest value still yielding low-state convergence and the lowest value yielding high-state convergence at low initial conditions for each of the three parameters of interest J_N, J_i and w_p by identifying values for which the maximal S_i of simulations using the low initial condition changed the most. The parameter exploration was then repeated using five evenly distributed values in this new interval. This procedure was repeated until at least one parameter combination resulted in a difference in maximal S_i between high and low initial conditions that exceeded 0.2, indicating that a bistable range had been identified. The range of parameter sets which exhibited bistable behaviour at each value of G was then selected as the relevant parameter space for further analysis

Full simulations were generated for 1000 combinations of values in the bistable range of each of the 101 values of G, using 10 equally distributed values for each of the three parameters J_N, J_i and w_p in the bistability, yielding a total of 101000 simulations. The simulations

produced time courses of 10000 seconds, approximately 17 minutes, of excitatory synaptic activity in each of the 70 regions present in the SC. A BOLD fMRI signal was then obtained from this data with the Balloon-Windkessel hemodynamic model (Buxton et al., 1998; Friston et al., 2003; Mandeville et al., 1999). This method assumes that an increase in neuronal activity in a brain region leads to an increase in vasodilation, which raises blood volume and alters blood deoxyhemoglobin content, producing a change in BOLD signal. This interaction is modelled using a set of equations linking blood flow, blood volume dynamics, and BOLD contrast. For each subject, the empirical FC was compared to the FC of the simulated time courses generated to determine the parameter combination which optimally reproduced that individual's brain activity.

stage	monitor	period	integrator	Integration step	length	I_0	G	J_N	J_i	w_p
parameter exploration	Temporal Average	1	EulerDeterministic	0.2	10^4 ms	0.3	start = 0 stop = 10 step = 0.1	start = 0.001 stop = 0.5 step = 0.1	start = 0.001 stop = 2 step = 0.4	start = 0 stop = 2 step = 0.4
simulation	Bold	2000	EulerStochastic	1	10^7 ms	0.3	start = 0 stop = 10 step = 0.1	Dependent on G	Dependent on G	Dependent on G
perturbation	Bold	2000	EulerStochastic	1	10^7 ms	0.3	1.4	0.5	2.0	0.67

Table 5: Simulation settings.

3.1.3 Calculation of FC measures

A set of static and dynamic FC measures was computed to evaluate the models. In order to describe meaningful and distinct characteristics of dynamic FC, three metrics were selected (Barber et al., 2021; Sizemore & Bassett, 2018): FC variance (FCV), temporal correlation (TC),

and node cohesion (NC). FC variance represents the amount of variability in the correlation between the activity of different brain regions over time. TC denotes the stability of each region's set of neighbours over time, measuring the abruptness of changes in connectivity pattern. NC signifies the number of times a pair of regions switches communities of nodes together. Pairs of regions with high NC are likely to contribute to the same networks and processes. To determine the static FC, the Pearson correlation between the time courses of each pair of regions was computed, resulting in a 70x70 matrix for each subject. The matrices were normalised with Fisher's z-transformation (Hotelling, 1953).

The first step in the computation of the dynamic FC parameters was the calculation of transient FC in 60 s windows. These windows were convolved with a Gaussian kernel of σ = 6 s and overlapped by 2 s, resulting in a 70x70x420 matrix for each subject (Leonardi & Van De Ville, 2015). The variance of the FC of each pair of regions over all windows yielded the FCV. The FC time course was then turned into a binary matrix, with the top 10 % of FC values represented as ones, and all other values as zeros. From this matrix, a dynamic graph was constructed whose edges changed over time. The temporal correlation of the dynamic graph was represented in a vector of 70 elements. After identifying communities of frequently connected nodes using the tnetwork python library (Cazabet et al., 2021, 2023) in the dynamic graph, the node cohesion was computed, another matrix of 70x70 elements. Static and dynamic FC values were computed separately in both fMRI scans from the first scanning session of the HCP data set, and averaged for further analysis. As one of the scans was acquired using left-right and the other right-left phase encoding, averaging the two reduces the effects of artefacts caused by the phase encoding direction (Van Essen et al., 2013).

The Pearson correlation between simulated and empirical data was computed for each of these metrics. As sFC, FC variance and NC were represented as symmetric matrices, only their upper triangulars were considered. Given that our aim was to identify models that reproduced both empirical static and dynamic FC, optimal models were selected according to a combined metric taking into account both sFC and TC using the global criterion method with

the l2-norm. The four models that achieved optimal fits on the individual metrics for each subject were also evaluated to analyse the comparative size of the fits for the combined metric. The fits for each metric were compared across the five optimal models. In order to validate the results obtained, the identification of optimal models and the subsequent analyses were repeated for the second fMRI session acquired as part of the HCP data set. Unless otherwise specified, the model fits and parameters used below are those belonging to the model which performed best according to the combined metric for the first fMRI session of each subject.

3.1.4 Correlation of fits and parameters with brain-derived features

In order to investigate whether FC patterns determine model fits, and to what extent variation in model parameters relate to individual differences in FC, we analysed the association between FC features and both parameters and fits. Pearson correlations were calculated between each of the eight model outcomes, including the four parameters and the four fit values according to the different metrics, and the static and dynamic connectivity features of each region or pair of regions, consisting of the sFC of 2415 region pairs and the TC of 70 regions, across the 200 subjects in our sample. In addition, we determined the correlation of model outcomes with 24 dynamic characteristics of regional BOLD time courses (Lubba et al., 2019) (listed in Supplementary Table 4) and 96 behavioural measures provided as part of the HCP data set (listed in Supplementary Table 5) The statistical significance of the correlations was determined using permutation testing. For each comparison, the values of the relevant model outcome variable were shuffled across all subjects, and the correlation recomputed. This was repeated 100000 times, yielding a null distribution of correlation values. P-values were adjusted for multiple comparisons using the false discovery rate (FDR). The values were aggregated for each of the seven canonical RSNs described by Yeo et al. (B. T. T. Yeo et al., 2011) to facilitate interpretation and visualisation.

In addition to investigating univariate associations of model outcomes and static and dynamic FC, we analysed whether larger FC patterns were predictive of model fits and parameters. Prediction models were built using the ridge regression algorithm. For each of the eight targets, four parameters and four fits, and each of the two sets of features, the sFC in all pairs of regions and the TC in all regions, a prediction model was generated, yielding a total of 16 prediction models. Preprocessing for the machine learning task consisted of scaling using a standard scaler and transformation via principal component analysis (PCA) (Maćkiewicz & Ratajczak, 1993). The PCA transforms the data to a new coordinate system of principal components which capture a descending amount of the variation in the data. Since the sFC feature set consists of 2415 pairs of regions, any prediction model taking into account the entire set is at risk of being overfitted, fitting too closely to the training data and not generalising well to unseen data, especially given the comparatively small number of subjects. As a result, only those transformed features which together explain more than 90 % of the variance in the data were kept for the machine learning analysis. The TC feature set only contains 70 features, one for each region, rendering dimensionality reduction unnecessary. To make the preprocessing comparable across the sFC-feature and TC-feature prediction models, PCA was nonetheless applied to the latter, but all components were kept.

The ridge regression models were fitted by searching a range of 100 values distributed on a logarithmic scale between 0.01 and 100 for the optimal value for alpha. A nested cross-validation (CV) approach was employed for hyperparameter estimation and evaluation of the prediction models (Varma & Simon, 2006). This technique allows for hyperparameter search and model evaluation to be performed on completely unseen data, ensuring that the calculated generalisability of the prediction performance is not biased due to hyperparameters that do not generalise. The data set was split into five outer folds, with four making up the training and one the test set. The training set was further split into five inner folds, again assigned to test and training sets. Scaling and PCA were performed independently on each training and test set to prevent information leakage. For each alpha value, a prediction model was fitted to the

training set and its prediction performance evaluated on the test set. This was repeated using each of the five folds as the test set, and the remaining folds as the training set. Then, the subjects were shuffled and five new folds formed, with prediction models trained and tested on each of them in turn. The alpha value which produced the highest prediction performances in the test sets across the 10 iterations was selected for evaluation in the outer CV. A regression model using this optimal alpha value was trained on the outer training set, and its prediction performance evaluated on the outer test set. Again, this process was repeated for all five folds of two permutations, and the mean overall test performance computed. Prediction performances were estimated using the coefficient of determination R^2, which represents the proportion of variance of the target variable that is explained by the prediction.

Furthermore, the contribution of each static and dynamic FC feature, or feature importance, to the prediction of each target variable was calculated (Breiman, 2001). A prediction model was trained on the entire data set using a single round of CV with five folds and two permutations and the prediction performance computed. Each feature was then permuted 1000 times, and a model trained and evaluated on the resulting data set under the same conditions. Shuffling the values of a feature removes any association between that feature and the target, rendering the feature uninformative without changing the number of features, which might alter prediction performance due to a lower risk of overfitting. The average reduction in prediction performance was computed for each feature, representing the feature importance. For sFC-feature models, the average importance of FCs between one region and all other regions was calculated, providing one importance value for each region. Feature importances were also aggregated for each RSN to improve interpretability and visualisability of the results.

3.1.5 Region-wise perturbation of parameters

We analysed the effects of changes in regional coupling on overall static and dynamic FC using a perturbation approach. The global coupling G was specifically altered in each individual region, with the G of all other regions remaining constant. The resulting changes in FC were analysed to determine in which regions G values had the greatest impact on FC, and in which they determined biological accuracy of FC most strongly. An average sFC matrix and a TC vector were produced by taking the mean of the 200 subjects in the HCP sample. The optimal parameters for this average FC based on the combined metric were then used as the default in our analyses. 7070 simulations were generated based on these default parameters, with the G value of each region in turn varied in a range of 101 values equally distributed between 0 and 10. The sFC, TC and global efficiency were determined for each of the simulations. The efficiency denotes the mean inverse shortest path length between each pair of regions, representing a measure for the ease with which information is exchanged within a network (Latora & Marchiori, 2001). The difference in sFC, TC and efficiency, as well as in the sFC and TC fit, were estimated between each of the simulated time courses resulting from the perturbations and the simulated time course produced by the default values. The sFC and TC differences were estimated using the cosine distance. These perturbation-related changes were then compared with graph properties, dynamic characteristics, and gene expression across brain regions in order to elucidate the role of regions in which alterations in coupling impact FC strongest in the establishment of brain connectivity.

The mean and variance of the sFC fit difference, TC fit difference and efficiency difference were correlated with a) graph metrics, including measures of the centrality and degree of SC weights, SC lengths, and mean FC and b) expression values of 15653 genes provided by the Allen brain atlas (Hawrylycz et al., 2012; Markello et al., 2021). Statistical significance of the correlations was estimated by permutation testing. In order to account for the spatial autocorrelation of the brain maps, null distributions of the permutation-induced differences were generated via spin-testing, rotating regional values across the surface of the brain, rather

than random shuffling (Alexander-Bloch et al., 2018) using the neuromaps python toolbox (Markello et al., 2022). The lists of genes which correlated significantly ($p < 0.05$, uncorrected) in their expression with the perturbation-induced differences were then compared to sets of genes identified as related to specific biological processes in the Gene Ontology database (Consortium, 2004) using the MetaScape (Y. Zhou et al., 2019) platform. Processes whose associated genes were significantly overrepresented in the lists associated with perturbation-induced differences were extracted, with clustering serving to combine redundant terms. This functional enrichment of genes allowed for the consideration of biological processes significantly associated with regions showing greater perturbation effects.

3.2 Results

3.2.1 Model Evaluation

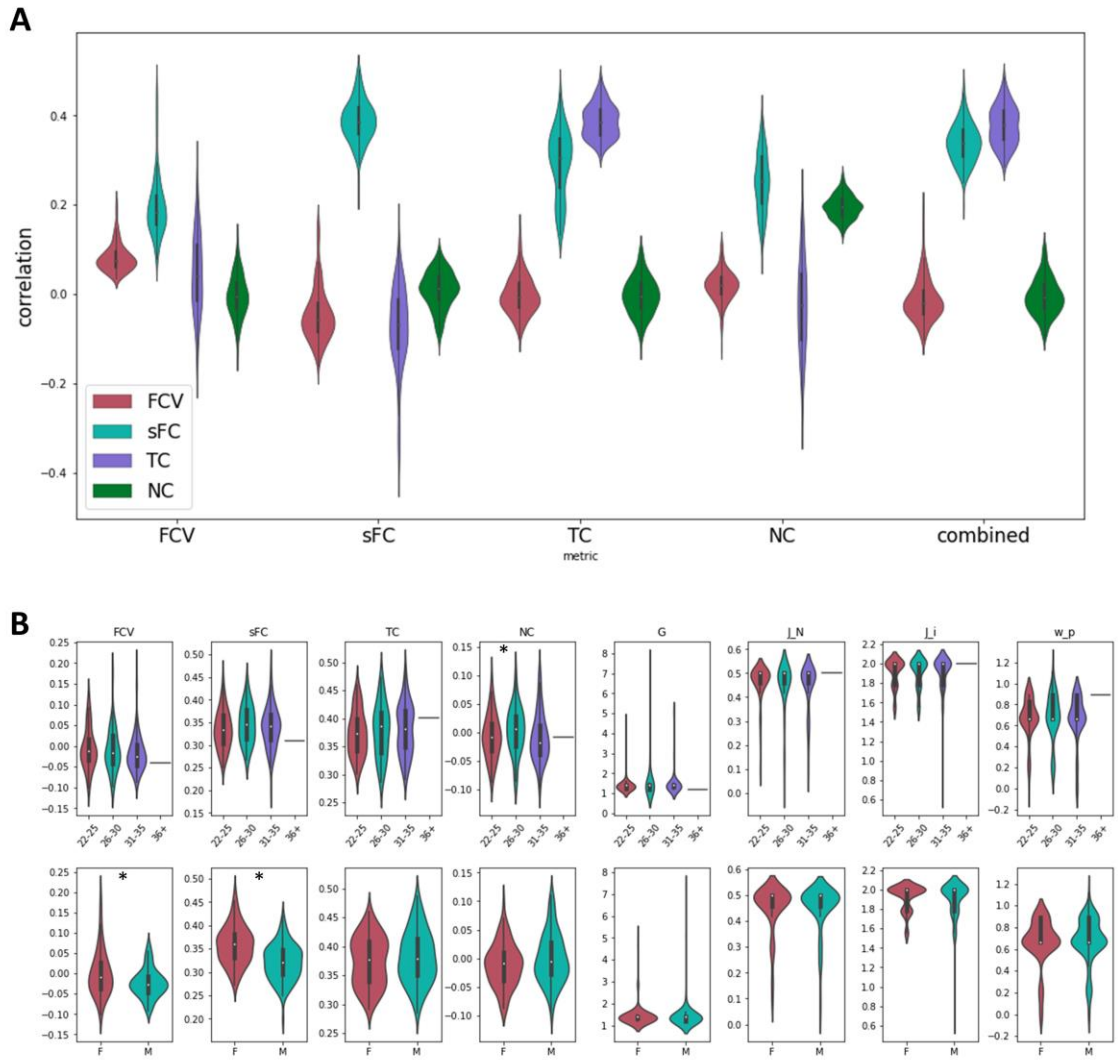

Figure 15: Outcomes of optimal simulations.

A Model fits on each of the four metrics (colours) of solutions optimised for each of the four metrics and the combined metric of sFC and TC (x-axis). B Analysis of covariate effects on parameters and fits of models optimised for the combined metric. Stars indicate significant differences ($p < 0.05$).

The optimal correlations produced between empirical and simulated sFC (r = 0.389, σ = 0.037) and TC (r = 0.388, σ = 0.046) were strong; however, we were less successful in replicating FCV (r = 0.082, σ = 0.032) and NC (r = 0.196, σ = 0.026) (Figure 15). Model optimisation based on sFC or TC produced high scores on the respective metric, but considerably lower scores on the other three metrics. When using the combined metric, which considered both sFC and TC fit, for optimisation, we achieved satisfactory fits for these two metrics, although there was notable variability in individual results. All models, even those optimised for FCV and NC failed to yield high correlations on these metrics. Models optimised for the combined metric produced average fits for sFC and TC of 0.339 (σ = 0.044) and 0.378 (σ = 0.044), respectively. We observed significant differences in sFC and FCV fits between male and female participants (p(sFC) < 0.001, p(FCV) = 0.003). NC fit varied significantly between the 22-25 and 26-30 age groups (p = 0.039). No other participant groups differed significantly in any other fits or parameters.

3.2.2 Association of model fits and parameters with FC features

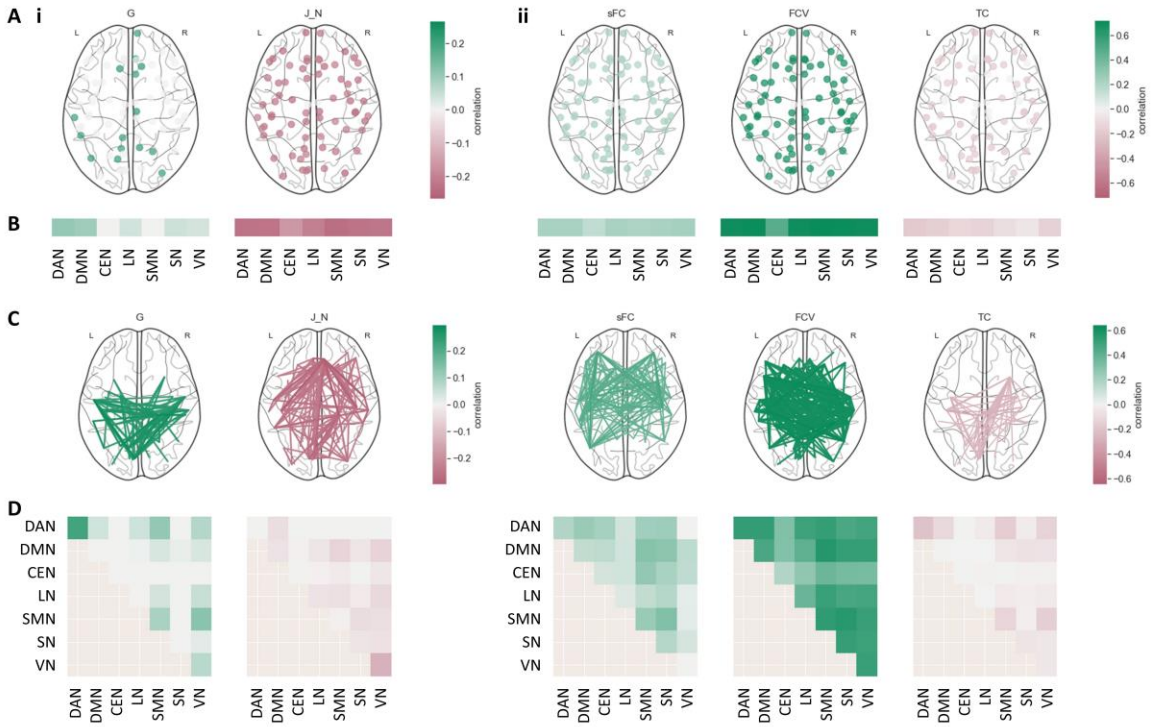

Figure 16: Relationship of model outcomes with static and dynamic FC features.

A Correlation of TC with i) optimal model parameters and ii) optimal fits. Only correlations above the significance threshold ($p_{FDR} < 0.05$) are shown. B Average correlation of TC with i) parameters and ii) fits for each resting-state network. Correlations below the significance threshold ($p_{FDR} >= 0.05$) were assigned a value of 0. C Correlation of sFC with i) parameters. and ii) fits. Only the strongest 30% of correlations above the significance threshold ($p_{FDR} < 0.05$) are shown. D Average correlation of sFC with i) parameters and ii) fits within and between resting-state networks. Correlations below the significance threshold ($p_{FDR} >= 0.05$) were assigned a value of 0. DAN: dorsal attention network, DMN: default mode network, CEN: central executive network, LN: limbic network, SMN: somatomotor network, SN: salience network, VN: visual network.

The optimal values of the model parameters G and J_N, derived for each participant based on the combined metric considering both static and dynamic FC, correlated significantly with sFC between and TC within several brain regions (Figure 16i). Specifically, the global coupling parameter G exhibited a strong positive relationship with the static and dynamic FC measures, while the excitatory synaptic coupling parameter J_N showed a negative correlation. G was most strongly correlated with sFC in connections within the DAN, and between the SMN and both the DAN and the VN. In contrast, J_N exhibited its strongest correlations with the sFC within the VN and in connections linking the CEN with the SMN and VN. TC in the DAN and DMN correlated most strongly with G, while TC in the DAN, DMN, and SMN exhibited strong correlations with J_N. No significant relationships were found between the feedback inhibitory synaptic coupling parameter J_i or the excitatory recurrence parameter w_p and either sFC or TC in any regions after correction for multiple comparisons. These results suggest that individual variations in certain patterns of static and dynamic FC are related to G and J_N, but not J_i or w_p.

The fit between simulated and empirical data, based on the sFC, FCV and TC also correlated strongly with TC and sFC in several regions (Figure 16ii). Participants with stronger sFC exhibited higher sFC and FCV fits. sFC in connections between the CEN and SMN was particularly strongly associated with sFC fit. Similarly, sFC in connections between the default mode network (DMN) and SMN was positively correlated with FCV fit. On the other hand, TC fit was negatively correlated with many sFC features, particularly those involving the DAN, SMN, and VN. The sFC and FC variance fits were positively associated with TC in all regions except the CEN, whereas the TC fit showed strong negative associations with TC, particularly in the DAN, DMN, limbic network (LN) and VN. Notably, NC fit did not show any significant correlation with sFC or TC in any regions, suggesting that individual patterns of static and dynamic FC influence sFC, FC variance, and TC fits, but not NC fit.

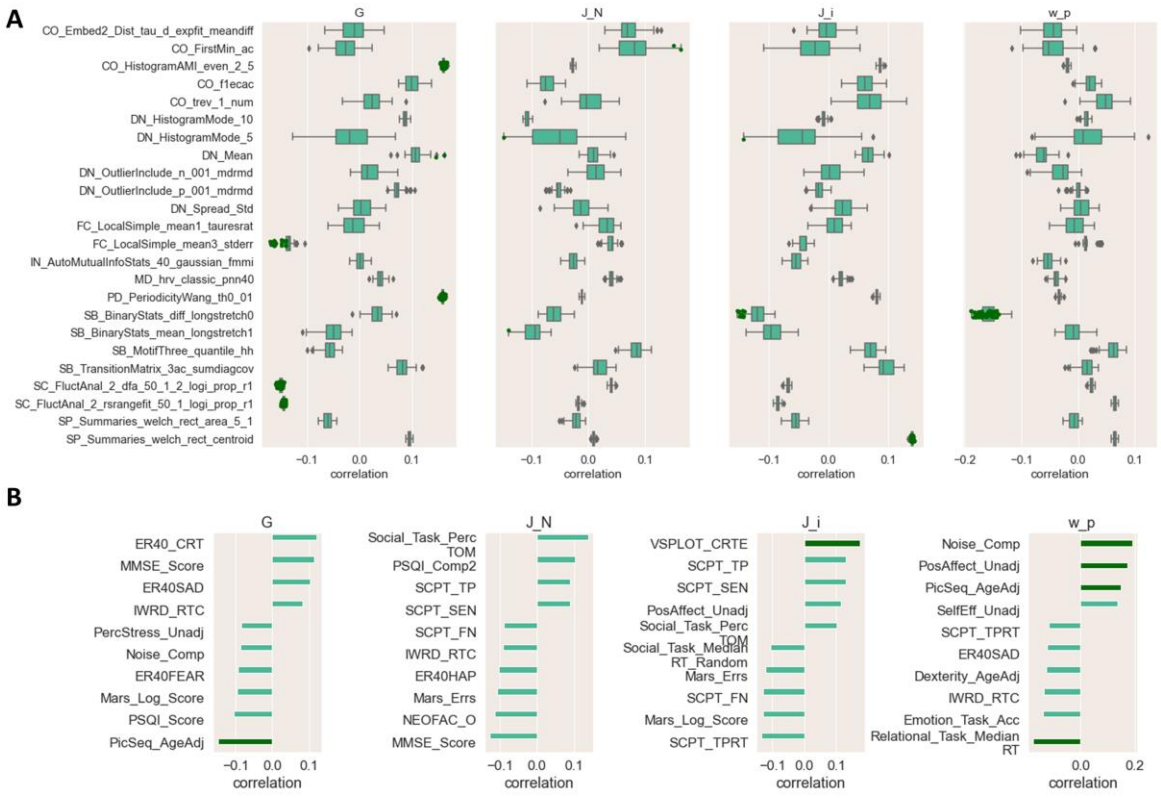

Figure 17: Association of optimal model parameters with brain dynamics and behavioural features.

A Correlation between optimal model parameters and characteristics of dynamic activity across all regional time courses. Regions for which the association is significant ($p_{uncorrected} < 0.05$) are plotted as green dots over the box plot. B Correlation between behavioural measures and parameters. Only the top 10% of absolute correlations are displayed. Light green regions are not significant, dark green regions are significant before FDR correction ($p_{uncorrected} < 0.05$). None of the initially significant correlations survive correction for multiple comparisons.

Significant correlations could be identified between model parameters and several dynamic features observed in the empirical fMRI time courses of various regions (Figure 17A). Specifically, G showed strong associations with the mean error derived from a rolling 3-sample mean forecast, as well as with automutual information (m=2, tau=5), the periodicity metric proposed by (X. Wang et al., 2007), and the proportion of slower timescale fluctuations consistent with detrended fluctuation analysis using 50% sampling. W_p exhibited a strong relationship with the longest sequence of successive incremental decreases across all regions. In contrast, correlations between J_N and J_i and these dynamic features were only significant in a few specific regions. The model parameters correlated only moderately with behavioural scores, with the highest correlation of 0.2 observed between w_p and performance on the Words-in-Noise Test, a measure of auditory function (Figure 17B). Although several of the associations between model parameters and dynamic characteristics as well as behavioural measures initially appeared significant, they did not withstand correction for multiple comparisons.

3.2.3 Prediction of model fits and parameters based on FC features

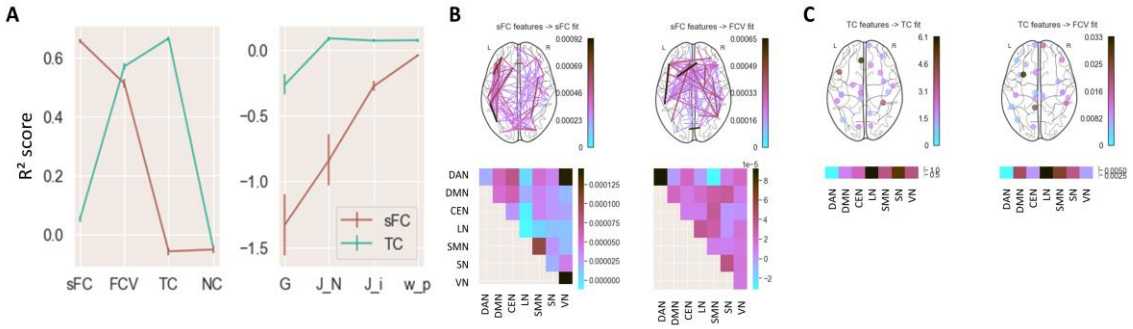

Figure 18: Estimation of individual fits and parameters based on sFC and TC.

A Average R² score produced by models predicting optimal fits and parameter values using either the sFC matrix or the TC vector as features. Error bars indicate the standard error of the mean R² score averaged over all folds and permutations of the outer CV. A baseline model predicting the average target value for each individual would receive an R² score of 0, with higher scores indicating better prediction performance. B Feature importance of TC, with only the 30% of regions with the highest importance presented. C Average feature importance of TC aggregated within each RSN. D Feature importance of sFC, with only the 5% of connections with the highest importance presented. E Feature importance of sFC aggregated within and between RSNs. Feature importance analysis was only conducted for models with an R² score of 0.25 or higher.

DAN: dorsal attention network, DMN: default mode network, CEN: central executive network, LN: limbic network, SMN: somatomotor network, SN: salience network, VN: visual network.

Patterns of TC and sFC features were able to predict some of the model fits with satisfactory accuracy. The correlation between empirical and simulated FCV was predicted with an R² value exceeding 0.5 (Figure 18A) by models using either the dynamic or the static FC as features. Models using sFC values as features could accurately predict sFC fit but not TC fit,

while models using TC values as features were able to predict TC fit, but not sFC fit. Neither model performed well in predicting the NC fit. For the model parameters, TC was the more effective predictor, but neither set of models achieved high R^2 scores. The scores obtained for J_N, J_i and w_p by the TC-based models were close to 0, with the score for G below 0. An R^2 score of 0 matches that of a constant model, predicting the mean target value for all participants irrespective of feature input, suggesting that the features could not predict the target accurately in the test data. sFC-based model predictions underperformed compared to a constant model for all parameter targets.

For models that achieved a high R^2 score, feature importance analysis was performed to identify key connections which were particularly predictive of the outcomes (Figure 18B-E). FCV fit exhibited the strongest relationship with the TC in the left temporal pole and left isthmus cingulate, as well as sFC in a broader network of regions. sFC in regions of the VN, SMN, and the connections between the VN and DAN were especially predictive of sFC fit. The TC within the LN and SN had a significant influence on TC fit, with the left medial orbitofrontal gyrus, left pars opercularis, and right fusiform gyrus the areas showing the greatest importance for the prediction.

3.2.4 Effects of perturbation of regional coupling on FC

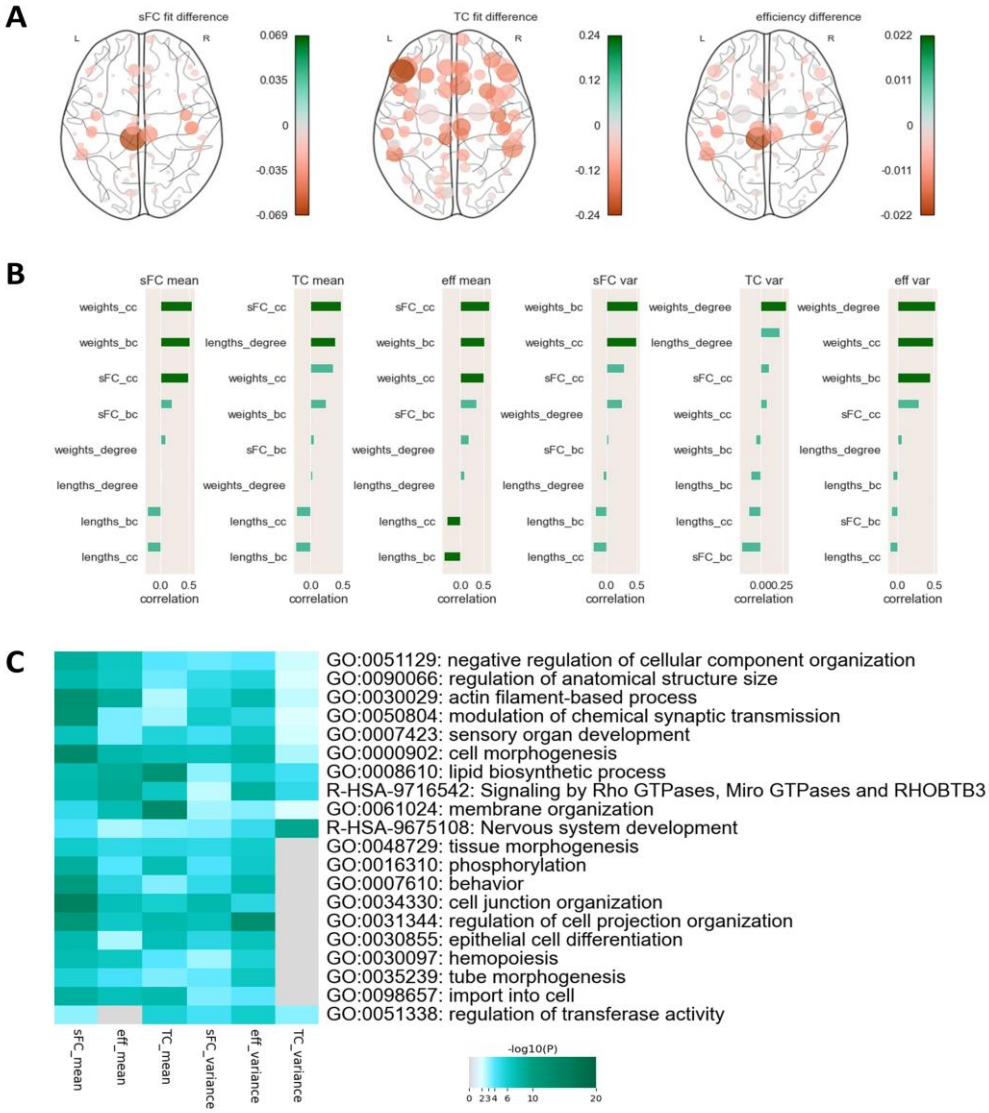

Figure 19: Alterations produced by perturbing regional coupling parameters.

A Changes in sFC fit, TC fit, and FC efficiency induced by the manipulation of G in each region. Average alteration across all G values is indicated by node colours, the variance of alterations by node sizes. B Correlation between mean and variance of perturbation-related changes and graph parameters. Features which did not correlate significantly are represented by light green bars, features which exhibited significant correlations before FDR correction ($p_{uncorrected} < 0.05$) are represented by dark green bars. C 10 biological processes which were most significantly

represented in the lists of genes which exhibited significant correlations ($p_{uncorrected} < 0.05$) with mean and variance of alterations produced by regional perturbation.

bc: betweenness centrality, cc: closeness centrality.

Perturbation analysis showed that altering the coupling in most regions resulted in a decrease in model fit and efficiency (Figure 19A). Nevertheless, the influence exerted by certain regions on overall network connectivity was greater than that of others. Perturbations in some regions even lead to slight improvements in fit and increases in efficiency. The perturbation-induced changes were strongest in the left and right paracentral gyri, right pre- and postcentral gyri, and right transverse temporal gyrus. Perturbations in the right medial orbitofrontal gyrus were found to enhance the sFC fit. The TC fit was affected more by the perturbations than the sFC fit and efficiency. Alterations in the left pars triangularis lead to a reduction in TC fit, whereas improvements in TC fit were observed after perturbation in the left inferior temporal gyrus. The impact on fit and efficiency in some of the regions varied substantially based on the degree of perturbation. In particular, perturbations in the left paracentral gyrus resulted in considerable variance in sFC fit and efficiency, while the TC fit was most sensitive to changes in the left pars triangularis and left pars orbitalis.

The six outcomes we derived from the perturbation analysis, the mean and variance of the sFC fit difference, the TC fit difference, and the efficiency difference, exhibited high correlations with graph parameters of the mean empirical sFC and SC matrices (Figure 19B). The mean and variance of the sFC fit difference and the efficiency difference were associated with betweenness centrality and closeness centrality of the SC weights. The average of the TC fit difference showed strong correlations with the closeness centrality of the sFC and the degree of SC lengths, while its variance had a strong relationship with the degree of SC weights. Regions which produced greater changes in global static and dynamic FC through the perturbation of their coupling exhibited stronger connections within the network. While the

association between network structure and perturbation-induced changes was strong, the comparison between perturbation outcomes and the dynamic characteristics of regional fMRI time courses produced lower correlation values.

The analysis of gene expression maps revealed strong correlations with all six outcome metrics of the perturbation analysis, and the identified genes were enriched to uncover several relevant biological processes (Figure 19C). The biological pathways associated with the mean of the sFC fit, TC fit, and efficiency differences, as well as with the variance of sFC fit and efficiency differences, were largely overlapping. These pathways included processes relevant to brain function, such as nervous system development, modulation of chemical synapse transmission, and behaviour. In contrast, the variance of the TC fit differences was linked to a more limited set of pathways. This pattern suggests that while the same biological processes that are involved in maintaining accurate global static and dynamic FC are associated with variability in static FC, not all of them are relevant in regions in which perturbation has an outsized effect on dynamic FC.

3.2.5 Validation analysis

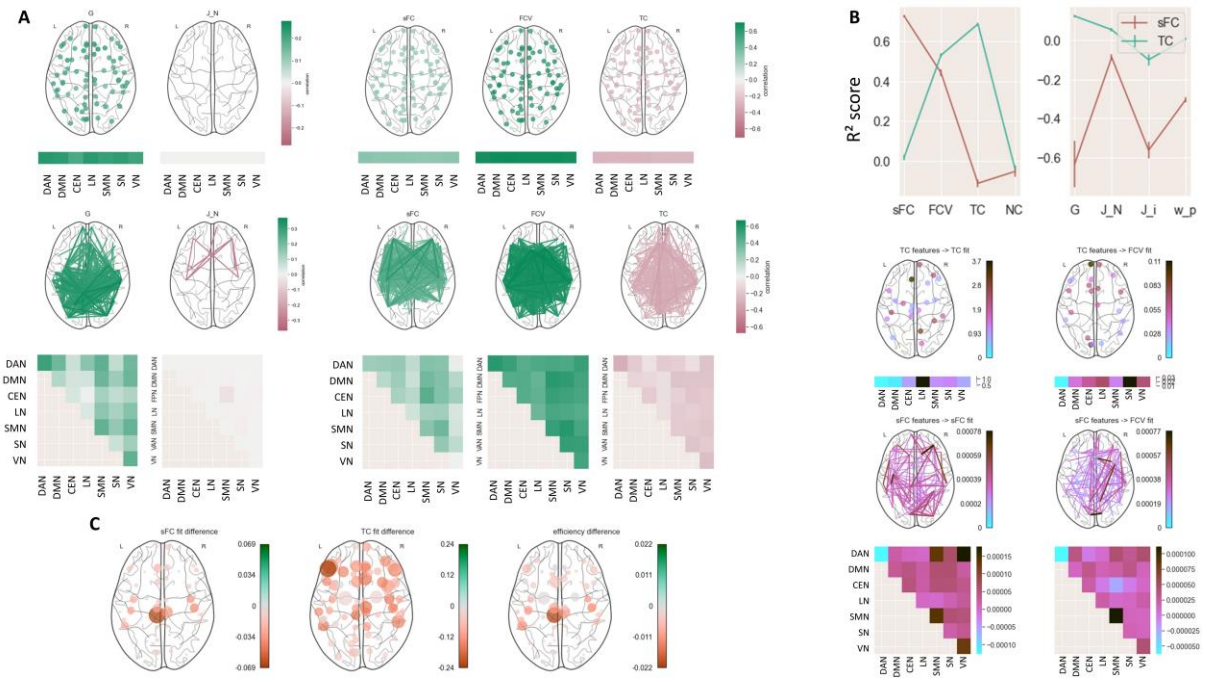

Figure 20: Replication of results in data from each subject's second scanning session.

A Replication of results of correlation analysis between FC patterns and fits and parameters. B Replication results of prediction of fits and parameters from FC patterns. C Replication of results of perturbation analysis.

The validation analysis conducted using the data of the second fMRI scanning session of each participant available in the HCP data set largely replicated the results of our initial analyses (Figure 20). The sFC and TC correlates of G, sFC fit, and FCV fit identified in the second session in particular matched those of the first session. Some additional connections showed significant correlations in their sFC with the optimal J_N in the second session that were not present in the first. However, not all significant associations between sFC and TC fit were preserved in the second session, and some regions did not exhibit the significant relationships in their TC with G that were detected in the first session. The machine learning models achieved matching prediction scores in the first and second sessions, with the accuracy in the prediction of sFC fit, TC fit and FCV fit preserved. The feature importance for these predictions exhibited similar patterns in both sessions, although the importance of sFC features for the prediction of FCV fit showed some changes. The coupling in the same areas was identified to have particularly large effects on the global static and dynamic FC in the second scans as in the first.

4. Study III

This study investigated neurobiological differences in patients with psychotic and affective disorders using computational modelling. While differences in static and dynamic FC have been well established in both conditions (Cattarinussi et al., 2023; Dong et al., 2018; Mulders et al., 2015; Sun et al., 2024), the processes underlying these abnormalities remain to be fully elucidated. In both disorders, neurobiological changes to global coupling and excitation-inhibition balance have been observed and linked to symptoms (Anticevic & Lisman, 2017; Hu et al., 2023; Jauhar et al., 2023; McCutcheon, Krystal, et al., 2020). However, it is still unclear how these mechanisms interact to produce shared and unique pathologies and symptoms. Using brain network modelling, we can infer individual neurobiological characteristics non-invasively from fMRI data (Schirner et al., 2018). Differences in the model-derived optimal parameters between patients and controls could provide new insights into the mechanisms underlying pathological alterations in static and dynamic FC, and potentially constitute novel biomarkers of psychiatric disorders. In light of the overlap in clinical characteristics (Conley et al., 2007; Ohayon & Schatzberg, 2002; Upthegrove et al., 2017) and FC alterations between psychotic and affective patients (Goodkind et al., 2015), comparing model-derived neurobiology between those patient groups could also provide information about common and unique mechanisms of psychiatric conditions. In addition, the analysis of optimal parameters in patients at clinical high risk for psychosis could reveal early signs of psychosis-related dysfunction.

Research in patients with epilepsy and Alzheimer's disease has demonstrated the utility of brain network models for understanding neurobiological abnormalities in brain disorders (H. E. Wang et al., 2023; Zimmermann et al., 2018). However, only a small number of computational modelling studies have been conducted in patients with psychiatric disorders, with evidence from affective patients and high-risk individuals particularly scarce. In addition, the findings of study II showed that optimising models for both static and dynamic FC allows for the identification of neurobiological characteristics underlying heterogeneity in both

measures. Thus, modelling static and dynamic FC enables us to investigate common and unique mechanisms contributing to pathological changes and individual variability of both measures in patients, providing a more comprehensive insight into the origins of abnormalities in brain connectivity.

Given these considerations, this study investigated the following hypotheses:

a) Neurobiological characteristics represented by optimal model parameters differ between patients and healthy controls
b) Neurobiological characteristics represented by optimal model parameters differ between patient groups

4.1 Methods

4.1.1 Data acquisition and preprocessing

For this study, we again utilised data from the PRONIA cohort. In contrast to study I, we initially considered the full sample in this analysis. Inclusion and exclusion criteria, data acquisition procedures, and preprocessing steps are detailed in sections 2.1.1 - 2.1.3. From the preprocessed brain volumes, we obtained regional BOLD time courses using the Desikan-Killiany parcellation (Desikan et al., 2006). We then calculated the sFC and TC for each individual according to the process outlined in section 3.1.3, using a window size of 30, an offset of 1 TR, and a σ of 3. We harmonised these four metrics across participants from different sites using the ComBat method (J. Fortin & Robert-Fitzgerald, 2018; J.-P. Fortin et al., 2018; Johnson et al., 2007). This technique assumes that relevant sources of variability affect the FC across regions or pairs of regions in similar ways, and pools the variance across FC features to provide robust confound removal while preserving both biologically relevant variance and the network structure of the FC. We selected the site as the batch variable whose effect should be removed, and provided age, sex and group as variables whose variance should be retained. The data acquired in Munich was chosen as the reference batch, as it included the largest number of participants. In order to maximise the validity of the harmonisation, we excluded individuals who were missing values in the age, sex, group and site variables. We also excluded individuals recruited in Bari, as the sample size was very low, and in Milan, as the MRI data was acquired at a different field strength at that site.

4.1.2 Brain network modelling

The brain network models were constructed according to the methodology detailed in section 3.1.2. We again used the reduced Wong-Wang model with excitatory and inhibitory populations to model regional activity, optimising the global coupling parameter G, the excitatory synaptic coupling parameter J_N, the inhibitory synaptic coupling parameter J_i,

and the excitatory recurrence parameter w_p. The regional models were integrated via the empirical group-averaged tract lengths and weights extracted from the HCP data. We explored the reduced parameter space provided by the bifurcation analysis performed in study II. However, instead of using a grid search to identify the optimal values for the three parameters governing excitation-inhibition balance, J_N, J_i, and w_p, simulating fMRI data for parameters spaced at fixed intervals, we employed a random grid search, selecting all three parameter values at random from their bifurcation range. This approach provides better coverage of the parameter space, as each of the three regional parameters takes on 1000 different values, one for each parameter combination, rather than only 10 different values, one at each fixed point. Table 6 shows the simulation specifications. We identified optimal model parameters based on sFC and TC fit using multi-objective optimisation as outlined in section 3.1.3.

stage	monitor	period	integrator	integration step	length	I_0	G	J_N	J_i	w_p
parameter exploration	Temporal Average	1	EulerDeterministic	0.2	10^4 ms	0.3	start = 0 stop = 10 step = 0.1	start = 0.001 stop = 0.5 step = 0.1	start = 0.001 stop = 3.0 step = 0.6	start = 0 stop = 2 step = 0.4
simulation	Bold	2000	EulerStochastic	1	10^7 ms	0.3	start = 0 stop = 10 step = 0.1	Dependent on G, random choice	Dependent on G, random choice	Dependent on G, random choice

Table 6: Simulation settings.

4.1.3 Comparison of model outcomes between patient groups

In order to isolate transdiagnostic and diagnosis-specific alterations, model outcomes were compared between the four subject groups. Differences in optimal parameters and fits were

assessed using Mann-Whitney U-tests. The association between covariates and model outcomes was determined to identify potential confounding effects. For continuous covariates, the Spearman correlation between each covariate and each outcome measure was calculated. For categorical covariates, the mean of each outcome measure was compared between all levels of the covariate using Mann-Whitney U-tests.

4.2 Results

4.2.1 Sample description

							HC v CHR		HC v ROP		HC v ROD		CHR v ROP		CHR v ROD		ROP v ROD	
	HC	CHR	ROP	ROD	χ^2/t-value	p-value	χ^2	p-value	χ^2	p-value	χ^2	p-value	χ^2	p-value	χ^2	p-value	χ^2	p-value
Subjects, n	356	216	217	196	-	-	-	-	-	-	-	-	-	-	-	-	-	-
Gender, male/female	148/208	103/113	129/88	86/110	18.462	< 0.001	1.799	0.180	16.540	< 0.001	0.189	0.664	5.557	0.018	0.456	0.499	9.388	0.002
Age, mean (sd)	27.8 (6.4)	25.9 (5.4)	27.9 (5.7)	28.3 (6.4)	20.067	< 0.001	45212.5	< 0.001	37960.5	0.729	33494.5	0.437	18540.5	< 0.001	16568.5	< 0.001	20781.5	0.689
Medication (daily dose in CPZE), mean (sd)	0.0 (0.0)	27.5 (79.2)	389.5 (1114.9)	29.3 (121.8)	365.282	< 0.001	29726.0	< 0.001	13350.0	< 0.001	29192.0	< 0.001	11174.0	< 0.001	22545.0	< 0.001	32924.5	< 0.001
PANSS positive scale, mean (sd)	-	11.7 (3.7)	19.1 (5.8)	8.5 (2.5)	332.929	< 0.001	-	-	-	-	-	-	6158.0	< 0.001	31104.0	< 0.001	37804.0	< 0.001
PANSS negative scale, mean (sd)	-	14.0 (8.0)	15.8 (10.6)	13.1 (7.7)	12.275	0.002	-	-	-	-	-	-	18719.5	0.009	20564.5	0.530	23572.5	0.001
PANSS general scale, mean (sd)	-	29.2 (6.7)	34.7 (7.5)	28.1 (5.3)	52.480	< 0.001	-	-	-	-	-	-	14705.0	< 0.001	20916.0	0.198	27268.0	< 0.001
BDI-II, mean (sd)	3.1 (4.6)	25.1 (11.5)	19.8 (11.2)	24.6 (12.3)	517.929	< 0.001	2605.5	< 0.001	4434.0	< 0.001	2047.0	< 0.001	22132.0	< 0.001	17455.5	0.400	12472.5	0.001
GAF Disability/ Impairment, mean (sd)	85.5 (6.0)	52.5 (13.1)	44.4 (13.3)	54.5 (14.7)	666.443	< 0.001	74989.5	< 0.001	75595.0	< 0.001	67709.5	< 0.001	31677.0	< 0.001	19002.5	0.101	12167.5	< 0.001
GAF Symptoms, mean (sd)	86.6 (6.0)	51.6 (11.2)	41.0 (14.1)	53.7 (12.8)	703.315	< 0.001	75978.0	< 0.001	75942.5	< 0.001	68177.5	< 0.001	34006.5	< 0.001	18428.5	0.034	9975.5	< 0.001

Table 7: Sample description.

CPZE: chlorpromazine equivalent units, PANSS: Positive and Negative Symptom Scale, BDI-II: Beck Depression Inventory-II, GAF: Global Assessment of Functioning

		Munich	Cologne	Basel	Udine	Birmingham	Turku	Muenster
	HC	60	64	56	72	42	51	11
	CHR	85	32	22	23	16	27	11
	ROP	87	29	25	15	14	39	8
	ROD	75	42	15	23	16	20	5
Muenster	χ^2	4.016	4.36	3.715	8.491	4.444	2.316	
	p-value	0.26	0.225	0.294	0.037	0.217	0.509	
Turku	χ^2	18.518	8.291	3.122	14.725	5.512		
	p-value	< 0.001	0.04	0.373	0.002	0.138		
Birmingham	χ^2	28.746	2.558	1.75	1.334			
	p-value	< 0.001	0.465	0.626	0.721			
Udine	χ^2	54.871	8.204	5.329				
	p-value	< 0.001	0.042	0.149				
Basel	χ^2	34.283	7.261					
	p-value	< 0.001	0.064					
Cologne	χ^2	23.111						
	p-value	< 0.001						

Table 8: Group assignment of participants at each site.

Out of the 1029 participants originally included in the sample, 22 were excluded due to missing data, and an additional 22 participants were excluded because of excessive motion during the fMRI scan. The final sample for the analysis comprised 356 HC participants, 216 CHR patients, 217 ROP patients, and 196 ROD patients (Table 7). Age and gender distributions differed significantly between some of the groups. The ROP group included a higher proportion of male participants than the HC, CHR and ROD groups ($p(\text{ROP-ROD}) = 0.002$, $p(\text{CHR-ROP}) = 0.018$, $p(\text{HC-ROP}) < 0.001$). The CHR group showed a significantly lower mean age than all other groups ($p < 0.001$). The CHR and ROD groups only differed significantly in the positive symptom subscale of the PANSS, medication dosage, and GAF symptom score, while the other groups differed significantly on all clinical scales and the medication dosage. Study

participants were recruited at seven different research centres, with the largest cohorts included in Munich (n=307) and Cologne (n=167). Additional participants were enrolled in Basel (n=118), Udine (n=133), Birmingham (n=88), Turku (n=137), and Muenster (n = 35). The number of participants included in each study group varied significantly between some research sites (Table 8).

4.2.2 Comparison of fits and parameters between groups

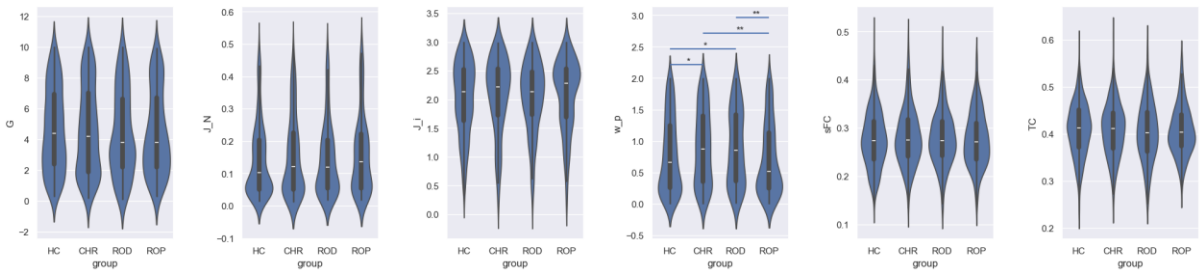

Figure 21: Comparison of model outcomes between subject groups.

Stars indicate significant differences (- $p_{uncorrected} < 0.05$, ** - $p_{FDR} < 0.05$).*

While G, J_N and J_i did not show significant differences between the groups, w_p was significantly higher in CHR and ROD patients than in HC individuals and ROP patients (Figure 21). The differences in w_p between CHR and ROP as well as between ROD and ROP were significant even after correction for multiple comparisons ($p_{FDR} < 0.013$), but the differences between CHR and HC and ROD and HC were not. The model fits were satisfactory, with a mean sFC fit of 0.278 and a mean TC fit of 0.408, although the variation between individuals was considerable. Neither the sFC fit nor the TC fit differed significantly between the groups, indicating that the comparison between groups was not biased by differences in model accuracy.

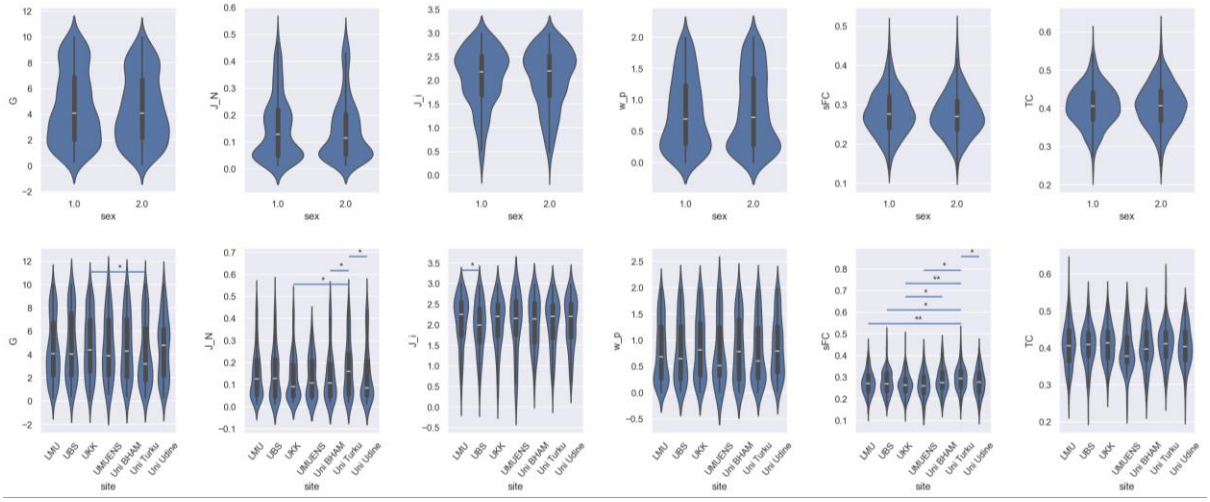

Figure 22: Association between categorical covariates and model parameters and fits.

Stars indicate significant differences (- $p_{uncorrected}$ < 0.05, ** - p_{FDR} < 0.05).*

		G	J_N	J_i	w_p	sFC	TC
age	r	-0.002	-0.002	-0.019	< 0.001	-0.033	0.024
	p-value	0.954	0.955	0.550	0.994	0.305	0.448
mean_FD	r	0.054	-0.020	0.100	-0.024	0.171	-0.045
	p-value	0.092	0.540	0.002	0.447	< 0.001	0.157
medication	r	0.105	-0.085	0.016	-0.081	0.036	-0.017
	p-value	0.116	0.206	0.810	0.226	0.592	0.801

Table 9: Association between continuous covariates and model parameters and fits.

The majority of covariates analysed did not show an association with parameter values. Motion, represented by mean framewise displacement, was significantly associated with J_i and sFC fit (Table 9), indicating that FC derived from scans with higher motion artifacts could be better replicated. The sFC of individuals recruited in Turku achieved significantly higher fits than that collected from other sites ($p_{uncorrected}$ < 0.017), with several differences remaining significant after correction for multiple comparisons (Figure 22). In addition, G, J_N, and J_i differed significantly between some sites before, but not after correction.

5. Discussion

Psychotic and affective disorders are serious and complex psychiatric conditions arising from a number of poorly understood mechanisms, including alterations in neurophysiology and brain connectivity. The objective of this PhD thesis is to contribute to the current understanding of alterations in FC and underlying neurobiological mechanisms in patients with these disorders. The three studies included in this thesis each explored a different facet of the relationship between neurobiological abnormalities and psychiatric illness via the intermediate phenotype of dynamic functional connectivity.

Study I compared dFC patterns between patients with recent-onset psychosis, recent-onset depression, and clinical high risk for psychosis, as well as healthy individuals. In addition, dynamic characteristics were associated with demographic, clinical, and cognitive variables across the patient groups. This study found evidence of alterations in dFC which were present across patient groups, as well as those which were specific to ROP and ROD patients respectively. Expression of one pattern of dFC was significantly associated with several clinical variables.

Study II used brain network modelling to examine the association of individual neurophysiology with static and dynamic FC, and tested the effect of altering regional brain activity on global FC. This study demonstrated that static and dynamic FC were strongly associated with, and predictive of, model fits. In addition, some FC patterns could be shown to be significantly correlated with neurobiological parameters, while perturbing regional models in some regions proved to have an outsized impact on FC.

Study III analysed neurobiological parameters in ROP patients, ROD patients, CHR patients and healthy individuals derived from brain network models optimised for both static and dynamic FC. This study determined that neurophysiology was significantly altered in CHR and ROD patients.

The findings of the three studies outlined here will first be discussed in detail individually, and then integrated in the context of potential mechanisms linking neurophysiology, FC, and clinical variables to describe novel insights produced by the research presented in this thesis.

5.1 Alterations of functional connectivity in psychotic and affective disorders

Study I investigated dynamic FC in CHR, ROP, and ROD patients and healthy controls. We identified a set of five recurrent FC patterns in each group, and found that this repertoire of states overlapped between the study groups. States 2, 4, and 5, which were most prevalent, were highly consistent, while the means of states 1 and 3 differed between the groups. This supports findings of previous research indicating the presence of a common set of dFC states that occurs across individuals and exhibits characteristic changes in its dynamic parameters in brain disorders (Y. Du et al., 2018; Yao et al., 2019). The size of this inventory of dFC states is still a matter of disagreement. Previous studies have identified two (Yao et al., 2019), three (Barber et al., 2018), four (Wu et al., 2019), and five (Snyder et al., 2021) recurrent FC patterns, suggesting that the optimal number of clusters is dependent on methodological choices. Some of the states identified in different studies show overlapping network architecture. In particular, several studies have identified a state characterised by low within- and between-network connectivity, which occurs with high frequency across subject groups (Damaraju et al., 2014; Schumacher et al., 2019; Yao et al., 2019). The states we obtained in our analysis proved to be highly reliable in validation analyses, and we were able to reproduce the finding of a commonly occurring, weakly connected state. The high correlation in several states between the subject groups, as well as between the first and second halves of the scans in the HC group, shows that these states could be robustly delineated in different data sets. States correlating highly with state 2, 4, and 5 were also generated when we clustered the sliding-window FC across all individuals. In addition, of the seven states produced by the k =

7 partition model, several corresponded strongly to one of the five original states, confirming that the same FC patterns could be identified irrespective of the number of clusters selected.

While the significant differences in the dynamic parameters of the less consistent states 1 and 3 represent a useful marker of dFC alterations between the groups, the information that can be gained from them is limited. On the other hand, the divergence in the architecture of rare states might itself constitute an important abnormality of brain FC in psychosis and depression. The states might represent intermediate patterns that occur during especially slow or common transitions between two other states, and reflect differences in the dynamic configuration of brain networks. These two states could also be additional states that are unique to the different groups. In that case, they might be a product of changes in neurophysiology, and might be active during pathologically altered cognitive processes. Additional analyses are necessary to investigate this phenomenon, and should involve studying state transitions at higher temporal resolution, and mapping the topography of the state space.

We observed significant differences in the dynamic parameters of several FC states between the study groups. State 4, characterised by low connectivity both within and between several networks but comparatively high connectivity in the SMN and SN, was active for significantly longer average lifetimes in all patient groups compared to the HC group. In the ROP group, this state occurred significantly more frequently than in the HC group. The ROP patients also exhibited a substantially higher transition frequency from state 5 into state 4 than individuals in the other study groups, indicating that an increase in the occurrence of this transition contributes to the higher frequency of this state in the ROP group compared to the other patient groups. While the frequency of this state was not significantly increased in CHR patients on average, this might be due to the heterogeneity of the CHR group. As an increase in state 4 frequency could prove to represent part of an early-onset pathological mechanism in psychosis, future studies should investigate whether individuals who exhibit a higher frequency are at increased risk of psychosis.

Evidence from static FC analyses indicate that increased dopamine levels lead to stronger connectivity in both the SMN and SN (Conio et al., 2020). As disruptions in dopamine signalling pathways have been shown to be an important neurophysiological marker in psychosis (McCutcheon, Krystal, et al., 2020), our findings indicate that this effect observed in the time-averaged FC might be produced by the increase in the frequency of a dFC state showing high connectivity in those networks. Future work should investigate the relationship between dopamine signalling, the dynamic synchronisation of the SMN and SN, and psychosis symptoms. The overlapping but distinct patterns of changes in the dynamic characteristics across patient groups suggest a psychosis-specific, potentially dopamine-related mechanism leading to a change in the transition behaviour, while an additional transdiagnostic mechanism causes patients to remain in this state for longer than healthy individuals. The increase in lifetime of a state with strong connectivity in the salience network, which has been hypothesised to mediate transitions between internal thought processes governed by the DMN and external thought processes governed by the CEN (Sridharan et al., 2008), might be caused by abnormal functioning within this network, and could contribute to impairments in higher-order cognitive processes observed in psychiatric disorders. The increase in the transitions into this state in ROP patients could indicate a lowered threshold for the activation of the salience network, potentially contributing to alterations in salience attribution in this disorder (Mallikarjun et al., 2018; Palaniyappan & Liddle, 2012).

State 5, which featured particularly low connectivities within and between most networks, and anticorrelations between some networks, occurred with longer lifetimes and higher frequencies in the ROD group compared to the other groups. This result is consistent with findings from previous studies, which have found a general increase in temporal stability (Demirtaş et al., 2016) which might be caused by this increased dominance of the weakly connected state. Activity of a weakly connected state has been previously linked to self-generated thought (Marusak et al., 2017), implicating an increase in the frequency and lifetime of this state in the origin of depressive symptoms such as rumination. Increased lifetimes of

this state have been previously observed in patients with depression (Yao et al., 2019), as well as in patients with Alzheimer's disease (Schumacher et al., 2019). Damaraju et al. (Damaraju et al., 2014) also identified an increase in the frequency of such a state in schizophrenia, which we were not able to replicate for the psychosis group. While this could have been the result of methodological differences or the higher heterogeneity of our sample, the behaviour of this state in schizophrenia needs to be further investigated before conclusions about its role can be drawn.

We identified a single pair of significantly correlated canonical covariates which captured a relationship between dFC and clinical characteristics in the patient groups. The dFC component was highly associated with the lifetime and frequency of state 1 and the transition frequencies between several states, while the clinical component was linked to positive psychosis symptom severity and antipsychotic medication dose. The distribution of the psychosis patients was shifted towards lower values on both dimensions compared to the ROD and CHR groups. The PANSS positive scale has previously been associated with the strength of changes in the CEN, DAN, and SMN (D. Wang et al., 2020), indicating a distributed but robust pattern of static FC correlates of psychosis symptom severity. These findings suggest that such wide-ranging symptom-related differences are also present in dFC. The association of medication dose with the clinical covariate initially indicated a potential confounding effect, as antipsychotic medication has been shown to produce alterations in FC (Abbott et al., 2013; Chopra et al., 2021). However, the link between positive psychosis symptom severity and the related dFC pattern continued to be significant even after correcting for medication dose, indicating that the difference in dFC is directly associated with symptom severity.

The fact that the CHR group shows much greater overlap with the ROD than the ROP group on the two canonical covariates, despite exhibiting significantly higher psychosis symptom severity than the ROD group in positive psychosis symptom severity, suggests that the identified dFC pattern is particularly affected in full psychosis. The distribution of patients

across the two dimensions might be the result of a psychosis-specific mechanism shifting individuals from normal variability towards a pathological change. Future work should compare the relevant dFC pattern between patients and healthy controls to determine whether it is altered from a healthy configuration in CHR and ROD patients, or only in the ROP group. The aggregation of CHR patients in a single group, rather than separate clusters, speaks against the utility of this set of dFC differences as a biomarker for transition to psychosis, although it is possible that a more complex relationship with psychosis risk could be identified.

Together, the findings from Study I indicate the presence of both diagnosis-specific and transdiagnostic alterations in dFC in psychotic and affective disorders. In addition, we identified a dFC correlate of positive psychosis symptoms across diagnoses.

5.2 Neurobiological contributions to static and dynamic FC patterns

Study II investigated brain network models of static and dynamic FC in healthy individuals. We were able to replicate sFC and TC well, obtaining reasonably high fits between simulated and empirical connectivity across individuals. Models with high sFC fit did not exhibit consistently high TC fit and vice versa, but models optimised for both metrics achieved sFC fits on par with those reported in previous literature (Klein et al., 2021; Zimmermann et al., 2018) and TC fits exceeding these. NC fit and FC variance fit were low for all individuals across all parameter combinations. The modelling approach could thus replicate some, but not all dynamic characteristics of FC. This finding should be considered in the interpretation of brain network modelling studies, and future work could focus on improving models to more comprehensively reproduce empirical dynamic FC.

While the optimal model fits were reasonably high, they exhibited significant correlations with both static and dynamic FC, showing that some individual connectivity patterns could be better simulated than others. The sFC and FCV fits were strongly positively associated with sFC and TC patterns, suggesting that these measures can be best reproduced in individuals with

integrated and stable connectomes. This is likely due to the influence of the SC on simulated activity (Sanz-Leon et al., 2015). Because activity in one area is passed onto connected areas along empirical fibre tracts, regional activity is synchronised across the brain. Using a sparser SC could improve fits for individuals with lower FC. In addition, increasing the noise added into the regional activity might produce less cohesive FC, as it would increase variability in regional activity. The sFC within and between the DAN, SN and LN correlated especially strongly with sFC fit.

TC fit was negatively associated with FC patterns across the brain, particularly in the DAN and VN, demonstrating that the model is better able to replicate the TC of less integrated and more dynamic networks. Thus, the model either cannot produce high TC, or patterns of high TC which the model produces are not biologically accurate. This phenomenon suggests the presence of a mechanism in the human brain which governs fluctuations in FC, determining which connections are more and which are less flexible, which is not included in the model specification. Together, these associations indicate that the models can reliably reproduce strong sFC patterns, but are less able to simulate the associated empirical TC, providing additional evidence for the importance of including both variables in the model fitting.

sFC and TC fit, as well as FCV fit, could be predicted from static and dynamic connectivity features. Prediction models based on sFC features performed well in the estimation of sFC and FCV fit, whereas TC features were able to predict TC and FCV fit well. For all prediction models which achieved high prediction scores, a small subset of connectivity features was particularly important for the estimation of the target. The sFC within the VN and SMN, and between the VN and VAN, contributed most strongly to the prediction of sFC fit, the TC in the left medial orbitofrontal gyrus, left pars opercularis, and right fusiform gyrus to the prediction of TC fit. The disparity in the reproducibility of individual static and dynamic FC patterns should be taken into account as a potential source of bias in future studies. If the connectivity in relevant regions or pairs of regions is statistically associated with a variable of interest, such as group affiliation or clinical scores, or a potential confounding factor, such as study centre

assignment or motion intensity, the resulting difference in the validity of optimal parameters could skew analysis outcomes.

Analysing the relationship between FC patterns and optimal model parameters, we were able to identify static and dynamic FC correlates of the global coupling parameter G and the excitatory synaptic coupling parameter J_N, suggesting that some of the individual variability in FC is related to neurobiological heterogeneity. G exhibited significant positive correlation with the FC of several regions, particularly those within and between the DAN, SMN and VN. This increase in connectivity with higher G values can be explained by the role of this parameter in scaling the contribution of external input to regional activity, with higher coupling leading to a greater integration between regions (Sanz-Leon et al., 2015). Pairs of regions which exhibit a particularly high correlation in their sFC with G likely receive similar inputs, which increasingly dominate regional activity at higher G values. G also exhibited positive correlations with the TC of several regions throughout the brain, showing that with higher coupling, FC changes are slower and less extensive over time. Presumably, this is similarly caused by the increased integration between regions, leading to the synchronisation of fluctuations in activity and thus producing strong and stable connectivity.

The association between the heterogeneity in the global coupling parameter and the variability in static and dynamic FC provides a potential explanation for the effect of neuromodulatory signalling on brain connectivity. Serotonin and dopamine receptor concentrations correlate with FC, and drugs affecting signalling pathways disturb normal FC patterns (Conio et al., 2020; Klaassens et al., 2015). These molecules can alter neuronal excitability and induce rewiring of synaptic connections in a targeted manner (Marder, 2012), which could impact global coupling, which in turn shapes FC. However, this potential mechanism is likely only a small part of the overall system linking neurophysiology and brain function, and further research is necessary to untangle this complex relationship.

J_N exhibited negative correlations with the sFC of several pairs of regions, mainly those in the VN and between the VN and DMN and most other networks, and with the TC of most brain regions. A higher J_N leads to stronger excitatory signalling both within and between regions, producing stronger and more variable regional activity and leading to lower functional connectivity. Regions which exhibit particularly high correlations with J_N are likely structurally isolated, so an increase in J_N strongly increases intrinsic regional signalling, which propagates the random noise added to the simulation within a region, while the external input, which synchronises regional activity, remains small. As J_N is closely associated with NMDA-mediated excitatory signalling, this observation is in line with previous evidence suggesting that a decrease in excitatory neurotransmission caused by administration of NMDA receptor antagonists leads to increased static connectivity (Anticevic et al., 2015; Driesen et al., 2013) and increased dynamic flexibility (Braun et al., 2016). However, most of the associations between J_N and FC were not significant in the validation analysis using the data from the second scanning session. As a result, this finding cannot be considered reliable, and further investigation is necessary to determine whether conclusions which might be drawn from it are valid.

Neither the two parameters for which we could identify FC correlates, G and J_N, nor the two parameters which were not associated with FC, J_i and w_p, could be reliably predicted from the sFC or TC. While the relationship between the parameters and some FC features was significant, it was not very strong for any regions or pairs of regions, limiting its predictive value. However, it is possible that a larger training set would improve the prediction performance on unseen test data. If a prediction of model parameters based on fMRI-derived FC could be realised, it would eliminate the computational effort of performing simulations based on large parameter sets, storing the resulting FC, and identifying optimal parameter combinations for each individual. Thus, future analyses should determine whether it is possible to achieve a sufficiently strong prediction performance to facilitate this approach.

The optimal model parameters did not show significant correlations with dynamic characteristics of regional fMRI BOLD time courses or behavioural test scores. The lack of association between parameters and regional dynamics represents a limitation of the modelling approach. While the choice of model parameters affects the dynamics of the simulated time courses (Sanz-Leon et al., 2015), we optimised the models using the static and dynamic FC, potentially masking differences in the underlying dynamics of the individual scans as different activity patterns could produce the same FC. Therefore, the static and dynamic FC of the simulated data matches that of the respective empirical data, but the correspondence of simulated and empirical dynamics of individual regions is lower, meaning that the parameters optimised to produce accurate FC do not correlate strongly with empirical regional dynamics.

Capturing the relationship between neurobiology and behaviour through modelling is equally challenging. Brain network models are limited to explaining mechanisms moderated by FC. While FC correlates have been identified for some behavioural tests (Smith et al., 2015), the prediction of behavioural phenotypes from FC has proven difficult (Kong et al., 2021), potentially due to limited reliability of behavioural scores (Calamia et al., 2013). Even if a behavioural feature exhibits a robust FC signature, parameters might be dominated by connectivities with the highest individual variability, even when these do not correlate with the variable of interest. This can result in simulated FC that poorly replicates behaviourally relevant but less variable patterns, leading to optimal parameters that lack meaningful behavioural associations. Enhancing model fits—either by refining optimization procedures or developing more detailed models—could help uncover neurobiological characteristics linked to behaviour.

When we altered the coupling parameter in each region separately, perturbations in some regions had a much greater effect on overall FC than in others. The sFC fit and efficiency exhibited particularly large variation depending on the G value in the left and right paracentral, and the right pre- and postcentral as well as the right transverse temporal gyrus, while TC fit

varied most with changes in G in the left pars triangularis. The former areas are thus likely involved in shaping the global network architecture, while the latter region controls the transition between network configurations. Another group of regions produces a disproportionate reduction in fits and efficiency if their coupling is perturbed in any way, indicating that this small set of regions determines the optimal coupling for the entire network. Since high fits can only be obtained if the coupling in these regions is set correctly, they presumably play an especially important role in maintaining biologically accurate FC. In contrast, regions in which perturbation improves FC fit seem to be less vital parts of the brain network, but might be relevant targets for further improving fits in future modelling analyses. sFC fit and efficiency were most strongly affected by perturbations in the same set of regions, which was distinct from the set of regions which most altered TC fit, suggesting the existence of separate networks shaping static and dynamic connectivity.

The regional perturbation effect correlated strongly with measures of centrality in the SC, suggesting that regions which are highly structurally interconnected shape global FC patterns. Regions which were particularly important in maintaining biological accurate FC, producing large reductions in fits under perturbation, also represented FC hubs, exhibiting high centrality in the FC. Previous studies of generative models of brain activity have shown that disrupting the underlying structural connectivity of hub nodes (Achard et al., 2006; Aerts et al., 2016), particularly in regions along the cortical midline (Alstott et al., 2009), leads to strong disturbances in FC. In addition, the regions that perturbation analysis revealed to be particularly important for maintaining FC, particularly the pre-, post- and paracentral gyri, tend to show preserved function after stroke (Thirugnanachandran et al., 2024). It is possible that mechanisms have evolved to protect these structures because disruptions would degrade brain function.

The perturbation outcomes also exhibited high correlations with the expression of a number of different genes, which could be clustered into several biological processes. Three of the relevant processes were directly related to the central nervous system, namely chemical

synapse transmission, nervous system development, and behaviour. The association with genes involved in chemical synapse transmission in particular suggests that regions which shape FC expend more resources toward sustaining synaptic signalling, providing additional evidence for the importance of neurophysiology in establishing FC patterns. Some additional processes relating to perturbation effects are active throughout the body, but are known to be crucial for brain function, including membrane organisation and phospholipid metabolism. These mechanisms are involved in establishing and maintaining the myelin sheaths which insulate nerve fibers (Raasakka et al., 2017), and play a key role in shaping the connectivity between regions (Huntenburg et al., 2017; Vandewouw et al., 2021).

The findings from Study II indicate that heterogeneity in neurobiological characteristics relating to coupling across regions contributed to individual variability in static and dynamic FC patterns and that global FC is predominantly shaped by a small subset of highly connected regions.

5.3 Modelling dynamic FC in psychotic and affective disorders

Study III investigated brain network models of static and dynamic FC in patients with psychotic and affective disorders. The fits we obtained were on par with those achieved in the HCP sample and did not differ between the study groups, indicating that the models could represent the neurobiology of patients and healthy controls in the PRONIA sample reasonably well. The global coupling parameter G, the excitatory synaptic coupling parameter J_N, and the inhibitory synaptic coupling parameter J_i did not differ between the groups. The excitatory recurrence parameter w_p was significantly increased in ROD and CHR patients compared to ROP patients and healthy controls. The alteration in this parameter in ROD and CHR patients suggests that it might be related to general psychopathology or affective symptomatology. The increase in w_p indicates an altered excitation-inhibition balance due to increased recurrent excitation within brain regions. While there is a growing body of evidence suggesting a role of

disruptions to the excitation-inhibition balance in the development of psychotic and depressive disorders, the findings are somewhat inconsistent and indicate regional differences in abnormalities. Patients with schizophrenia as well as CHR and depression exhibit alterations in the concentration of glutamate metabolites, with an increase identified in some and a decrease in other regions (Hu et al., 2023; Merritt et al., 2023; Wenneberg et al., 2020). Future research should investigate the spatial distribution of model parameters in these disorders to identify areas in which they are altered, and determine whether these overlap with areas exhibiting altered glutamatergic signalling.

In addition, our findings indicate that potential disturbances in glutamatergic excitatory signalling in depression and CHR have a more pronounced effect on excitatory feedback currents than excitatory global connections. This observation suggests the presence of different mechanisms contributing to external and internal regional excitatory signalling, and highlights the importance of computational modelling for the investigation of the effects of neurobiology on brain activity. Both affective symptom severity and psychiatric disease burden were also high in the ROP group, but patients did not exhibit significantly increased w_p compared to healthy controls. This observation might be caused by the administration of antipsychotic medication in psychosis patients, which has been shown to alter both the excitation-inhibition balance (de la Fuente-Sandoval et al., 2018; Lidsky et al., 1997) and brain connectivity (Abbott et al., 2013; Chopra et al., 2021). Further analysis is necessary to elucidate the relationship between model parameters and disease- and medication-related processes across patient groups.

Klein et al. (Klein et al., 2021) previously found an increase in w_p in healthy individuals exhibiting a genetic polymorphism linked to schizophrenia risk, suggesting a potential shared mechanism of neurobiological alterations with CHR patients. However, that study also identified differences in other model parameters which we did not find in our analysis. In addition, previous work on computational modelling in schizophrenia has suggested a role of abnormalities in global coupling (Cabral et al., 2013), which was not significantly altered in our

sample. This discrepancy could be related to the inclusion of dynamic FC in our modelling, highlighting the importance of building and analysing models describing the association between neurobiology and both static and dynamic FC.

While there was generally little effect of covariates on model parameters or fits, two observations warrant further consideration. First, the sFC fit was higher for individuals with stronger head motion. This finding is somewhat unexpected, particularly given that study II found that sFC fit was increased in individuals with stronger connectivity. Even though we could show that head motion only affected J_i and not the other model parameters in our sample, future work should analyse the impact of motion strength, as well as the impact of the choice of preprocessing steps, on model fits and parameters more comprehensively. Second, several parameters differed significantly between sites before correction for multiple comparisons, and the sFC fit showed differences which persisted after correction. Although we corrected the empirical sFC and TC for site effects using the powerful ComBat technique (J.-P. Fortin et al., 2018), it is possible that not all site-related differences could be accounted for. These might relate to nuisance variables such as experimental or scanner effects, although they might also reflect relevant variations in the individuals recruited at the different sites. The differences seen in the J_i parameter and the sFC fit could be connected to differences in motion across the sites. Thus, site effects on model outcomes should also be further investigated, particularly given that the clinical utility of parameters depends on the generalisability of findings across sites.

5.4 Linking individual heterogeneity in neurophysiology, FC, and behaviour

The findings of study I provide additional evidence for the utility of dynamic FC as a marker of abnormalities in brain function in psychiatric disorders. We were able to identify a transdiagnostic increase in the lifetime of a low-connectivity state with characteristic connectivities in the SMN and the SN, as well as an increase in the frequency of this state in

ROP patients and an increase in the lifetime and frequency of a weakly connected state in ROD patients. In addition, dFC patterns were related to positive psychosis symptom severity across the patient groups. These observations suggest a complex set of shared as well as diagnosis-specific and symptom-related mechanisms contributing to alterations in brain network communication in psychotic and affective disorders. The changes in the dynamic characteristics of the SMN-SN state point to a role of dysfunction of the triple network system in these conditions, and might be related to dopaminergic signalling.

Study II showed that individual variability in dFC of the DAN and DMN, and sFC of the DAN, SMN and VN were related to heterogeneity in global coupling, while dFC across the brain and sFC in the VN were linked to excitatory synaptic recurrence, although not robustly. The static and dynamic FC patterns correlating with model parameters do not substantially overlap with the dFC alterations identified in study I. This might indicate that dFC changes in patients are not related to the computational characteristics investigated, or the methodology is insufficient for the detection of such an association. However, the increase in the excitatory recurrence parameter identified in study III, which was not associated with FC in study II, suggests that the disease-related differences in both FC and model parameters are distinct from normal individual variation. In that case, an association between FC and excitatory recurrence would not be observable in healthy individuals due to low variance, and global coupling and excitatory synaptic coupling would not differ significantly between patients and controls as both groups would exhibit similar levels of variation. Thus, further research is needed to investigate the relationship between neurophysiological differences and alterations in FC in psychiatric disorders.

The perturbation analysis conducted in study II revealed that changes in coupling in a small number of frontal regions, particularly the left pars triangularis, affected global dynamic FC most strongly. These regions are thus likely to govern the dynamic restructuring of the functional connectome, potentially by mediating switches between brain states. Research in patients with schizophrenia has identified structural and functional abnormalities in the inferior

frontal gyrus (Jeong et al., 2009), which encompasses the pars triangularis, pars opercularis and pars orbitalis. The left pars triangularis and pars opercularis constitute Broca's area, which has long been known to play a vital role in speech production (Flinker et al., 2015). The equivalent regions in the right hemisphere are also considered to be involved in language processing, and abnormalities have been associated with impairment in language-related cognitive processes in schizophrenia (Jeong et al., 2009). It is possible that alterations in the structure and physiology of this region additionally contribute to alterations in dFC, and thus might be linked to positive psychosis symptoms.

Our findings contribute to the understanding of alterations in brain connectivity in psychiatric patients and their association with symptoms and neurophysiological systems. However, our results also support previous analyses which found that dFC changes in psychiatric disorders are widely distributed over the brain and cannot be consistently identified across methodologies (Cattarinussi et al., 2023; Sun et al., 2024). Future studies into alterations of FC in brain disorders would benefit from basic research providing a better understanding of the fundamental principles of large-scale brain dynamics, as well as a comprehensive theoretical model linking different dynamic characteristics of FC.

5.5 Clinical implications and future perspective

While the analyses presented in this thesis were not primarily translational, the findings should be used to inform future clinical research. The presence of robust alterations in dFC in patients and their relationship with symptoms provides further evidence for the relevance of this measure for the investigation of psychiatric disorders. While the utility of dFC as a biomarker for diagnosis is likely low, it carries some promise for the identification of subgroups and the prediction of clinical trajectories and treatment outcomes. Our findings show that an increase in the frequency of an FC state characterised by low connectivities overall, but higher connectivities in the SN and SMN, is distinctive of psychosis patients, and occurs in some, but

not all CHR patients. Future work should investigate whether this quantity is linked to the probability of conversion to psychosis in CHR patients. In addition, dFC could be useful as an intermediate phenotype for the development of new therapeutic approaches. By investigating how medication or brain stimulation affect dFC in healthy individuals, or even in computational or preclinical models, researchers can identify promising candidates for new treatments.

Brain network modelling has shown considerable promise in clinical research. In epilepsy, computational models of individual patient brains have been used to investigate seizure propagation (Jirsa et al., 2017; Proix et al., 2018), and a clinical trial is currently underway which is studying the use of personalised models to improve surgical strategies for the removal of seizure-generating regions in patients with drug-resistant epilepsy (H. E. Wang et al., 2023). In addition, work in patients with Alzheimer's disease has shown that personalised optimal model parameters can predict cognitive function (Zimmermann et al., 2018), and a new project is evaluating the utility of brain models for the diagnosis and treatment planning in neurodegenerative diseases (virtualbraincloud-2020.eu). Research on brain network models in psychiatric patients is still limited, and the translation potential has not yet been tested in these populations. Our study found that CHR and ROD patients exhibited alterations in model parameters, whereas ROP did not. A further examination of this observation could elucidate mechanisms contributing to alterations in FC in psychiatric patients, and identify associations with clinical variables. In addition, further validation and testing of this difference in model parameters might reveal that it provides clinically relevant predictive value.

5.6 Limitations

While this thesis presents novel insights into alterations of dynamic FC in psychiatric disorders and the neurobiology underlying heterogeneity in FC patterns, some methodological limitations need to be considered.

One major challenge was the quality of the data used in the analyses presented. The fMRI data from the PRONIA study was obtained at different sites from different populations by different researchers. While we used well-established procedures to account for this issue, fully removing potential effects is not possible. Even the HCP data, which was acquired and preprocessed according to strict protocols to maximise quality (Glasser et al., 2013; Smith et al., 2013; Sotiropoulos et al., 2013; Van Essen et al., 2013) and has been widely used and extensively analysed (Elam et al., 2021), is not free of all confound effects. As a result, replication of these analyses under different conditions is necessary to further validate the findings presented here.

Another limitation is the use of fMRI data for the estimation of dFC. Since it measures changes in blood flow as a result of neural activity and not the neural activity directly (Heeger & Ress, 2002), its temporal resolution is limited by the comparatively slow hemodynamic response, and the processes involved in this response could bias the findings. As a result, it is essential to integrate findings from fMRI and EEG or MEG studies, and future research should include multimodal approaches. In addition, the spatial resolution determined by the choice of atlas could influence analysis outcomes. While structural and functional specialisation of brain regions has been well established (B. T. T. Yeo et al., 2011), the number of distinct regions and networks, and the boundaries between them, vary between atlases (Dosenbach et al., 2010; Uddin et al., 2019; B. T. T. Yeo et al., 2011). Research has also shown that the exact topography of brain networks varies between individuals (Laumann et al., 2015). Some of this heterogeneity is lost when distinguishing regions based on group-average parcellations. For the modelling analysis, the choice of a purely cortical atlas introduced the additional limitation of neglecting the influence of subcortical areas.

The methodology used to quantify dynamic FC limits the extent of the information that can be captured, and might affect the resulting findings. There has been some debate about the optimal size of the sliding windows used to compute time-varying FC, with a length of 60 s or more generally considered appropriate (Leonardi & Van De Ville, 2015). While there is a lower

limit for the optimal window length, it is possible that windows of different lengths capture dynamic fluctuations at different time scales, resulting in divergent, but still valid observations depending on the length selected. The k-means-based consensus clustering approach we employed yielded highly robust clusters, but also has its disadvantages. The k-means algorithm is known to perform less well in identifying clusters of different sizes or densities, and is vulnerable to outliers (Jain, 2010). The repetition of the analysis with a different clustering algorithm might produce additional insights into the topography of the state space, particularly with regard to the rare and inconsistent clusters we identified. In order to test the validity of our findings and contextualise them, it is necessary to systematically evaluate the impact of methodological choices.

The brain network modelling approach is naturally limited by the specifications of the model, which need to balance accuracy against computational effort. The quality of the models could be improved by fitting the parameters not just globally across the entire brain, but for each region individually. Inherent differences in global coupling and local excitation-inhibition ratio exist across the brain (X.-J. Wang, 2020), and there is some suggestion that neurobiological alterations in psychiatric disorders are focused on certain areas (Crossley et al., 2014). The perturbation analysis described in Study II also showed that altering the coupling parameter from the global optimum in some regions produced an improvement in fit. However, increasing the number of variables to cover individual parameter values for each region would have required a substantial increase in computational resources, and was not feasible in the context of this thesis. Future work should consider this regional variation in neurobiology. We also showed that brain network modelling was not able to replicate all dynamic characteristics of empirical FC, achieving only low FC variance and node cohesion fits. Developing improved regional models able to more comprehensively capture dynamic FC processes would provide more accurate model outcomes, and allow for a more detailed investigation of neurobiological correlates of dynamic FC.

6. Summary

This dissertation explores the role of dynamic functional connectivity (dFC) as an intermediate phenotype linking neurobiological characteristics and clinical outcomes in psychotic and affective disorders. The thesis aims to reveal alterations in dFC in psychotic and affective patients (Study I), study the impact of neurobiology on static and dynamic FC patterns (Study II), and identify neurobiological processes which might contribute to static and dynamic FC changes in psychotic and affective disorders (Study III).

Study I, which compared dFC patterns of patients with recent-onset psychosis, patients with recent-onset depression, individuals with a clinical high risk for psychosis, and healthy individuals, found diagnosis-specific alterations in recent-onset psychosis (ROP) and recent-onset depression (ROD) patients as well as transdiagnostic alterations exhibited by all patient groups. These results support findings of previous research in depression and provide additional evidence of dFC alterations in psychotic disorders, presenting a potential link between disruptions in dopaminergic signalling and changes in brain connectivity. We also identified a dFC pattern which was significantly correlated with psychosis symptom severity across the patient groups. This transdiagnostic association of clinical heterogeneity with dFC highlights the importance of investigating variability across a spectrum of psychiatric disorders to reveal information about pathological changes and mechanisms.

Study II investigated the relationship between neurobiological characteristics and static and dynamic FC using brain network modelling, identifying FC correlates of global coupling and excitatory synaptic coupling, as well as model fits. These associations indicate a contribution of neurobiological heterogeneity to individual variability in static and dynamic FC patterns, but also show that brain network models are able to reproduce some FC patterns more accurately than others. In addition, this study investigated the effect of altering regional model parameters on global FC, showing that distinct small subsets of regions produced outsized effects on static

and dynamic FC and regional effects were correlated with network structure and expression of genes involved in processes relating to brain function.

Study III employed brain network modelling of static and dynamic FC to reveal an increase in regional recurrent excitation in clinical high risk (CHR) individuals and ROD patients compared to healthy controls and ROP patients. While this finding requires further validation, it supports the importance of disruptions in excitatory signalling as a computational mechanism contributing to altered brain connectivity. Moreover, the increase in the excitatory recurrence model parameter might represent a useful clinical biomarker.

Integrating the findings from these three studies, this dissertation contributes to the understanding of the role of dFC in psychotic and affective disorders, providing evidence for neurobiological underpinnings and clinical consequences of alterations to dFC. In addition, the thesis highlights the importance of studying individual variability in clinical presentation, brain connectivity and neurophysiology to produce insights into heterogeneous mechanisms of psychiatric disorders across diagnoses.

7. Zusammenfassung

In dieser Dissertation wird die Rolle der dynamischen funktionellen Konnektivität (dFC) als intermediärer Phänotyp untersucht, der neurobiologische Merkmale und klinische Präsentation bei psychotischen und affektiven Störungen miteinander verbindet. Die Dissertation zielt darauf ab, Veränderungen der dFC bei psychotischen und affektiven Patienten aufzudecken (Studie I), den Einfluss der Neurobiologie auf statische und dynamische FC-Muster zu untersuchen (Studie II) und neurobiologische Prozesse zu identifizieren, die zu statischen und dynamischen FC-Veränderungen bei psychotischen und affektiven Störungen beitragen könnten (Studie III).

Studie I, in der die dFC-Muster von Patienten mit einer kürzlich aufgetretenen Psychose (ROP), von Patienten mit einer kürzlich aufgetretenen Depression (ROD), von Personen mit einem klinischen Hochrisiko für eine Psychose (CHR) und von gesunden Personen verglichen wurden, zeigte diagnosespezifische Veränderungen bei ROP-Patienten und ROD-Patienten sowie transdiagnostische Veränderungen, die bei allen Patientengruppen zu beobachten waren. Diese Ergebnisse unterstützen frühere Forschungsergebnisse bei depressiven Störungen und liefern zusätzliche Belege für dFC-Veränderungen bei psychotischen Störungen, die einen möglichen Zusammenhang zwischen Unregelmäßigkeiten der dopaminergen Signalübertragung und Veränderungen der Konnektivität des Gehirns darstellen. Ebenso konnte ein dFC-Muster identifiziert werden, das in allen Patientengruppen signifikant mit der Schwere von psychotischen Symptomen korreliert war. Diese transdiagnostische Assoziation der klinischen Heterogenität mit der dFC unterstreicht die Bedeutung der Untersuchung der Variabilität über ein Spektrum psychiatrischer Störungen, um Informationen über pathologische Veränderungen zu erhalten.

Studie II untersuchte die Beziehung zwischen neurobiologischen Merkmalen und statischer und dynamischer FC durch Hirnnetzwerkmodellierung, und identifizierte FC-Korrelate der

globalen Kopplung und der exzitatorischen synaptischen Kopplung sowie der Übereinstimmung zwischen simulierten und empirischen Daten. Diese Assoziationen deuten auf einen Beitrag der neurobiologischen Heterogenität zur individuellen Variabilität in statischen und dynamischen FC-Mustern hin, zeigen aber auch, dass Hirnnetzwerkmodelle in der Lage sind, einige FC-Muster genauer zu reproduzieren als andere. Darüber hinaus untersuchte diese Studie die Auswirkung der Veränderung regionaler Modellparameter auf die globale FC. Es zeigte sich, dass bestimmte kleine Untergruppen von Regionen übergroße Auswirkungen auf die statische und dynamische FC hatten, und dass die regionalen Auswirkungen mit der Netzwerkstruktur des Gehirns und der Expression von Genen korrelierten, die an Prozessen beteiligt sind, die mit der Gehirnfunktion zusammenhängen.

In Studie III wurde durch Hirnnetzwerkmodellierung der statischen und dynamischen FC eine Zunahme der regionalen Selbstexzitation bei CHR-Personen und ROD-Patienten im Vergleich zu gesunden Kontrollen und ROP-Patienten identifiziert. Dieser Befund muss zwar noch weiter validiert werden, er untermauert jedoch die Bedeutung von Störungen der exzitatorischen Signalübertragung als computationalen Mechanismus, der zu einer veränderten Konnektivität des Gehirns beiträgt. Darüber hinaus könnte die Erhöhung des Modellparameters, der die Selbstexzitation repräsentiert, ein nützlicher klinischer Biomarker sein.

Durch die Integration der Ergebnisse dieser drei Studien trägt diese Dissertation zum Verständnis der Rolle der dFC bei psychotischen und affektiven Störungen bei und liefert Belege für die neurobiologischen Grundlagen und klinischen Konsequenzen von Veränderungen der dFC. Darüber hinaus unterstreicht die Dissertation, wie wichtig es ist, die individuelle Variabilität in der klinischen Präsentation, der Konnektivität des Gehirns und der Neurophysiologie zu untersuchen, um Einblicke in die heterogenen und diagnoseübergreifenden Mechanismen psychiatrischer Störungen zu gewinnen.

8. References

Abbott, C. C., Jaramillo, A., Wilcox, C. E., & Hamilton, D. A. (2013). Antipsychotic drug effects in schizophrenia: A review of longitudinal FMRI investigations and neural interpretations. *Current Medicinal Chemistry*, *20*(3), 428–437. https://doi.org/10.2174/0929867311320030014

Achard, S., Salvador, R., Whitcher, B., Suckling, J., & Bullmore, E. (2006). A Resilient, Low-Frequency, Small-World Human Brain Functional Network with Highly Connected Association Cortical Hubs. *The Journal of Neuroscience*, *26*(1), 63–72. https://doi.org/10.1523/JNEUROSCI.3874-05.2006

Addington, J., Cornblatt, B. A., Cadenhead, K. S., Cannon, T. D., McGlashan, T. H., Perkins, D. O., Seidman, L. J., Tsuang, M. T., Walker, E. F., Woods, S. W., & Heinssen, R. (2011). At Clinical High Risk for Psychosis: Outcome for Nonconverters. *American Journal of Psychiatry*, *168*(8), 800–805. https://doi.org/10.1176/appi.ajp.2011.10081191

Adhikari, M. H., Hacker, C. D., Siegel, J. S., Griffa, A., Hagmann, P., Deco, G., & Corbetta, M. (2017). Decreased integration and information capacity in stroke measured by whole brain models of resting state activity. *Brain*, *140*(4), 1068–1085. https://doi.org/10.1093/brain/awx021

Aerts, H., Fias, W., Caeyenberghs, K., & Marinazzo, D. (2016). Brain networks under attack: Robustness properties and the impact of lesions. *Brain*, *139*(12), 3063–3083. https://doi.org/10.1093/brain/aww194

Alexander-Bloch, A. F., Shou, H., Liu, S., Satterthwaite, T. D., Glahn, D. C., Shinohara, R. T., Vandekar, S. N., & Raznahan, A. (2018). On testing for spatial correspondence between maps of human brain structure and function. *NeuroImage*, *178*, 540–551. https://doi.org/10.1016/j.neuroimage.2018.05.070

Allen, E. A., Damaraju, E., Plis, S. M., Erhardt, E. B., Eichele, T., & Calhoun, V. D. (2014). Tracking Whole-Brain Connectivity Dynamics in the Resting State. *Cerebral Cortex (New York, NY)*, *24*(3), 663–676. https://doi.org/10.1093/cercor/bhs352

Almulla, A. F., Thipakorn, Y., Vasupanrajit, A., Abo Algon, A. A., Tunvirachaisakul, C., Hashim Aljanabi, A. A., Oxenkrug, G., Al-Hakeim, H. K., & Maes, M. (2022). The tryptophan catabolite or kynurenine pathway in major depressive and bipolar disorder: A systematic review and meta-analysis. *Brain, Behavior, & Immunity - Health*, *26*, 100537. https://doi.org/10.1016/j.bbih.2022.100537

Alstott, J., Breakspear, M., Hagmann, P., Cammoun, L., & Sporns, O. (2009). Modeling the Impact of Lesions in the Human Brain. *PLOS Computational Biology*, *5*(6), e1000408. https://doi.org/10.1371/journal.pcbi.1000408

Anticevic, A., Corlett, P. R., Cole, M. W., Savic, A., Gancsos, M., Tang, Y., Repovs, G., Murray, J. D., Driesen, N. R., Morgan, P. T., Xu, K., Wang, F., & Krystal, J. H. (2015). *N*-Methyl-D-Aspartate Receptor Antagonist Effects on Prefrontal Cortical Connectivity Better Model Early Than Chronic Schizophrenia. *Biological Psychiatry*, *77*(6), 569–580. https://doi.org/10.1016/j.biopsych.2014.07.022

Anticevic, A., & Lisman, J. (2017). How Can Global Alteration of Excitation/Inhibition Balance Lead to the Local Dysfunctions That Underlie Schizophrenia? *Biological Psychiatry*, *81*(10), 818–820. https://doi.org/10.1016/j.biopsych.2016.12.006

Arnaud, A. M., Brister, T. S., Duckworth, K., Foxworth, P., Fulwider, T., Suthoff, E. D.,

Werneburg, B., Aleksanderek, I., & Reinhart, M. L. (2022). Impact of Major Depressive Disorder on Comorbidities: A Systematic Literature Review. *The Journal of Clinical Psychiatry*, *83*(6), 43390. https://doi.org/10.4088/JCP.21r14328

Artigas, F., Nutt, D. J., & Shelton, R. (2002). Mechanism of action of antidepressants. *Psychopharmacology Bulletin*, *36 Suppl 2*, 123–132.

Auther, A. M., Smith, C. W., & Cornblatt, B. A. (2006). *Global Functioning: Social Scale (GF: Social)*. Glen Oaks, NY: Zucker Hillside Hospital.

Bansal, K., Nakuci, J., & Muldoon, S. F. (2018). Personalized brain network models for assessing structure–function relationships. *Current Opinion in Neurobiology*, *52*, 42–47. https://doi.org/10.1016/j.conb.2018.04.014

Barber, A. D., Hegarty, C. E., Lindquist, M., & Karlsgodt, K. H. (2021). Heritability of Functional Connectivity in Resting State: Assessment of the Dynamic Mean, Dynamic Variance, and Static Connectivity across Networks. *Cerebral Cortex*, *31*(6), 2834–2844. https://doi.org/10.1093/cercor/bhaa391

Barber, A. D., Lindquist, M. A., DeRosse, P., & Karlsgodt, K. H. (2018). Dynamic Functional Connectivity States Reflecting Psychotic-Like Experiences. *Biological Psychiatry. Cognitive Neuroscience and Neuroimaging*, *3*(5), 443–453. https://doi.org/10.1016/j.bpsc.2017.09.008

Barttfeld, P., Uhrig, L., Sitt, J. D., Sigman, M., Jarraya, B., & Dehaene, S. (2015). Signature of consciousness in the dynamics of resting-state brain activity. *Proceedings of the National Academy of Sciences*, *112*(3), 887–892. https://doi.org/10.1073/pnas.1418031112

Beck, A. T., Steer, R. A., Ball, R., & Ranieri, W. (1996). Comparison of Beck Depression Inventories -IA and -II in psychiatric outpatients. *Journal of Personality Assessment*, *67*(3), 588–597. https://doi.org/10.1207/s15327752jpa6703_13

Beck, K., Hindley, G., Borgan, F., Ginestet, C., McCutcheon, R., Brugger, S., Driesen, N., Ranganathan, M., D'Souza, D. C., Taylor, M., Krystal, J. H., & Howes, O. D. (2020). Association of Ketamine With Psychiatric Symptoms and Implications for Its Therapeutic Use and for Understanding Schizophrenia: A Systematic Review and Meta-analysis. *JAMA Network Open*, *3*(5), e204693. https://doi.org/10.1001/jamanetworkopen.2020.4693

Beijers, L., Wardenaar, K. J., van Loo, H. M., & Schoevers, R. A. (2019). Data-driven biological subtypes of depression: Systematic review of biological approaches to depression subtyping. *Molecular Psychiatry*, *24*(6), 888–900. https://doi.org/10.1038/s41380-019-0385-5

Bentall, R. P., Wickham, S., Shevlin, M., & Varese, F. (2012). Do Specific Early-Life Adversities Lead to Specific Symptoms of Psychosis? A Study from the 2007 The Adult Psychiatric Morbidity Survey. *Schizophrenia Bulletin*, *38*(4), 734–740. https://doi.org/10.1093/schbul/sbs049

Biswal, B., Zerrin Yetkin, F., Haughton, V. M., & Hyde, J. S. (1995). Functional connectivity in the motor cortex of resting human brain using echo-planar mri. *Magnetic Resonance in Medicine*, *34*(4), 537–541. https://doi.org/10.1002/mrm.1910340409

Braun, U., Schäfer, A., Bassett, D. S., Rausch, F., Schweiger, J. I., Bilek, E., Erk, S., Romanczuk-Seiferth, N., Grimm, O., Geiger, L. S., Haddad, L., Otto, K., Mohnke, S., Heinz, A., Zink, M., Walter, H., Schwarz, E., Meyer-Lindenberg, A., & Tost, H. (2016). Dynamic brain network reconfiguration as a potential schizophrenia genetic risk mechanism modulated by NMDA receptor function. *Proceedings of the National Academy of Sciences*, *113*(44), 12568–12573.

https://doi.org/10.1073/pnas.1608819113
Breakspear, M. (2017). Dynamic models of large-scale brain activity. *Nature Neuroscience*, *20*(3), Article 3. https://doi.org/10.1038/nn.4497
Breiman, L. (2001). Random Forests. *Machine Learning*, *45*(1), 5–32. https://doi.org/10.1023/A:1010933404324
Brink, R. L. van den, Pfeffer, T., Warren, C. M., Murphy, P. R., Tona, K.-D., Wee, N. J. A. van der, Giltay, E., Noorden, M. S. van, Rombouts, S. A. R. B., Donner, T. H., & Nieuwenhuis, S. (2016). Catecholaminergic Neuromodulation Shapes Intrinsic MRI Functional Connectivity in the Human Brain. *Journal of Neuroscience*, *36*(30), 7865–7876. https://doi.org/10.1523/JNEUROSCI.0744-16.2016
Buckley, P. F., Miller, B. J., Lehrer, D. S., & Castle, D. J. (2009). Psychiatric Comorbidities and Schizophrenia. *Schizophrenia Bulletin*, *35*(2), 383–402. https://doi.org/10.1093/schbul/sbn135
Bullmore, E., & Sporns, O. (2009). Complex brain networks: Graph theoretical analysis of structural and functional systems. *Nature Reviews Neuroscience*, *10*(3), 186–198. https://doi.org/10.1038/nrn2575
Buxton, R. B., Wong, E. C., & Frank, L. R. (1998). Dynamics of blood flow and oxygenation changes during brain activation: The balloon model. *Magnetic Resonance in Medicine*, *39*(6), 855–864. https://doi.org/10.1002/mrm.1910390602
Cabral, J., Fernandes, H. M., Van Hartevelt, T. J., James, A. C., Kringelbach, M. L., & Deco, G. (2013). Structural connectivity in schizophrenia and its impact on the dynamics of spontaneous functional networks. *Chaos: An Interdisciplinary Journal of Nonlinear Science*, *23*(4), 046111. https://doi.org/10.1063/1.4851117
Cabral, J., Vidaurre, D., Marques, P., Magalhães, R., Silva Moreira, P., Miguel Soares, J., Deco, G., Sousa, N., & Kringelbach, M. L. (2017). Cognitive performance in healthy older adults relates to spontaneous switching between states of functional connectivity during rest. *Scientific Reports*, *7*(1), Article 1. https://doi.org/10.1038/s41598-017-05425-7
Calamia, M., Markon, K., & Tranel, D. (2013). The robust reliability of neuropsychological measures: Meta-analyses of test-retest correlations. *The Clinical Neuropsychologist*, *27*(7), 1077–1105. https://doi.org/10.1080/13854046.2013.809795
Calhoun, V. D., Miller, R., Pearlson, G., & Adalı, T. (2014). The Chronnectome: Time-Varying Connectivity Networks as the Next Frontier in fMRI Data Discovery. *Neuron*, *84*(2), 262–274. https://doi.org/10.1016/j.neuron.2014.10.015
Caliński, T., & Harabasz, J. (1974). A dendrite method for cluster analysis. *Communications in Statistics*, *3*(1), 1–27. https://doi.org/10.1080/03610927408827101
Cattarinussi, G., Di Giorgio, A., Moretti, F., Bondi, E., & Sambataro, F. (2023). Dynamic functional connectivity in schizophrenia and bipolar disorder: A review of the evidence and associations with psychopathological features. *Progress in Neuro-Psychopharmacology and Biological Psychiatry*, *127*, 110827. https://doi.org/10.1016/j.pnpbp.2023.110827
Cazabet, R., Boudebza, S., & Jorquera, T. (2023). *Tnetwork* [Computer software]. GitHub. https://github.com/Yquetzal/tnetwork
Cazabet, R., Boudebza, S., & Rossetti, G. (2021). Evaluating community detection algorithms for progressively evolving graphs. *Journal of Complex Networks*, *8*(6), cnaa027. https://doi.org/10.1093/comnet/cnaa027
Chopra, S., Francey, S. M., O'Donoghue, B., Sabaroedin, K., Arnatkeviciute, A., Cropley, V., Nelson, B., Graham, J., Baldwin, L., Tahtalian, S., Yuen, H. P., Allott, K., Alvarez-

Jimenez, M., Harrigan, S., Pantelis, C., Wood, S. J., McGorry, P., & Fornito, A. (2021). Functional Connectivity in Antipsychotic-Treated and Antipsychotic-Naive Patients With First-Episode Psychosis and Low Risk of Self-harm or Aggression: A Secondary Analysis of a Randomized Clinical Trial. *JAMA Psychiatry*, *78*(9), 994–1004. https://doi.org/10.1001/jamapsychiatry.2021.1422

Choquet, D., & Triller, A. (2013). The Dynamic Synapse. *Neuron*, *80*(3), 691–703. https://doi.org/10.1016/j.neuron.2013.10.013

Cohen, J. R. (2018). The behavioral and cognitive relevance of time-varying, dynamic changes in functional connectivity. *NeuroImage*, *180*, 515–525. https://doi.org/10.1016/j.neuroimage.2017.09.036

Colodro-Conde, L., Couvy-Duchesne, B., Zhu, G., Coventry, W. L., Byrne, E. M., Gordon, S., Wright, M. J., Montgomery, G. W., Madden, P. a. F., Ripke, S., Eaves, L. J., Heath, A. C., Wray, N. R., Medland, S. E., & Martin, N. G. (2018). A direct test of the diathesis–stress model for depression. *Molecular Psychiatry*, *23*(7), 1590–1596. https://doi.org/10.1038/mp.2017.130

Conio, B., Martino, M., Magioncalda, P., Escelsior, A., Inglese, M., Amore, M., & Northoff, G. (2020). Opposite effects of dopamine and serotonin on resting-state networks: Review and implications for psychiatric disorders. *Molecular Psychiatry*, *25*(1), Article 1. https://doi.org/10.1038/s41380-019-0406-4

Conley, R. R., Ascher-Svanum, H., Zhu, B., Faries, D. E., & Kinon, B. J. (2007). The burden of depressive symptoms in the long-term treatment of patients with schizophrenia. *Schizophrenia Research*, *90*(1), 186–197. https://doi.org/10.1016/j.schres.2006.09.027

Consortium, G. O. (2004). The Gene Ontology (GO) database and informatics resource. *Nucleic Acids Research*, *32*(suppl_1), D258–D261. https://doi.org/10.1093/nar/gkh036

Coppen, A. (1967). The Biochemistry of Affective Disorders. *The British Journal of Psychiatry*, *113*(504), 1237–1264. https://doi.org/10.1192/bjp.113.504.1237

Correll, C. U., Abi-Dargham, A., & Howes, O. (2022). Emerging Treatments in Schizophrenia. *The Journal of Clinical Psychiatry*, *83*(1), 39683. https://doi.org/10.4088/JCP.SU21204IP1

Crossley, N. A., Mechelli, A., Scott, J., Carletti, F., Fox, P. T., McGuire, P., & Bullmore, E. T. (2014). The hubs of the human connectome are generally implicated in the anatomy of brain disorders. *Brain*, *137*(8), 2382–2395. https://doi.org/10.1093/brain/awu132

Cryan, J. F., & Dinan, T. G. (2012). Mind-altering microorganisms: The impact of the gut microbiota on brain and behaviour. *Nature Reviews Neuroscience*, *13*(10), 701–712. https://doi.org/10.1038/nrn3346

Damaraju, E., Allen, E. A., Belger, A., Ford, J. M., McEwen, S., Mathalon, D. H., Mueller, B. A., Pearlson, G. D., Potkin, S. G., Preda, A., Turner, J. A., Vaidya, J. G., van Erp, T. G., & Calhoun, V. D. (2014). Dynamic functional connectivity analysis reveals transient states of dysconnectivity in schizophrenia. *NeuroImage: Clinical*, *5*, 298–308. https://doi.org/10.1016/j.nicl.2014.07.003

Davies, D. L., & Bouldin, D. W. (1979). A Cluster Separation Measure. *IEEE Transactions on Pattern Analysis and Machine Intelligence*, *PAMI-1*(2), 224–227. IEEE Transactions on Pattern Analysis and Machine Intelligence. https://doi.org/10.1109/TPAMI.1979.4766909

de la Fuente-Sandoval, C., Reyes-Madrigal, F., Mao, X., León-Ortiz, P., Rodríguez-Mayoral, O., Jung-Cook, H., Solís-Vivanco, R., Graff-Guerrero, A., & Shungu, D. C. (2018).

Prefrontal and Striatal Gamma-Aminobutyric Acid Levels and the Effect of Antipsychotic Treatment in First-Episode Psychosis Patients. *Biological Psychiatry*, *83*(6), 475–483. https://doi.org/10.1016/j.biopsych.2017.09.028

Deco, G., Jirsa, V. K., Robinson, P. A., Breakspear, M., & Friston, K. (2008). The Dynamic Brain: From Spiking Neurons to Neural Masses and Cortical Fields. *PLOS Computational Biology*, *4*(8), e1000092. https://doi.org/10.1371/journal.pcbi.1000092

Deco, G., Kringelbach, M. L., Arnatkeviciute, A., Oldham, S., Sabaroedin, K., Rogasch, N. C., Aquino, K. M., & Fornito, A. (2021). Dynamical consequences of regional heterogeneity in the brain's transcriptional landscape. *Science Advances*, *7*(29), eabf4752. https://doi.org/10.1126/sciadv.abf4752

Deco, G., Ponce-Alvarez, A., Hagmann, P., Romani, G. L., Mantini, D., & Corbetta, M. (2014). How Local Excitation–Inhibition Ratio Impacts the Whole Brain Dynamics. *Journal of Neuroscience*, *34*(23), 7886–7898. https://doi.org/10.1523/JNEUROSCI.5068-13.2014

Del Fabro, L., Schmidt, A., Fortea, L., Delvecchio, G., D'Agostino, A., Radua, J., Borgwardt, S., & Brambilla, P. (2021). Functional brain network dysfunctions in subjects at high-risk for psychosis: A meta-analysis of resting-state functional connectivity. *Neuroscience & Biobehavioral Reviews*, *128*, 90–101. https://doi.org/10.1016/j.neubiorev.2021.06.020

Demirtaş, M., Falcon, C., Tucholka, A., Gispert, J. D., Molinuevo, J. L., & Deco, G. (2017). A whole-brain computational modeling approach to explain the alterations in resting-state functional connectivity during progression of Alzheimer's disease. *NeuroImage. Clinical*, *16*, 343–354. https://doi.org/10.1016/j.nicl.2017.08.006

Demirtaş, M., Tornador, C., Falcón, C., López-Solà, M., Hernández-Ribas, R., Pujol, J., Menchón, J. M., Ritter, P., Cardoner, N., Soriano-Mas, C., & Deco, G. (2016). Dynamic functional connectivity reveals altered variability in functional connectivity among patients with major depressive disorder. *Human Brain Mapping*, *37*(8), 2918–2930. https://doi.org/10.1002/hbm.23215

Deng, Y., Han, S., Cheng, D., Li, H., Zhang, B., Kong, Y., Lin, Y., Li, Y., Wen, G., & Liu, K. (2021). Simultaneously decreased temporal variability and enhanced variability-strength coupling of emotional network connectivities are related to positive symptoms in patients with schizophrenia. *Brain Imaging and Behavior*, *15*(1), 76–84. https://doi.org/10.1007/s11682-019-00234-0

Deng, Y., Liu, K., Cheng, D., Zhang, J., Chen, H., Chen, B., Li, Y., Wang, W., Kong, Y., & Wen, G. (2019). Ventral and dorsal visual pathways exhibit abnormalities of static and dynamic connectivities, respectively, in patients with schizophrenia. *Schizophrenia Research*, *206*, 103–110. https://doi.org/10.1016/j.schres.2018.12.005

Desikan, R. S., Ségonne, F., Fischl, B., Quinn, B. T., Dickerson, B. C., Blacker, D., Buckner, R. L., Dale, A. M., Maguire, R. P., Hyman, B. T., Albert, M. S., & Killiany, R. J. (2006). An automated labeling system for subdividing the human cerebral cortex on MRI scans into gyral based regions of interest. *NeuroImage*, *31*(3), 968–980. https://doi.org/10.1016/j.neuroimage.2006.01.021

DGPPN e.V. (Ed.). (2019). *S3 Guideline for Schizophrenia*.

Domhof, J. W. M., Jung, K., Eickhoff, S. B., & Popovych, O. V. (2021). Parcellation-induced variation of empirical and simulated brain connectomes at group and subject levels. *Network Neuroscience*, *5*(3), 798–830. https://doi.org/10.1162/netn_a_00202

Domhof, J. W. M., Jung, K., Eickhoff, S. B., & Popovych, O. V. (2022a). *Parcellation-based resting-state blood-oxygen-level-dependent (BOLD) signals of a healthy cohort*

(v1.0). EBRAINS. https://doi.org/10.25493/F9DP-WCQ
Domhof, J. W. M., Jung, K., Eickhoff, S. B., & Popovych, O. V. (2022b). *Parcellation-based structural and resting-state functional brain connectomes of a healthy cohort (v1.1)*. EBRAINS. https://doi.org/10.25493/NVS8-XS5
Dong, D., Duan, M., Wang, Y., Zhang, X., Jia, X., Li, Y., Xin, F., Yao, D., & Luo, C. (2019). Reconfiguration of Dynamic Functional Connectivity in Sensory and Perceptual System in Schizophrenia. *Cerebral Cortex*, *29*(8), 3577–3589. https://doi.org/10.1093/cercor/bhy232
Dong, D., Wang, Y., Chang, X., Luo, C., & Yao, D. (2018). Dysfunction of Large-Scale Brain Networks in Schizophrenia: A Meta-analysis of Resting-State Functional Connectivity. *Schizophrenia Bulletin*, *44*(1), 168–181. https://doi.org/10.1093/schbul/sbx034
Dosenbach, N. U. F., Nardos, B., Cohen, A. L., Fair, D. A., Power, J. D., Church, J. A., Nelson, S. M., Wig, G. S., Vogel, A. C., Lessov-Schlaggar, C. N., Barnes, K. A., Dubis, J. W., Feczko, E., Coalson, R. S., Pruett, J. R., Barch, D. M., Petersen, S. E., & Schlaggar, B. L. (2010). Prediction of individual brain maturity using fMRI. *Science (New York, N.Y.)*, *329*(5997), 1358–1361. https://doi.org/10.1126/science.1194144
Douglas, R. J., Koch, C., Mahowald, M., Martin, K. A. C., & Suarez, H. H. (1995). Recurrent Excitation in Neocortical Circuits. *Science*, *269*(5226), 981–985. https://doi.org/10.1126/science.7638624
Driesen, N. R., McCarthy, G., Bhagwagar, Z., Bloch, M., Calhoun, V., D'Souza, D. C., Gueorguieva, R., He, G., Ramachandran, R., Suckow, R. F., Anticevic, A., Morgan, P. T., & Krystal, J. H. (2013). Relationship of resting brain hyperconnectivity and schizophrenia-like symptoms produced by the NMDA receptor antagonist ketamine in humans. *Molecular Psychiatry*, *18*(11), 1199–1204. https://doi.org/10.1038/mp.2012.194
Drysdale, A. T., Grosenick, L., Downar, J., Dunlop, K., Mansouri, F., Meng, Y., Fetcho, R. N., Zebley, B., Oathes, D. J., Etkin, A., Schatzberg, A. F., Sudheimer, K., Keller, J., Mayberg, H. S., Gunning, F. M., Alexopoulos, G. S., Fox, M. D., Pascual-Leone, A., Voss, H. U., … Liston, C. (2017). Resting-state connectivity biomarkers define neurophysiological subtypes of depression. *Nature Medicine*, *23*(1), 28–38. https://doi.org/10.1038/nm.4246
Du, M., Zhang, L., Li, L., Ji, E., Han, X., Huang, G., Liang, Z., Shi, L., Yang, H., & Zhang, Z. (2021). Abnormal transitions of dynamic functional connectivity states in bipolar disorder: A whole-brain resting-state fMRI study. *Journal of Affective Disorders*, *289*, 7–15. https://doi.org/10.1016/j.jad.2021.04.005
Du, Y., Fryer, S. L., Fu, Z., Lin, D., Sui, J., Chen, J., Damaraju, E., Mennigen, E., Stuart, B., Mathalon, D. H., & Calhoun, V. D. (2018). Dynamic functional connectivity impairments in early schizophrenia and clinical high-risk for psychosis. *NeuroImage*, *180*(Pt B), 632–645. https://doi.org/10.1016/j.neuroimage.2017.10.022
Dubovsky, S. L., Ghosh, B. M., Serotte, J. C., & Cranwell, V. (2021). Psychotic Depression: Diagnosis, Differential Diagnosis, and Treatment. *Psychotherapy and Psychosomatics*, *90*(3), 160–177. https://doi.org/10.1159/000511348
Dunn, O. J. (1961). Multiple Comparisons among Means. *Journal of the American Statistical Association*, *56*(293), 52–64. https://doi.org/10.1080/01621459.1961.10482090
Elam, J. S., Glasser, M. F., Harms, M. P., Sotiropoulos, S. N., Andersson, J. L. R., Burgess, G. C., Curtiss, S. W., Oostenveld, R., Larson-Prior, L. J., Schoffelen, J.-M., Hodge, M. R., Cler, E. A., Marcus, D. M., Barch, D. M., Yacoub, E., Smith, S. M., Ugurbil, K.,

& Van Essen, D. C. (2021). The Human Connectome Project: A retrospective. *NeuroImage*, *244*, 118543. https://doi.org/10.1016/j.neuroimage.2021.118543

El-Baba, M., Lewis, D. J., Fang, Z., Owen, A. M., Fogel, S. M., & Morton, J. B. (2019). Functional connectivity dynamics slow with descent from wakefulness to sleep. *PLOS ONE*, *14*(12), e0224669. https://doi.org/10.1371/journal.pone.0224669

Eliason, M. J., & Richman, L. C. (1987). The Continuous Performance Test in Learning Disabled and Nondisabled Children. *Journal of Learning Disabilities*, *20*(10), 614–619. https://doi.org/10.1177/002221948702001007

Espinoza, F. A., Vergara, V. M., Damaraju, E., Henke, K. G., Faghiri, A., Turner, J. A., Belger, A. A., Ford, J. M., McEwen, S. C., Mathalon, D. H., Mueller, B. A., Potkin, S. G., Preda, A., Vaidya, J. G., van Erp, T. G. M., & Calhoun, V. D. (2019). Characterizing Whole Brain Temporal Variation of Functional Connectivity via Zero and First Order Derivatives of Sliding Window Correlations. *Frontiers in Neuroscience*, *13*. https://doi.org/10.3389/fnins.2019.00634

Fiorentini, A., Cantù, F., Crisanti, C., Cereda, G., Oldani, L., & Brambilla, P. (2021). Substance-Induced Psychoses: An Updated Literature Review. *Frontiers in Psychiatry*, *12*. https://doi.org/10.3389/fpsyt.2021.694863

First, M. B., Spitzer, R. L., Gibbon, M., & Williams, J. B. W. (2002). *Structured Clinical Interview DSM-IV-TR Axis I Disorders, Research Version, Patient Edition. (SCID-I/P)*. New York: Biometrics Research, New York State Psychiatric Institute.

Flinker, A., Korzeniewska, A., Shestyuk, A. Y., Franaszczuk, P. J., Dronkers, N. F., Knight, R. T., & Crone, N. E. (2015). Redefining the role of Broca's area in speech. *Proceedings of the National Academy of Sciences*, *112*(9), 2871–2875. https://doi.org/10.1073/pnas.1414491112

Fortin, J., & Robert-Fitzgerald, T. (2018). *neuroCombat* [Computer software]. GitHub. https://github.com/Jfortin1/neuroCombat

Fortin, J.-P., Cullen, N., Sheline, Y. I., Taylor, W. D., Aselcioglu, I., Cook, P. A., Adams, P., Cooper, C., Fava, M., McGrath, P. J., McInnis, M., Phillips, M. L., Trivedi, M. H., Weissman, M. M., & Shinohara, R. T. (2018). Harmonization of cortical thickness measurements across scanners and sites. *NeuroImage*, *167*, 104–120. https://doi.org/10.1016/j.neuroimage.2017.11.024

Fransson, P., & Thompson, W. H. (2020). Temporal flow of hubs and connectivity in the human brain. *NeuroImage*, *223*, 117348. https://doi.org/10.1016/j.neuroimage.2020.117348

Friston, K. J., Harrison, L., & Penny, W. (2003). Dynamic causal modelling. *NeuroImage*, *19*(4), 1273–1302. https://doi.org/10.1016/S1053-8119(03)00202-7

Fu, Z., Sui, J., Turner, J. A., Du, Y., Assaf, M., Pearlson, G. D., & Calhoun, V. D. (2021). Dynamic functional network reconfiguration underlying the pathophysiology of schizophrenia and autism spectrum disorder. *Human Brain Mapping*, *42*(1), 80–94. https://doi.org/10.1002/hbm.25205

Fusar-Poli, P., Borgwardt, S., Bechdolf, A., Addington, J., Riecher-Rössler, A., Schultze-Lutter, F., Keshavan, M., Wood, S., Ruhrmann, S., Seidman, L. J., Valmaggia, L., Cannon, T., Velthorst, E., De Haan, L., Cornblatt, B., Bonoldi, I., Birchwood, M., McGlashan, T., Carpenter, W., … Yung, A. (2013). The Psychosis High-Risk State. *JAMA Psychiatry*, *70*(1), 107–120. https://doi.org/10.1001/jamapsychiatry.2013.269

Fusar-Poli, P., McGorry, P. D., & Kane, J. M. (2017). Improving outcomes of first-episode psychosis: An overview. *World Psychiatry*, *16*(3), 251–265. https://doi.org/10.1002/wps.20446

Gage, S. H., Hickman, M., & Zammit, S. (2016). Association Between Cannabis and Psychosis: Epidemiologic Evidence. *Biological Psychiatry*, *79*(7), 549–556. https://doi.org/10.1016/j.biopsych.2015.08.001

Gallo, S., El-Gazzar, A., Zhutovsky, P., Thomas, R. M., Javaheripour, N., Li, M., Bartova, L., Bathula, D., Dannlowski, U., Davey, C., Frodl, T., Gotlib, I., Grimm, S., Grotegerd, D., Hahn, T., Hamilton, P. J., Harrison, B. J., Jansen, A., Kircher, T., … van Wingen, G. (2023). Functional connectivity signatures of major depressive disorder: Machine learning analysis of two multicenter neuroimaging studies. *Molecular Psychiatry*, *28*(7), 3013–3022. https://doi.org/10.1038/s41380-023-01977-5

Gaser, C., Dahnke, R., Thompson, P. M., Kurth, F., Luders, E., & the Alzheimer's Disease Neuroimaging Initiative. (2024). CAT: A computational anatomy toolbox for the analysis of structural MRI data. *GigaScience*, *13*, giae049. https://doi.org/10.1093/gigascience/giae049

GBD 2021 Diseases and Injuries Collaborators. (2024). Global incidence, prevalence, years lived with disability (YLDs), disability-adjusted life-years (DALYs), and healthy life expectancy (HALE) for 371 diseases and injuries in 204 countries and territories and 811 subnational locations, 1990–2021: A systematic analysis for the Global Burden of Disease Study 2021. *Lancet (London, England)*, *403*(10440), 2133–2161. https://doi.org/10.1016/S0140-6736(24)00757-8

Geerligs, L., Renken, R. J., Saliasi, E., Maurits, N. M., & Lorist, M. M. (2015). A Brain-Wide Study of Age-Related Changes in Functional Connectivity. *Cerebral Cortex*, *25*(7), 1987–1999. https://doi.org/10.1093/cercor/bhu012

Glasser, M. F., Sotiropoulos, S. N., Wilson, J. A., Coalson, T. S., Fischl, B., Andersson, J. L., Xu, J., Jbabdi, S., Webster, M., Polimeni, J. R., Van Essen, D. C., & Jenkinson, M. (2013). The minimal preprocessing pipelines for the Human Connectome Project. *NeuroImage*, *80*, 105–124. https://doi.org/10.1016/j.neuroimage.2013.04.127

Godin, S.-L., & Shehata, S. (2022). Adolescent cannabis use and later development of schizophrenia: An updated systematic review of longitudinal studies. *Journal of Clinical Psychology*, *78*(7), 1331–1340. https://doi.org/10.1002/jclp.23312

Gonzalez-Castillo, J., & Bandettini, P. A. (2018). Task-based dynamic functional connectivity: Recent findings and open questions. *NeuroImage*, *180*, 526–533. https://doi.org/10.1016/j.neuroimage.2017.08.006

Goodkind, M., Eickhoff, S. B., Oathes, D. J., Jiang, Y., Chang, A., Jones-Hagata, L. B., Ortega, B. N., Zaiko, Y. V., Roach, E. L., Korgaonkar, M. S., Grieve, S. M., Galatzer-Levy, I., Fox, P. T., & Etkin, A. (2015). Identification of a common neurobiological substrate for mental illness. *JAMA Psychiatry*, *72*(4), 305–315. https://doi.org/10.1001/jamapsychiatry.2014.2206

Grace, A. A. (2016). Dysregulation of the dopamine system in the pathophysiology of schizophrenia and depression. *Nature Reviews Neuroscience*, *17*(8), Article 8. https://doi.org/10.1038/nrn.2016.57

Griffanti, L., Salimi-Khorshidi, G., Beckmann, C. F., Auerbach, E. J., Douaud, G., Sexton, C. E., Zsoldos, E., Ebmeier, K. P., Filippini, N., Mackay, C. E., Moeller, S., Xu, J., Yacoub, E., Baselli, G., Ugurbil, K., Miller, K. L., & Smith, S. M. (2014). ICA-based artefact removal and accelerated fMRI acquisition for improved resting state network imaging. *NeuroImage*, *95*, 232–247. https://doi.org/10.1016/j.neuroimage.2014.03.034

Gu, H., Hu, Y., Chen, X., He, Y., & Yang, Y. (2019). Regional excitation-inhibition balance predicts default-mode network deactivation via functional connectivity. *NeuroImage*,

185, 388–397. https://doi.org/10.1016/j.neuroimage.2018.10.055

Haas, S. S., Antonucci, L. A., Wenzel, J., Ruef, A., Biagianti, B., Paolini, M., Rauchmann, B.-S., Weiske, J., Kambeitz, J., Borgwardt, S., Brambilla, P., Meisenzahl, E., Salokangas, R. K. R., Upthegrove, R., Wood, S. J., Koutsouleris, N., & Kambeitz-Ilankovic, L. (2021). A multivariate neuromonitoring approach to neuroplasticity-based computerized cognitive training in recent onset psychosis. *Neuropsychopharmacology*, *46*(4), Article 4. https://doi.org/10.1038/s41386-020-00877-4

Hansen, J. Y., Shafiei, G., Markello, R. D., Smart, K., Cox, S. M. L., Nørgaard, M., Beliveau, V., Wu, Y., Gallezot, J.-D., Aumont, É., Servaes, S., Scala, S. G., DuBois, J. M., Wainstein, G., Bezgin, G., Funck, T., Schmitz, T. W., Spreng, R. N., Galovic, M., … Misic, B. (2022). Mapping neurotransmitter systems to the structural and functional organization of the human neocortex. *Nature Neuroscience*, *25*(11), 1569–1581. https://doi.org/10.1038/s41593-022-01186-3

Hawrylycz, M. J., Lein, E. S., Guillozet-Bongaarts, A. L., Shen, E. H., Ng, L., Miller, J. A., van de Lagemaat, L. N., Smith, K. A., Ebbert, A., Riley, Z. L., Abajian, C., Beckmann, C. F., Bernard, A., Bertagnolli, D., Boe, A. F., Cartagena, P. M., Chakravarty, M. M., Chapin, M., Chong, J., … Jones, A. R. (2012). An anatomically comprehensive atlas of the adult human brain transcriptome. *Nature*, *489*(7416), 391–399. https://doi.org/10.1038/nature11405

He, H., Shang, Y., Yang, X., Di, Y., Lin, J., Zhu, Y., Zheng, W., Zhao, J., Ji, M., Dong, L., Deng, N., Lei, Y., & Chai, Z. (2019). Constructing an Associative Memory System Using Spiking Neural Network. *Frontiers in Neuroscience*, *13*. https://doi.org/10.3389/fnins.2019.00650

Heeger, D. J., & Ress, D. (2002). What does fMRI tell us about neuronal activity? *Nature Reviews Neuroscience*, *3*(2), 142–151. https://doi.org/10.1038/nrn730

Herzog, R., Mediano, P. A. M., Rosas, F. E., Lodder, P., Carhart-Harris, R., Perl, Y. S., Tagliazucchi, E., & Cofre, R. (2023). A whole-brain model of the neural entropy increase elicited by psychedelic drugs. *Scientific Reports*, *13*(1), Article 1. https://doi.org/10.1038/s41598-023-32649-7

Hjorthøj, C., Arnfred, B., Behrendt, S., Møller, S. B., & Nordentoft, M. (2021). Substance-induced psychosis as a risk factor for unipolar depression or anxiety disorders–A nationwide register-based prospective cohort study. *Journal of Affective Disorders*, *295*, 960–966. https://doi.org/10.1016/j.jad.2021.09.004

Ho, B.-C., Andreasen, N. C., Ziebell, S., Pierson, R., & Magnotta, V. (2011). Long-term Antipsychotic Treatment and Brain Volumes: A Longitudinal Study of First-Episode Schizophrenia. *Archives of General Psychiatry*, *68*(2), 128–137. https://doi.org/10.1001/archgenpsychiatry.2010.199

Ho, V. M., Lee, J.-A., & Martin, K. C. (2011). The Cell Biology of Synaptic Plasticity. *Science*, *334*(6056), 623–628. https://doi.org/10.1126/science.1209236

Honey, C. J., Kötter, R., Breakspear, M., & Sporns, O. (2007). Network structure of cerebral cortex shapes functional connectivity on multiple time scales. *Proceedings of the National Academy of Sciences*, *104*(24), 10240–10245. https://doi.org/10.1073/pnas.0701519104

Honey, C. J., Sporns, O., Cammoun, L., Gigandet, X., Thiran, J. P., Meuli, R., & Hagmann, P. (2009). Predicting human resting-state functional connectivity from structural connectivity. *Proceedings of the National Academy of Sciences*, *106*(6), 2035–2040. https://doi.org/10.1073/pnas.0811168106

Horan, W. P., Blanchard, J. J., Clark, L. A., & Green, M. F. (2008). Affective Traits in Schizophrenia and Schizotypy. *Schizophrenia Bulletin*, *34*(5), 856–874. https://doi.org/10.1093/schbul/sbn083

Hotelling, H. (1936). Relations Between Two Sets of Variates. *Biometrika*, *28*(3/4), 321–377. https://doi.org/10.2307/2333955

Hotelling, H. (1953). New Light on the Correlation Coefficient and its Transforms. *Journal of the Royal Statistical Society: Series B (Methodological)*, *15*(2), 193–225. https://doi.org/10.1111/j.2517-6161.1953.tb00135.x

Howard, D. M., Adams, M. J., Clarke, T.-K., Hafferty, J. D., Gibson, J., Shirali, M., Coleman, J. R. I., Hagenaars, S. P., Ward, J., Wigmore, E. M., Alloza, C., Shen, X., Barbu, M. C., Xu, E. Y., Whalley, H. C., Marioni, R. E., Porteous, D. J., Davies, G., Deary, I. J., … McIntosh, A. M. (2019). Genome-wide meta-analysis of depression identifies 102 independent variants and highlights the importance of the prefrontal brain regions. *Nature Neuroscience*, *22*(3), 343–352. https://doi.org/10.1038/s41593-018-0326-7

Howes, O. D., Hird, E. J., Adams, R. A., Corlett, P. R., & McGuire, P. (2020). Aberrant Salience, Information Processing, and Dopaminergic Signaling in People at Clinical High Risk for Psychosis. *Biological Psychiatry*, *88*(4), 304–314. https://doi.org/10.1016/j.biopsych.2020.03.012

Howes, O. D., Kambeitz, J., Kim, E., Stahl, D., Slifstein, M., Abi-Dargham, A., & Kapur, S. (2012). The nature of dopamine dysfunction in schizophrenia and what this means for treatment. *Archives of General Psychiatry*, *69*(8), 776–786. https://doi.org/10.1001/archgenpsychiatry.2012.169

Hu, Y.-T., Tan, Z.-L., Hirjak, D., & Northoff, G. (2023). Brain-wide changes in excitation-inhibition balance of major depressive disorder: A systematic review of topographic patterns of GABA- and glutamatergic alterations. *Molecular Psychiatry*, *28*(8), 3257–3266. https://doi.org/10.1038/s41380-023-02193-x

Hull, J. V., Dokovna, L. B., Jacokes, Z. J., Torgerson, C. M., Irimia, A., & Van Horn, J. D. (2017). Resting-State Functional Connectivity in Autism Spectrum Disorders: A Review. *Frontiers in Psychiatry*, *7*. https://doi.org/10.3389/fpsyt.2016.00205

Huntenburg, J. M., Bazin, P.-L., Goulas, A., Tardif, C. L., Villringer, A., & Margulies, D. S. (2017). A Systematic Relationship Between Functional Connectivity and Intracortical Myelin in the Human Cerebral Cortex. *Cerebral Cortex*, *27*(2), 981–997. https://doi.org/10.1093/cercor/bhx030

Hutchison, R. M., Womelsdorf, T., Allen, E. A., Bandettini, P. A., Calhoun, V. D., Corbetta, M., Della Penna, S., Duyn, J. H., Glover, G. H., Gonzalez-Castillo, J., Handwerker, D. A., Keilholz, S., Kiviniemi, V., Leopold, D. A., de Pasquale, F., Sporns, O., Walter, M., & Chang, C. (2013). Dynamic functional connectivity: Promise, issues, and interpretations. *NeuroImage*, *80*, 360–378. https://doi.org/10.1016/j.neuroimage.2013.05.079

Hutchison, R. M., Womelsdorf, T., Gati, J. S., Everling, S., & Menon, R. S. (2012). Resting-state networks show dynamic functional connectivity in awake humans and anesthetized macaques. *Human Brain Mapping*, *34*(9), 2154–2177. https://doi.org/10.1002/hbm.22058

Jain, A. K. (2010). Data clustering: 50 years beyond K-means. *Pattern Recognition Letters*, *31*(8), 651–666. https://doi.org/10.1016/j.patrec.2009.09.011

Jauhar, S., Cowen, P. J., & Browning, M. (2023). Fifty years on: Serotonin and depression. *Journal of Psychopharmacology*, *37*(3), 237–241. https://doi.org/10.1177/02698811231161813

Jenkins, J. H., & Schumacher, J. G. (1999). Family burden of schizophrenia and depressive illness: Specifying the effects of ethnicity, gender and social ecology. *The British Journal of Psychiatry*, *174*(1), 31–38. https://doi.org/10.1192/bjp.174.1.31

Jeong, B., Wible, C. G., Hashimoto, R.-I., & Kubicki, M. (2009). Functional and anatomical connectivity abnormalities in left inferior frontal gyrus in schizophrenia. *Human Brain Mapping*, *30*(12), 4138–4151. https://doi.org/10.1002/hbm.20835

Jirsa, V. K., Proix, T., Perdikis, D., Woodman, M. M., Wang, H., Gonzalez-Martinez, J., Bernard, C., Bénar, C., Guye, M., Chauvel, P., & Bartolomei, F. (2017). The Virtual Epileptic Patient: Individualized whole-brain models of epilepsy spread. *NeuroImage*, *145*, 377–388. https://doi.org/10.1016/j.neuroimage.2016.04.049

Johnson, W. E., Li, C., & Rabinovic, A. (2007). Adjusting batch effects in microarray expression data using empirical Bayes methods. *Biostatistics*, *8*(1), 118–127. https://doi.org/10.1093/biostatistics/kxj037

Jongsma, H. E., Turner, C., Kirkbride, J. B., & Jones, P. B. (2019). International incidence of psychotic disorders, 2002–17: A systematic review and meta-analysis. *The Lancet Public Health*, *4*(5), e229–e244. https://doi.org/10.1016/S2468-2667(19)30056-8

Kaar, S. J., Natesan, S., McCutcheon, R., & Howes, O. D. (2020). Antipsychotics: Mechanisms underlying clinical response and side-effects and novel treatment approaches based on pathophysiology. *Neuropharmacology*, *172*, 107704. https://doi.org/10.1016/j.neuropharm.2019.107704

Kajumba, M. M., Kakooza-Mwesige, A., Nakasujja, N., Koltai, D., & Canli, T. (2024). Treatment-resistant depression: Molecular mechanisms and management. *Molecular Biomedicine*, *5*(1), 43. https://doi.org/10.1186/s43556-024-00205-y

Kambeitz, J., Cabral, C., Sacchet, M. D., Gotlib, I. H., Zahn, R., Serpa, M. H., Walter, M., Falkai, P., & Koutsouleris, N. (2017). Detecting Neuroimaging Biomarkers for Depression: A Meta-analysis of Multivariate Pattern Recognition Studies. *Biological Psychiatry*, *82*(5), 330–338. https://doi.org/10.1016/j.biopsych.2016.10.028

Kambeitz, J., Kambeitz-Ilankovic, L., Leucht, S., Wood, S., Davatzikos, C., Malchow, B., Falkai, P., & Koutsouleris, N. (2015). Detecting Neuroimaging Biomarkers for Schizophrenia: A Meta-Analysis of Multivariate Pattern Recognition Studies. *Neuropsychopharmacology*, *40*(7), 1742–1751. https://doi.org/10.1038/npp.2015.22

Kambeitz, J. P., & Howes, O. D. (2015). The serotonin transporter in depression: Meta-analysis of in vivo and post mortem findings and implications for understanding and treating depression. *Journal of Affective Disorders*, *186*, 358–366. https://doi.org/10.1016/j.jad.2015.07.034

Kay, S. R., Fiszbein, A., & Opler, L. A. (1987). The positive and negative syndrome scale (PANSS) for schizophrenia. *Schizophrenia Bulletin*, *13*(2), 261–276. https://doi.org/10.1093/schbul/13.2.261

Kern, R. S., Nuechterlein, K. H., Green, M. F., Baade, L. E., Fenton, W. S., Gold, J. M., Keefe, R. S. E., Mesholam-Gately, R., Mintz, J., Seidman, L. J., Stover, E., & Marder, S. R. (2008). The MATRICS Consensus Cognitive Battery, Part 2: Co-Norming and Standardization. *American Journal of Psychiatry*, *165*(2), 214–220. https://doi.org/10.1176/appi.ajp.2007.07010043

Klaassens, B. L., van Gorsel, H. C., Khalili-Mahani, N., van der Grond, J., Wyman, B. T., Whitcher, B., Rombouts, S. A. R. B., & van Gerven, J. M. A. (2015). Single-dose serotonergic stimulation shows widespread effects on functional brain connectivity. *NeuroImage*, *122*, 440–450. https://doi.org/10.1016/j.neuroimage.2015.08.012

Klein, P. C., Ettinger, U., Schirner, M., Ritter, P., Rujescu, D., Falkai, P., Koutsouleris, N.,

Kambeitz-Ilankovic, L., & Kambeitz, J. (2021). Brain Network Simulations Indicate Effects of Neuregulin-1 Genotype on Excitation-Inhibition Balance in Cortical Dynamics. *Cerebral Cortex*, *31*(4), 2013–2025. https://doi.org/10.1093/cercor/bhaa339

Kochunov, P., Thompson, P. M., & Hong, L. E. (2019). Toward High Reproducibility and Accountable Heterogeneity in Schizophrenia Research. *JAMA Psychiatry*, *76*(7), 680–681. https://doi.org/10.1001/jamapsychiatry.2019.0208

Kong, R., Yang, Q., Gordon, E., Xue, A., Yan, X., Orban, C., Zuo, X.-N., Spreng, N., Ge, T., Holmes, A., Eickhoff, S., & Yeo, B. T. T. (2021). Individual-Specific Areal-Level Parcellations Improve Functional Connectivity Prediction of Behavior. *Cerebral Cortex*, *31*(10), 4477–4500. https://doi.org/10.1093/cercor/bhab101

Koutsouleris, N., Dwyer, D. B., Degenhardt, F., Maj, C., Urquijo-Castro, M. F., Sanfelici, R., Popovic, D., Oeztuerk, O., Haas, S. S., Weiske, J., Ruef, A., Kambeitz-Ilankovic, L., Antonucci, L. A., Neufang, S., Schmidt-Kraepelin, C., Ruhrmann, S., Penzel, N., Kambeitz, J., Haidl, T. K., … PRONIA Consortium. (2021). Multimodal Machine Learning Workflows for Prediction of Psychosis in Patients With Clinical High-Risk Syndromes and Recent-Onset Depression. *JAMA Psychiatry*, *78*(2), 195–209. https://doi.org/10.1001/jamapsychiatry.2020.3604

Koutsouleris, N., & Fusar-Poli, P. (2024). From Heterogeneity to Precision: Redefining Diagnosis, Prognosis, and Treatment of Mental Disorders. *Biological Psychiatry*, *96*(7), 508–510. https://doi.org/10.1016/j.biopsych.2024.07.015

Koutsouleris, N., Kambeitz-Ilankovic, L., Ruhrmann, S., Rosen, M., Ruef, A., Dwyer, D. B., Paolini, M., Chisholm, K., Kambeitz, J., Haidl, T., Schmidt, A., Gillam, J., Schultze-Lutter, F., Falkai, P., Reiser, M., Riecher-Rössler, A., Upthegrove, R., Hietala, J., Salokangas, R. K. R., … PRONIA Consortium. (2018). Prediction Models of Functional Outcomes for Individuals in the Clinical High-Risk State for Psychosis or With Recent-Onset Depression: A Multimodal, Multisite Machine Learning Analysis. *JAMA Psychiatry*, *75*(11), 1156–1172. https://doi.org/10.1001/jamapsychiatry.2018.2165

Kugaya, A., Seneca, N. M., Snyder, P. J., Williams, S. A., Malison, R. T., Baldwin, R. M., Seibyl, J. P., & Innis, R. B. (2003). Changes in human in vivo serotonin and dopamine transporter availabilities during chronic antidepressant administration. *Neuropsychopharmacology: Official Publication of the American College of Neuropsychopharmacology*, *28*(2), 413–420. https://doi.org/10.1038/sj.npp.1300036

Kunze, T., Hunold, A., Haueisen, J., Jirsa, V., & Spiegler, A. (2016). Transcranial direct current stimulation changes resting state functional connectivity: A large-scale brain network modeling study. *NeuroImage*, *140*, 174–187. https://doi.org/10.1016/j.neuroimage.2016.02.015

Latora, V., & Marchiori, M. (2001). Efficient Behavior of Small-World Networks. *Physical Review Letters*, *87*(19), 198701. https://doi.org/10.1103/PhysRevLett.87.198701

Laumann, T. O., Gordon, E. M., Adeyemo, B., Snyder, A. Z., Joo, S. J., Chen, M.-Y., Gilmore, A. W., McDermott, K. B., Nelson, S. M., Dosenbach, N. U. F., Schlaggar, B. L., Mumford, J. A., Poldrack, R. A., & Petersen, S. E. (2015). Functional system and areal organization of a highly sampled individual human brain. *Neuron*, *87*(3), 657–670. https://doi.org/10.1016/j.neuron.2015.06.037

Leonardi, N., & Van De Ville, D. (2015). On spurious and real fluctuations of dynamic functional connectivity during rest. *NeuroImage*, *104*, 430–436. https://doi.org/10.1016/j.neuroimage.2014.09.007

Levar, N., Van Doesum, T. J., Denys, D., & Van Wingen, G. A. (2019). Anterior cingulate GABA and glutamate concentrations are associated with resting-state network connectivity. *Scientific Reports*, *9*(1), 2116. https://doi.org/10.1038/s41598-018-38078-1

Li, T., Wang, Q., Zhang, J., Rolls, E. T., Yang, W., Palaniyappan, L., Zhang, L., Cheng, W., Yao, Y., Liu, Z., Gong, X., Luo, Q., Tang, Y., Crow, T. J., Broome, M. R., Xu, K., Li, C., Wang, J., Liu, Z., … Feng, J. (2017). Brain-Wide Analysis of Functional Connectivity in First-Episode and Chronic Stages of Schizophrenia. *Schizophrenia Bulletin*, *43*(2), 436–448. https://doi.org/10.1093/schbul/sbw099

Li, Y., Zhu, Y., Nguchu, B. A., Wang, Y., Wang, H., Qiu, B., & Wang, X. (2020). Dynamic Functional Connectivity Reveals Abnormal Variability and Hyper-connected Pattern in Autism Spectrum Disorder. *Autism Research*, *13*(2), 230–243. https://doi.org/10.1002/aur.2212

Lidsky, T. I., Yablonsky-Alter, E., Zuck, L. G., & Banerjee, S. P. (1997). Antipsychotic drug effects on glutamatergic activity. *Brain Research*, *764*(1), 46–52. https://doi.org/10.1016/S0006-8993(97)00423-X

Liégeois, R., Li, J., Kong, R., Orban, C., Van De Ville, D., Ge, T., Sabuncu, M. R., & Yeo, B. T. T. (2019). Resting brain dynamics at different timescales capture distinct aspects of human behavior. *Nature Communications*, *10*(1), 2317. https://doi.org/10.1038/s41467-019-10317-7

Lloyd, S. (1982). Least squares quantization in PCM. *IEEE Transactions on Information Theory*, *28*(2), 129–137. IEEE Transactions on Information Theory. https://doi.org/10.1109/TIT.1982.1056489

Lubba, C. H., Sethi, S. S., Knaute, P., Schultz, S. R., Fulcher, B. D., & Jones, N. S. (2019). catch22: CAnonical Time-series CHaracteristics. *Data Mining and Knowledge Discovery*, *33*(6), 1821–1852. https://doi.org/10.1007/s10618-019-00647-x

Luppi, A. I., Carhart-Harris, R. L., Roseman, L., Pappas, I., Menon, D. K., & Stamatakis, E. A. (2021). LSD alters dynamic integration and segregation in the human brain. *NeuroImage*, *227*, 117653. https://doi.org/10.1016/j.neuroimage.2020.117653

Lurie, D. J., Kessler, D., Bassett, D. S., Betzel, R. F., Breakspear, M., Kheilholz, S., Kucyi, A., Liégeois, R., Lindquist, M. A., McIntosh, A. R., Poldrack, R. A., Shine, J. M., Thompson, W. H., Bielczyk, N. Z., Douw, L., Kraft, D., Miller, R. L., Muthuraman, M., Pasquini, L., … Calhoun, V. D. (2020). Questions and controversies in the study of time-varying functional connectivity in resting fMRI. *Network Neuroscience*, *4*(1), 30–69. https://doi.org/10.1162/netn_a_00116

Lynch, C. J., Gunning, F. M., & Liston, C. (2020). Causes and Consequences of Diagnostic Heterogeneity in Depression: Paths to Discovering Novel Biological Depression Subtypes. *Biological Psychiatry*, *88*(1), 83–94. https://doi.org/10.1016/j.biopsych.2020.01.012

Maćkiewicz, A., & Ratajczak, W. (1993). Principal components analysis (PCA). *Computers & Geosciences*, *19*(3), 303–342. https://doi.org/10.1016/0098-3004(93)90090-R

Mallikarjun, P. K., Lalousis, P. A., Dunne, T. F., Heinze, K., Reniers, R. L., Broome, M. R., Farmah, B., Oyebode, F., Wood, S. J., & Upthegrove, R. (2018). Aberrant salience network functional connectivity in auditory verbal hallucinations: A first episode psychosis sample. *Translational Psychiatry*, *8*(1), Article 1. https://doi.org/10.1038/s41398-018-0118-6

Mandeville, J. B., Marota, J. J. A., Ayata, C., Zaharchuk, G., Moskowitz, M. A., Rosen, B. R., & Weisskoff, R. M. (1999). *Evidence of a Cerebrovascular Postarteriole Windkessel*

with Delayed Compliance. https://journals.sagepub.com/doi/full/10.1097/00004647-199906000-00012

Manjón, J. V., Carbonell-Caballero, J., Lull, J. J., García-Martí, G., Martí-Bonmatí, L., & Robles, M. (2008). MRI denoising using non-local means. *Medical Image Analysis*, *12*(4), 514–523. https://doi.org/10.1016/j.media.2008.02.004

Mann, H. B., & Whitney, D. R. (1947). On a Test of Whether one of Two Random Variables is Stochastically Larger than the Other. *The Annals of Mathematical Statistics*, *18*(1), 50–60. https://doi.org/10.1214/aoms/1177730491

Marder, E. (2012). Neuromodulation of Neuronal Circuits: Back To The Future. *Neuron*, *76*(1), 1–11. https://doi.org/10.1016/j.neuron.2012.09.010

Markello, R. D., Arnatkeviciute, A., Poline, J.-B., Fulcher, B. D., Fornito, A., & Misic, B. (2021). Standardizing workflows in imaging transcriptomics with the abagen toolbox. *eLife*, *10*, e72129. https://doi.org/10.7554/eLife.72129

Markello, R. D., Hansen, J. Y., Liu, Z.-Q., Bazinet, V., Shafiei, G., Suárez, L. E., Blostein, N., Seidlitz, J., Baillet, S., Satterthwaite, T. D., Chakravarty, M. M., Raznahan, A., & Misic, B. (2022). neuromaps: Structural and functional interpretation of brain maps. *Nature Methods*, *19*(11), 1472–1479. https://doi.org/10.1038/s41592-022-01625-w

Marshall, C. R., Howrigan, D. P., Merico, D., Thiruvahindrapuram, B., Wu, W., Greer, D. S., Antaki, D., Shetty, A., Holmans, P. A., Pinto, D., Gujral, M., Brandler, W. M., Malhotra, D., Wang, Z., Fajarado, K. V. F., Maile, M. S., Ripke, S., Agartz, I., Albus, M., … Sebat, J. (2017). Contribution of copy number variants to schizophrenia from a genome-wide study of 41,321 subjects. *Nature Genetics*, *49*(1), 27–35. https://doi.org/10.1038/ng.3725

Marusak, H. A., Calhoun, V. D., Brown, S., Crespo, L. M., Sala-Hamrick, K., Gotlib, I. H., & Thomason, M. E. (2017). Dynamic functional connectivity of neurocognitive networks in children. *Human Brain Mapping*, *38*(1), 97–108. https://doi.org/10.1002/hbm.23346

Marwaha, S., Palmer, E., Suppes, T., Cons, E., Young, A. H., & Upthegrove, R. (2023). Novel and emerging treatments for major depression. *The Lancet*, *401*(10371), 141–153. https://doi.org/10.1016/S0140-6736(22)02080-3

McCutcheon, R. A., Krystal, J. H., & Howes, O. D. (2020). Dopamine and glutamate in schizophrenia: Biology, symptoms and treatment. *World Psychiatry*, *19*(1), 15–33. https://doi.org/10.1002/wps.20693

McCutcheon, R. A., Nour, M. M., Dahoun, T., Jauhar, S., Pepper, F., Expert, P., Veronese, M., Adams, R. A., Turkheimer, F., Mehta, M. A., & Howes, O. D. (2019). Mesolimbic Dopamine Function Is Related to Salience Network Connectivity: An Integrative Positron Emission Tomography and Magnetic Resonance Study. *Biological Psychiatry*, *85*(5), 368–378. https://doi.org/10.1016/j.biopsych.2018.09.010

McCutcheon, R. A., Reis Marques, T., & Howes, O. D. (2020). Schizophrenia—An Overview. *JAMA Psychiatry*, *77*(2), 201–210. https://doi.org/10.1001/jamapsychiatry.2019.3360

McGlashan, T., Walsh, B., & Woods, S. (2010). *The Psychosis Risk Syndrome: Handbook for Diagnosis and Follow-Up*. Oxford University Press.

McGorry, P. D., Nelson, B., Goldstone, S., & Yung, A. R. (2010). Clinical Staging: A Heuristic and Practical Strategy for New Research and Better Health and Social Outcomes for Psychotic and Related Mood Disorders. *The Canadian Journal of Psychiatry*, *55*(8), 486–497. https://doi.org/10.1177/070674371005500803

McIntyre, R. S., Filteau, M.-J., Martin, L., Patry, S., Carvalho, A., Cha, D. S., Barakat, M., & Miguelez, M. (2014). Treatment-resistant depression: Definitions, review of the evidence, and algorithmic approach. *Journal of Affective Disorders*, *156*, 1–7.

https://doi.org/10.1016/j.jad.2013.10.043
Mehta, U. M., Ibrahim, F. A., Sharma, M. S., Venkatasubramanian, G., Thirthalli, J., Bharath, R. D., Bolo, N. R., Gangadhar, B. N., & Keshavan, M. S. (2021). Resting-state functional connectivity predictors of treatment response in schizophrenia – A systematic review and meta-analysis. *Schizophrenia Research*, *237*, 153–165. https://doi.org/10.1016/j.schres.2021.09.004
Meier, J. M., Perdikis, D., Blickensdörfer, A., Stefanovski, L., Liu, Q., Maith, O., Dinkelbach, H. Ü., Baladron, J., Hamker, F. H., & Ritter, P. (2022). Virtual deep brain stimulation: Multiscale co-simulation of a spiking basal ganglia model and a whole-brain mean-field model with The Virtual Brain. *Experimental Neurology*, *354*, 114111. https://doi.org/10.1016/j.expneurol.2022.114111
Menon, V. (2011). Large-scale brain networks and psychopathology: A unifying triple network model. *Trends in Cognitive Sciences*, *15*(10), 483–506. https://doi.org/10.1016/j.tics.2011.08.003
Merritt, K., Egerton, A., Kempton, M. J., Taylor, M. J., & McGuire, P. K. (2016). Nature of Glutamate Alterations in Schizophrenia: A Meta-analysis of Proton Magnetic Resonance Spectroscopy Studies. *JAMA Psychiatry*, *73*(7), 665–674. https://doi.org/10.1001/jamapsychiatry.2016.0442
Merritt, K., McCutcheon, R. A., Aleman, A., Ashley, S., Beck, K., Block, W., Bloemen, O. J. N., Borgan, F., Boules, C., Bustillo, J. R., Capizzano, A. A., Coughlin, J. M., David, A., de la Fuente-Sandoval, C., Demjaha, A., Dempster, K., Do, K. Q., Du, F., Falkai, P., … Egerton, A. (2023). Variability and magnitude of brain glutamate levels in schizophrenia: A meta and mega-analysis. *Molecular Psychiatry*, *28*(5), 2039–2048. https://doi.org/10.1038/s41380-023-01991-7
Miao, J., Tantawi, M., Alizadeh, M., Thalheimer, S., Vedaei, F., Romo, V., Mohamed, F. B., & Wu, C. (2023). Characteristic dynamic functional connectivity during sevoflurane-induced general anesthesia. *Scientific Reports*, *13*(1), 21014. https://doi.org/10.1038/s41598-023-43832-1
Mietus, J. E., Peng, C.-K., Henry, I., Goldsmith, R. L., & Goldberger, A. L. (2002). The pNNx files: Re-examining a widely used heart rate variability measure. *Heart*, *88*(4), 378–380. https://doi.org/10.1136/heart.88.4.378
Milaneschi, Y., Lamers, F., Berk, M., & Penninx, B. W. J. H. (2020). Depression Heterogeneity and Its Biological Underpinnings: Toward Immunometabolic Depression. *Biological Psychiatry*, *88*(5), 369–380. https://doi.org/10.1016/j.biopsych.2020.01.014
Misiak, B., Krefft, M., Bielawski, T., Moustafa, A. A., Sąsiadek, M. M., & Frydecka, D. (2017). Toward a unified theory of childhood trauma and psychosis: A comprehensive review of epidemiological, clinical, neuropsychological and biological findings. *Neuroscience & Biobehavioral Reviews*, *75*, 393–406. https://doi.org/10.1016/j.neubiorev.2017.02.015
Moncrieff, J., Cooper, R. E., Stockmann, T., Amendola, S., Hengartner, M. P., & Horowitz, M. A. (2023). The serotonin theory of depression: A systematic umbrella review of the evidence. *Molecular Psychiatry*, *28*(8), 3243–3256. https://doi.org/10.1038/s41380-022-01661-0
Moran, L. V., Ongur, D., Hsu, J., Castro, V. M., Perlis, R. H., & Schneeweiss, S. (2019). Psychosis with Methylphenidate or Amphetamine in Patients with ADHD. *New England Journal of Medicine*, *380*(12), 1128–1138. https://doi.org/10.1056/NEJMoa1813751

Moret, C., & Briley, M. (2011). The importance of norepinephrine in depression. *Neuropsychiatric Disease and Treatment*, *7*(sup1), 9–13. https://doi.org/10.2147/NDT.S19619

Muenzenmaier, K. H., Seixas, A. A., Schneeberger, A. R., Castille, D. M., Battaglia, J., & Link, B. G. (2015). Cumulative Effects of Stressful Childhood Experiences on Delusions and Hallucinations. *Journal of Trauma & Dissociation*, *16*(4), 442–462. https://doi.org/10.1080/15299732.2015.1018475

Mulders, P. C., van Eijndhoven, P. F., Schene, A. H., Beckmann, C. F., & Tendolkar, I. (2015). Resting-state functional connectivity in major depressive disorder: A review. *Neuroscience & Biobehavioral Reviews*, *56*, 330–344. https://doi.org/10.1016/j.neubiorev.2015.07.014

Najjar, S., & Pearlman, D. M. (2015). Neuroinflammation and white matter pathology in schizophrenia: Systematic review. *Schizophrenia Research*, *161*(1), 102–112. https://doi.org/10.1016/j.schres.2014.04.041

Nasrallah, F. A., Singh, K. K. D. /O. R., Yeow, L. Y., & Chuang, K.-H. (2017). GABAergic effect on resting-state functional connectivity: Dynamics under pharmacological antagonism. *NeuroImage*, *149*, 53–62. https://doi.org/10.1016/j.neuroimage.2017.01.040

Nemani, K., Hosseini Ghomi, R., McCormick, B., & Fan, X. (2015). Schizophrenia and the gut–brain axis. *Progress in Neuro-Psychopharmacology and Biological Psychiatry*, *56*, 155–160. https://doi.org/10.1016/j.pnpbp.2014.08.018

Niendam, T. A., Bearden, C. E., Johnson, J. K., & Cannon, T. D. (2006). *Global Functioning: Role Scale (GF: Role)*. Los Angeles, CA: University of California, Los Angeles.

Nostro, A. D., Müller, V. I., Varikuti, D. P., Pläschke, R. N., Hoffstaedter, F., Langner, R., Patil, K. R., & Eickhoff, S. B. (2018). Predicting personality from network-based resting-state functional connectivity. *Brain Structure and Function*, *223*(6), 2699–2719. https://doi.org/10.1007/s00429-018-1651-z

Nowicki, S., & Duke, M. P. (1994). Individual differences in the nonverbal communication of affect: The diagnostic analysis of nonverbal accuracy scale. *Journal of Nonverbal Behavior*, *18*(1), 9–35. https://doi.org/10.1007/BF02169077

Nuechterlein, K. H., Green, M. F., Kern, R. S., Baade, L. E., Barch, D. M., Cohen, J. D., Essock, S., Fenton, W. S., Frese, F. J., Gold, J. M., Goldberg, T., Heaton, R. K., Keefe, R. S. E., Kraemer, H., Mesholam-Gately, R., Seidman, L. J., Stover, E., Weinberger, D. R., Young, A. S., … Marder, S. R. (2008). The MATRICS Consensus Cognitive Battery, Part 1: Test Selection, Reliability, and Validity. *American Journal of Psychiatry*, *165*(2), 203–213. https://doi.org/10.1176/appi.ajp.2007.07010042

Ohayon, M. M., & Schatzberg, A. F. (2002). Prevalence of Depressive Episodes With Psychotic Features in the General Population. *American Journal of Psychiatry*, *159*(11), 1855–1861. https://doi.org/10.1176/appi.ajp.159.11.1855

Olsen, A. S., Lykkebo-Valløe, A., Ozenne, B., Madsen, M. K., Stenbæk, D. S., Armand, S., Mørup, M., Ganz, M., Knudsen, G. M., & Fisher, P. M. (2022). Psilocybin modulation of time-varying functional connectivity is associated with plasma psilocin and subjective effects. *NeuroImage*, *264*, 119716. https://doi.org/10.1016/j.neuroimage.2022.119716

Ooi, L. Q. R., Chen, J., Zhang, S., Kong, R., Tam, A., Li, J., Dhamala, E., Zhou, J. H., Holmes, A. J., & Yeo, B. T. T. (2022). Comparison of individualized behavioral predictions across anatomical, diffusion and functional connectivity MRI. *NeuroImage*, *263*, 119636. https://doi.org/10.1016/j.neuroimage.2022.119636

Orhan, F., Fatouros-Bergman, H., Goiny, M., Malmqvist, A., Piehl, F., Cervenka, S., Collste, K., Victorsson, P., Sellgren, C. M., Flyckt, L., Erhardt, S., & Engberg, G. (2018). CSF GABA is reduced in first-episode psychosis and associates to symptom severity. *Molecular Psychiatry*, *23*(5), 1244–1250. https://doi.org/10.1038/mp.2017.25

Palaniyappan, L., & Liddle, P. F. (2012). Does the salience network play a cardinal role in psychosis? An emerging hypothesis of insular dysfunction. *Journal of Psychiatry and Neuroscience*, *37*(1), 17–27. https://doi.org/10.1503/jpn.100176

Patel, A. X., Kundu, P., Rubinov, M., Jones, P. S., Vértes, P. E., Ersche, K. D., Suckling, J., & Bullmore, E. T. (2014). A wavelet method for modeling and despiking motion artifacts from resting-state fMRI time series. *NeuroImage*, *95*(100), 287–304. https://doi.org/10.1016/j.neuroimage.2014.03.012

Pearson, K. (1895). Note on Regression and Inheritance in the Case of Two Parents. *Proceedings of the Royal Society of London Series I*, *58*, 240–242.

Pedersen, G., Hagtvet, K. A., & Karterud, S. (2007). Generalizability studies of the Global Assessment of Functioning-Split version. *Comprehensive Psychiatry*, *48*(1), 88–94. https://doi.org/10.1016/j.comppsych.2006.03.008

Penttilä, M., Jääskeläinen, E., Hirvonen, N., Isohanni, M., & Miettunen, J. (2014). Duration of untreated psychosis as predictor of long-term outcome in schizophrenia: Systematic review and meta-analysis. *The British Journal of Psychiatry*, *205*(2), 88–94. https://doi.org/10.1192/bjp.bp.113.127753

Peralta, V., García de Jalón, E., Moreno-Izco, L., Peralta, D., Janda, L., Sánchez-Torres, A. M., Cuesta, M. J., & SEGPEPs Group. (2022). Long-Term Outcomes of First-Admission Psychosis: A Naturalistic 21-Year Follow-Up Study of Symptomatic, Functional and Personal Recovery and Their Baseline Predictors. *Schizophrenia Bulletin*, *48*(3), 631–642. https://doi.org/10.1093/schbul/sbab145

Petrides, M., & Milner, B. (1982). Deficits on subject-ordered tasks after frontal- and temporal-lobe lesions in man. *Neuropsychologia*, *20*(3), 249–262. https://doi.org/10.1016/0028-3932(82)90100-2

Phillips, M. L., Chase, H. W., Sheline, Y. I., Etkin, A., Almeida, J. R. C., Deckersbach, T., & Trivedi, M. H. (2015). Identifying Predictors, Moderators, and Mediators of Antidepressant Response in Major Depressive Disorder: Neuroimaging Approaches. *American Journal of Psychiatry*, *172*(2), 124–138. https://doi.org/10.1176/appi.ajp.2014.14010076

Picardi, A., Viroli, C., Tarsitani, L., Miglio, R., de Girolamo, G., Dell'Acqua, G., & Biondi, M. (2012). Heterogeneity and symptom structure of schizophrenia. *Psychiatry Research*, *198*(3), 386–394. https://doi.org/10.1016/j.psychres.2011.12.051

Power, J. D., Barnes, K. A., Snyder, A. Z., Schlaggar, B. L., & Petersen, S. E. (2012). Spurious but systematic correlations in functional connectivity MRI networks arise from subject motion. *NeuroImage*, *59*(3), 2142–2154. https://doi.org/10.1016/j.neuroimage.2011.10.018

Power, J. D., Mitra, A., Laumann, T. O., Snyder, A. Z., Schlaggar, B. L., & Petersen, S. E. (2014). Methods to detect, characterize, and remove motion artifact in resting state fMRI. *NeuroImage*, *84*, 320–341. https://doi.org/10.1016/j.neuroimage.2013.08.048

Proix, T., Jirsa, V. K., Bartolomei, F., Guye, M., & Truccolo, W. (2018). Predicting the spatiotemporal diversity of seizure propagation and termination in human focal epilepsy. *Nature Communications*, *9*(1), 1088. https://doi.org/10.1038/s41467-018-02973-y

Pronold, J., van Meegen, A., Shimoura, R. O., Vollenbröker, H., Senden, M., Hilgetag, C. C.,

Bakker, R., & van Albada, S. J. (2024). Multi-scale spiking network model of human cerebral cortex. *Cerebral Cortex*, *34*(10), bhae409. https://doi.org/10.1093/cercor/bhae409

Purcell, S. M., Wray, N. R., Stone, J. L., Visscher, P. M., O'Donovan, M. C., Sullivan, P. F., Sklar, P., Purcell (Leader), S. M., Stone, J. L., Sullivan, P. F., Ruderfer, D. M., McQuillin, A., Morris, D. W., O'Dushlaine, C. T., Corvin, A., Holmans, P. A., O'Donovan, M. C., Sklar, P., Wray, N. R., … Stanley Center for Psychiatric Research and Broad Institute of MIT and Harvard. (2009). Common polygenic variation contributes to risk of schizophrenia and bipolar disorder. *Nature*, *460*(7256), 748–752. https://doi.org/10.1038/nature08185

Raasakka, A., Ruskamo, S., Kowal, J., Barker, R., Baumann, A., Martel, A., Tuusa, J., Myllykoski, M., Bürck, J., Ulrich, A. S., Stahlberg, H., & Kursula, P. (2017). Membrane Association Landscape of Myelin Basic Protein Portrays Formation of the Myelin Major Dense Line. *Scientific Reports*, *7*(1), 4974. https://doi.org/10.1038/s41598-017-05364-3

Rajapakse, J. C., Giedd, J. N., & Rapoport, J. L. (1997). Statistical approach to segmentation of single-channel cerebral MR images. *IEEE Transactions on Medical Imaging*, *16*(2), 176–186. https://doi.org/10.1109/42.563663

Rasic, D., Hajek, T., Alda, M., & Uher, R. (2014). Risk of Mental Illness in Offspring of Parents With Schizophrenia, Bipolar Disorder, and Major Depressive Disorder: A Meta-Analysis of Family High-Risk Studies. *Schizophrenia Bulletin*, *40*(1), 28–38. https://doi.org/10.1093/schbul/sbt114

Rocha, R. P., Koçillari, L., Suweis, S., De Filippo De Grazia, M., de Schotten, M. T., Zorzi, M., & Corbetta, M. (2022). Recovery of neural dynamics criticality in personalized whole-brain models of stroke. *Nature Communications*, *13*(1), 3683. https://doi.org/10.1038/s41467-022-30892-6

Royer, J., Bernhardt, B. C., Larivière, S., Gleichgerrcht, E., Vorderwülbecke, B. J., Vulliémoz, S., & Bonilha, L. (2022). Epilepsy and brain network hubs. *Epilepsia*, *63*(3), 537–550. https://doi.org/10.1111/epi.17171

Rubinov, M., & Bullmore, Ed. (2013). Schizophrenia and abnormal brain network hubs. *Dialogues in Clinical Neuroscience*, *15*(3), 339–349. https://doi.org/10.31887/DCNS.2013.15.3/mrubinov

Ruff, R. M., Light, R. H., Parker, S. B., & Levin, H. S. (1996). Benton controlled oral word association test: Reliability and updated norms. *Archives of Clinical Neuropsychology*, *11*(4), 329–338. https://doi.org/10.1093/arclin/11.4.329

Ruhé, H. G., Mason, N. S., & Schene, A. H. (2007). Mood is indirectly related to serotonin, norepinephrine and dopamine levels in humans: A meta-analysis of monoamine depletion studies. *Molecular Psychiatry*, *12*(4), 331–359. https://doi.org/10.1038/sj.mp.4001949

Saarni, S. I., Suvisaari, J., Sintonen, H., Pirkola, S., Koskinen, S., Aromaa, A., & Lönnqvist, J. (2007). Impact of psychiatric disorders on health-related quality of life: General population survey. *The British Journal of Psychiatry*, *190*(4), 326–332. https://doi.org/10.1192/bjp.bp.106.025106

Sahle, B. W., Reavley, N. J., Li, W., Morgan, A. J., Yap, M. B. H., Reupert, A., & Jorm, A. F. (2022). The association between adverse childhood experiences and common mental disorders and suicidality: An umbrella review of systematic reviews and meta-analyses. *European Child & Adolescent Psychiatry*, *31*(10), 1489–1499. https://doi.org/10.1007/s00787-021-01745-2

Salazar de Pablo, G., Radua, J., Pereira, J., Bonoldi, I., Arienti, V., Besana, F., Soardo, L., Cabras, A., Fortea, L., Catalan, A., Vaquerizo-Serrano, J., Coronelli, F., Kaur, S., Da Silva, J., Shin, J. I., Solmi, M., Brondino, N., Politi, P., McGuire, P., & Fusar-Poli, P. (2021). Probability of Transition to Psychosis in Individuals at Clinical High Risk: An Updated Meta-analysis. *JAMA Psychiatry*, *78*(9), 970–978. https://doi.org/10.1001/jamapsychiatry.2021.0830

Salimi-Khorshidi, G., Douaud, G., Beckmann, C. F., Glasser, M. F., Griffanti, L., & Smith, S. M. (2014). Automatic denoising of functional MRI data: Combining independent component analysis and hierarchical fusion of classifiers. *NeuroImage*, *90*, 449–468. https://doi.org/10.1016/j.neuroimage.2013.11.046

Sanfratello, L., Houck, J. M., & Calhoun, V. D. (2019). Dynamic Functional Network Connectivity in Schizophrenia with Magnetoencephalography and Functional Magnetic Resonance Imaging: Do Different Timescales Tell a Different Story? *Brain Connectivity*, *9*(3), 251–262. https://doi.org/10.1089/brain.2018.0608

Sanz Leon, P., Knock, S., Woodman, M., Domide, L., Mersmann, J., McIntosh, A., & Jirsa, V. (2013). The Virtual Brain: A simulator of primate brain network dynamics. *Frontiers in Neuroinformatics*, *7*. https://www.frontiersin.org/articles/10.3389/fninf.2013.00010

Sanz-Leon, P., Knock, S. A., Spiegler, A., & Jirsa, V. K. (2015). Mathematical framework for large-scale brain network modeling in The Virtual Brain. *NeuroImage*, *111*, 385–430. https://doi.org/10.1016/j.neuroimage.2015.01.002

Satterthwaite, T. D., Elliott, M. A., Gerraty, R. T., Ruparel, K., Loughead, J., Calkins, M. E., Eickhoff, S. B., Hakonarson, H., Gur, R. C., Gur, R. E., & Wolf, D. H. (2013). An improved framework for confound regression and filtering for control of motion artifact in the preprocessing of resting-state functional connectivity data. *NeuroImage*, *64*, 240–256. https://doi.org/10.1016/j.neuroimage.2012.08.052

Schirner, M., McIntosh, A. R., Jirsa, V., Deco, G., & Ritter, P. (2018). Inferring multi-scale neural mechanisms with brain network modelling. *eLife*, *7*, e28927. https://doi.org/10.7554/eLife.28927

Schmidt, M. (1996). *Rey auditory verbal learning test: A handbook: Vol. Vol. 17*. Western Psychological Services.

Schnack, H. G., & Kahn, R. S. (2016). Detecting neuroimaging biomarkers for psychiatric disorders: Sample size matters. *Frontiers in Psychiatry*, *7*(MAR). Scopus. https://doi.org/10.3389/fpsyt.2016.00050

Schultze-Lutter, F., Addington, J., Ruhrmann, S., & Klosterkötter, J. (2007). *Schizophrenia Proneness Instrument, Adult Version (SPI-A)*. Giovanni Fioriti Editore.

Schumacher, J., Peraza, L. R., Firbank, M., Thomas, A. J., Kaiser, M., Gallagher, P., O'Brien, J. T., Blamire, A. M., & Taylor, J.-P. (2019). Dynamic functional connectivity changes in dementia with Lewy bodies and Alzheimer's disease. *NeuroImage: Clinical*, *22*, 101812. https://doi.org/10.1016/j.nicl.2019.101812

Seeman, P. (2013). Schizophrenia and dopamine receptors. *European Neuropsychopharmacology*, *23*(9), 999–1009. https://doi.org/10.1016/j.euroneuro.2013.06.005

Shappell, H., Caffo, B. S., Pekar, J. J., & Lindquist, M. A. (2019). Improved state change estimation in dynamic functional connectivity using hidden semi-Markov models. *NeuroImage*, *191*, 243–257. https://doi.org/10.1016/j.neuroimage.2019.02.013

Sheline, Y. I., & Raichle, M. E. (2013). Resting State Functional Connectivity in Preclinical Alzheimer's Disease. *Biological Psychiatry*, *74*(5), 340–347. https://doi.org/10.1016/j.biopsych.2012.11.028

Shevlin, M., Houston, J. E., Dorahy, M. J., & Adamson, G. (2008). Cumulative traumas and psychosis: An analysis of the national comorbidity survey and the British Psychiatric Morbidity Survey. *Schizophrenia Bulletin*, *34*(1), 193–199. Scopus. https://doi.org/10.1093/schbul/sbm069

Shine, J. M., Bissett, P. G., Bell, P. T., Koyejo, O., Balsters, J. H., Gorgolewski, K. J., Moodie, C. A., & Poldrack, R. A. (2016). The Dynamics of Functional Brain Networks: Integrated Network States during Cognitive Task Performance. *Neuron*, *92*(2), 544–554. https://doi.org/10.1016/j.neuron.2016.09.018

Shine, J. M., Müller, E. J., Munn, B., Cabral, J., Moran, R. J., & Breakspear, M. (2021). Computational models link cellular mechanisms of neuromodulation to large-scale neural dynamics. *Nature Neuroscience*, *24*(6), 765–776. https://doi.org/10.1038/s41593-021-00824-6

Siskind, D., Orr, S., Sinha, S., Yu, O., Brijball, B., Warren, N., MacCabe, J. H., Smart, S. E., & Kisely, S. (2022). Rates of treatment-resistant schizophrenia from first-episode cohorts: Systematic review and meta-analysis. *The British Journal of Psychiatry*, *220*(3), 115–120. https://doi.org/10.1192/bjp.2021.61

Sizemore, A. E., & Bassett, D. S. (2018). Dynamic graph metrics: Tutorial, toolbox, and tale. *NeuroImage*, *180*, 417–427. https://doi.org/10.1016/j.neuroimage.2017.06.081

Smith, S. M., Beckmann, C. F., Andersson, J., Auerbach, E. J., Bijsterbosch, J., Douaud, G., Duff, E., Feinberg, D. A., Griffanti, L., Harms, M. P., Kelly, M., Laumann, T., Miller, K. L., Moeller, S., Petersen, S., Power, J., Salimi-Khorshidi, G., Snyder, A. Z., Vu, A. T., … Glasser, M. F. (2013). Resting-state fMRI in the Human Connectome Project. *NeuroImage*, *80*, 144–168. https://doi.org/10.1016/j.neuroimage.2013.05.039

Smith, S. M., Nichols, T. E., Vidaurre, D., Winkler, A. M., Behrens, T. E. J., Glasser, M. F., Ugurbil, K., Barch, D. M., Van Essen, D. C., & Miller, K. L. (2015). A positive-negative mode of population covariation links brain connectivity, demographics and behavior. *Nature Neuroscience*, *18*(11), 1565–1567. https://doi.org/10.1038/nn.4125

Snyder, W., Uddin, L. Q., & Nomi, J. S. (2021). Dynamic functional connectivity profile of the salience network across the life span. *Human Brain Mapping*, *42*(14), 4740–4749. https://doi.org/10.1002/hbm.25581

Sohal, V. S., & Rubenstein, J. L. R. (2019). Excitation-inhibition balance as a framework for investigating mechanisms in neuropsychiatric disorders. *Molecular Psychiatry*, *24*(9), 1248–1257. https://doi.org/10.1038/s41380-019-0426-0

Solmi, M., Radua, J., Olivola, M., Croce, E., Soardo, L., Salazar de Pablo, G., Il Shin, J., Kirkbride, J. B., Jones, P., Kim, J. H., Kim, J. Y., Carvalho, A. F., Seeman, M. V., Correll, C. U., & Fusar-Poli, P. (2022). Age at onset of mental disorders worldwide: Large-scale meta-analysis of 192 epidemiological studies. *Molecular Psychiatry*, *27*(1), 281–295. https://doi.org/10.1038/s41380-021-01161-7

Song, X.-W., Dong, Z.-Y., Long, X.-Y., Li, S.-F., Zuo, X.-N., Zhu, C.-Z., He, Y., Yan, C.-G., & Zang, Y.-F. (2011). REST: A toolkit for resting-state functional magnetic resonance imaging data processing. *PloS One*, *6*(9), e25031. https://doi.org/10.1371/journal.pone.0025031

Sotiropoulos, S. N., Jbabdi, S., Xu, J., Andersson, J. L., Moeller, S., Auerbach, E. J., Glasser, M. F., Hernandez, M., Sapiro, G., Jenkinson, M., Feinberg, D. A., Yacoub, E., Lenglet, C., Van Essen, D. C., Ugurbil, K., & Behrens, T. E. J. (2013). Advances in diffusion MRI acquisition and processing in the Human Connectome Project. *NeuroImage*, *80*, 125–143. https://doi.org/10.1016/j.neuroimage.2013.05.057

Sridharan, D., Levitin, D. J., & Menon, V. (2008). A critical role for the right fronto-insular

cortex in switching between central-executive and default-mode networks. *Proceedings of the National Academy of Sciences of the United States of America*, *105*(34), 12569–12574. https://doi.org/10.1073/pnas.0800005105

Sun, S., Yan, C., Qu, S., Luo, G., Liu, X., Tian, F., Dong, Q., Li, X., & Hu, B. (2024). Resting-state dynamic functional connectivity in major depressive disorder: A systematic review. *Progress in Neuro-Psychopharmacology and Biological Psychiatry*, *135*, 111076. https://doi.org/10.1016/j.pnpbp.2024.111076

Tandon, R., Nasrallah, H., Akbarian, S., Carpenter, W. T., DeLisi, L. E., Gaebel, W., Green, M. F., Gur, R. E., Heckers, S., Kane, J. M., Malaspina, D., Meyer-Lindenberg, A., Murray, R., Owen, M., Smoller, J. W., Yassin, W., & Keshavan, M. (2024). The schizophrenia syndrome, circa 2024: What we know and how that informs its nature. *Schizophrenia Research*, *264*, 1–28. https://doi.org/10.1016/j.schres.2023.11.015

Tang, Y., Martin, N. L., & Cotes, R. O. (2014). Cocaine-Induced Psychotic Disorders: Presentation, Mechanism, and Management. *Journal of Dual Diagnosis*, *10*(2), 98–106. https://doi.org/10.1080/15504263.2014.906133

Thirugnanachandran, T., Ma, H., Donnan, G. A., Reutens, D. C., & Phan, T. G. (2024). Introducing the Concept of Sanctuary Sites in Ischemic Stroke. *Stroke*, *55*(5), 1405–1408. https://doi.org/10.1161/STROKEAHA.123.046083

Tombaugh, T. N. (2004). Trail Making Test A and B: Normative data stratified by age and education. *Archives of Clinical Neuropsychology*, *19*(2), 203–214. https://doi.org/10.1016/S0887-6177(03)00039-8

Tost, H., Alam, T., & Meyer-Lindenberg, A. (2010). Dopamine and psychosis: Theory, pathomechanisms and intermediate phenotypes. *Neuroscience & Biobehavioral Reviews*, *34*(5), 689–700. https://doi.org/10.1016/j.neubiorev.2009.06.005

Trivedi, M. H., Rush, A. J., Wisniewski, S. R., Nierenberg, A. A., Warden, D., Ritz, L., Norquist, G., Howland, R. H., Lebowitz, B., McGrath, P. J., Shores-Wilson, K., Biggs, M. M., Balasubramani, G. K., Fava, M., & STAR*D Study Team. (2006). Evaluation of Outcomes With Citalopram for Depression Using Measurement-Based Care in STAR*D: Implications for Clinical Practice. *American Journal of Psychiatry*, *163*(1), 28–40. https://doi.org/10.1176/appi.ajp.163.1.28

Troubat, R., Barone, P., Leman, S., Desmidt, T., Cressant, A., Atanasova, B., Brizard, B., El Hage, W., Surget, A., Belzung, C., & Camus, V. (2021). Neuroinflammation and depression: A review. *European Journal of Neuroscience*, *53*(1), 151–171. https://doi.org/10.1111/ejn.14720

Uddin, L. Q., Yeo, B. T. T., & Spreng, R. N. (2019). Towards a Universal Taxonomy of Macro-scale Functional Human Brain Networks. *Brain Topography*, *32*(6), 926–942. https://doi.org/10.1007/s10548-019-00744-6

Upthegrove, R., Marwaha, S., & Birchwood, M. (2017). Depression and Schizophrenia: Cause, Consequence, or Trans-diagnostic Issue? *Schizophrenia Bulletin*, *43*(2), 240–244. https://doi.org/10.1093/schbul/sbw097

van den Heuvel, M. P., & Hulshoff Pol, H. E. (2010). Exploring the brain network: A review on resting-state fMRI functional connectivity. *European Neuropsychopharmacology*, *20*(8), 519–534. https://doi.org/10.1016/j.euroneuro.2010.03.008

Van Essen, D. C., Smith, S. M., Barch, D. M., Behrens, T. E. J., Yacoub, E., & Ugurbil, K. (2013). The WU-Minn Human Connectome Project: An overview. *NeuroImage*, *80*, 62–79. https://doi.org/10.1016/j.neuroimage.2013.05.041

van Hooijdonk, C. F. M., Drukker, M., van de Giessen, E., Booij, J., Selten, J.-P., & van Amelsvoort, T. A. M. J. (2022). Dopaminergic alterations in populations at increased

risk for psychosis: A systematic review of imaging findings. *Progress in Neurobiology*, *213*, 102265. https://doi.org/10.1016/j.pneurobio.2022.102265

Vandewouw, M. M., Hunt, B. A. E., Ziolkowski, J., & Taylor, M. J. (2021). The developing relations between networks of cortical myelin and neurophysiological connectivity. *NeuroImage*, *237*, 118142. https://doi.org/10.1016/j.neuroimage.2021.118142

Varma, S., & Simon, R. (2006). Bias in error estimation when using cross-validation for model selection. *BMC Bioinformatics*, *7*(1), 91. https://doi.org/10.1186/1471-2105-7-91

Walder, D. J., Faraone, S. V., Glatt, S. J., Tsuang, M. T., & Seidman, L. J. (2014). Genetic liability, prenatal health, stress and family environment: Risk factors in the Harvard Adolescent Family High Risk for Schizophrenia Study. *Schizophrenia Research*, *157*(1), 142–148. https://doi.org/10.1016/j.schres.2014.04.015

Wang, C., Ong, J. L., Patanaik, A., Zhou, J., & Chee, M. W. L. (2016). Spontaneous eyelid closures link vigilance fluctuation with fMRI dynamic connectivity states. *Proceedings of the National Academy of Sciences*, *113*(34), 9653–9658. https://doi.org/10.1073/pnas.1523980113

Wang, D., Li, M., Wang, M., Schoeppe, F., Ren, J., Chen, H., Öngür, D., Brady, R. O., Baker, J. T., & Liu, H. (2020). Individual-specific functional connectivity markers track dimensional and categorical features of psychotic illness. *Molecular Psychiatry*, *25*(9), Article 9. https://doi.org/10.1038/s41380-018-0276-1

Wang, H. E., Triebkorn, P., Breyton, M., Dollomaja, B., Lemarechal, J.-D., Petkoski, S., Sorrentino, P., Depannemaecker, D., Hashemi, M., & Jirsa, V. K. (2024). Virtual brain twins: From basic neuroscience to clinical use. *National Science Review*, *11*(5), nwae079. https://doi.org/10.1093/nsr/nwae079

Wang, H. E., Woodman, M., Triebkorn, P., Lemarechal, J.-D., Jha, J., Dollomaja, B., Vattikonda, A. N., Sip, V., Medina Villalon, S., Hashemi, M., Guye, M., Makhalova, J., Bartolomei, F., & Jirsa, V. (2023). Delineating epileptogenic networks using brain imaging data and personalized modeling in drug-resistant epilepsy. *Science Translational Medicine*, *15*(680), eabp8982. https://doi.org/10.1126/scitranslmed.abp8982

Wang, H.-T., Smallwood, J., Mourao-Miranda, J., Xia, C. H., Satterthwaite, T. D., Bassett, D. S., & Bzdok, D. (2020). Finding the needle in a high-dimensional haystack: Canonical correlation analysis for neuroscientists. *NeuroImage*, *216*, 116745. https://doi.org/10.1016/j.neuroimage.2020.116745

Wang, X., Wirth, A., & Wang, L. (2007). Structure-Based Statistical Features and Multivariate Time Series Clustering. *Seventh IEEE International Conference on Data Mining (ICDM 2007)*, 351–360. https://doi.org/10.1109/ICDM.2007.103

Wang, X.-J. (2020). Macroscopic gradients of synaptic excitation and inhibition in the neocortex. *Nature Reviews Neuroscience*, *21*(3), 169–178. https://doi.org/10.1038/s41583-020-0262-x

Ward Jr., J. H. (1963). Hierarchical Grouping to Optimize an Objective Function. *Journal of the American Statistical Association*, *58*(301), 236–244. https://doi.org/10.1080/01621459.1963.10500845

Weber, S., Johnsen, E., Kroken, R. A., Løberg, E.-M., Kandilarova, S., Stoyanov, D., Kompus, K., & Hugdahl, K. (2020). Dynamic Functional Connectivity Patterns in Schizophrenia and the Relationship With Hallucinations. *Frontiers in Psychiatry*, *11*, 227. https://doi.org/10.3389/fpsyt.2020.00227

Wechsler, D. (1955). *Manual for the Wechsler Adult Intelligence Scale*. Psychological Corp.

Wenneberg, C., Glenthøj, B. Y., Hjorthøj, C., Buchardt Zingenberg, F. J., Glenthøj, L. B., Rostrup, E., Broberg, B. V., & Nordentoft, M. (2020). Cerebral glutamate and GABA levels in high-risk of psychosis states: A focused review and meta-analysis of 1H-MRS studies. *Schizophrenia Research*, *215*, 38–48. https://doi.org/10.1016/j.schres.2019.10.050

Woodward, N. D., & Cascio, C. J. (2015). Resting-State Functional Connectivity in Psychiatric Disorders. *JAMA Psychiatry*, *72*(8), 743–744. https://doi.org/10.1001/jamapsychiatry.2015.0484

World Health Organization. (2004). *ICD-10: International statistical classification of diseases and related health problems : tenth revision*. World Health Organization. https://iris.who.int/handle/10665/42980

Wray, N. R., Ripke, S., Mattheisen, M., Trzaskowski, M., Byrne, E. M., Abdellaoui, A., Adams, M. J., Agerbo, E., Air, T. M., Andlauer, T. M. F., Bacanu, S.-A., Bækvad-Hansen, M., Beekman, A. F. T., Bigdeli, T. B., Binder, E. B., Blackwood, D. R. H., Bryois, J., Buttenschøn, H. N., Bybjerg-Grauholm, J., … Sullivan, P. F. (2018). Genome-wide association analyses identify 44 risk variants and refine the genetic architecture of major depression. *Nature Genetics*, *50*(5), 668–681. https://doi.org/10.1038/s41588-018-0090-3

Wu, X., He, H., Shi, L., Xia, Y., Zuang, K., Feng, Q., Zhang, Y., Ren, Z., Wei, D., & Qiu, J. (2019). Personality traits are related with dynamic functional connectivity in major depression disorder: A resting-state analysis. *Journal of Affective Disorders*, *245*, 1032–1042. https://doi.org/10.1016/j.jad.2018.11.002

Xu, J., Van Dam, N. T., Feng, C., Luo, Y., Ai, H., Gu, R., & Xu, P. (2019). Anxious brain networks: A coordinate-based activation likelihood estimation meta-analysis of resting-state functional connectivity studies in anxiety. *Neuroscience & Biobehavioral Reviews*, *96*, 21–30. https://doi.org/10.1016/j.neubiorev.2018.11.005

Yan, C.-G., Chen, X., Li, L., Castellanos, F. X., Bai, T.-J., Bo, Q.-J., Cao, J., Chen, G.-M., Chen, N.-X., Chen, W., Cheng, C., Cheng, Y.-Q., Cui, X.-L., Duan, J., Fang, Y.-R., Gong, Q.-Y., Guo, W.-B., Hou, Z.-H., Hu, L., … Zang, Y.-F. (2019). Reduced default mode network functional connectivity in patients with recurrent major depressive disorder. *Proceedings of the National Academy of Sciences*, *116*(18), 9078–9083. https://doi.org/10.1073/pnas.1900390116

Yang, J., Huber, L., Yu, Y., & Bandettini, P. A. (2021). Linking cortical circuit models to human cognition with laminar fMRI. *Neuroscience & Biobehavioral Reviews*, *128*, 467–478. https://doi.org/10.1016/j.neubiorev.2021.07.005

Yao, Z., Shi, J., Zhang, Z., Zheng, W., Hu, T., Li, Y., Yu, Y., Zhang, Z., Fu, Y., Zou, Y., Zhang, W., Wu, X., & Hu, B. (2019). Altered dynamic functional connectivity in weakly-connected state in major depressive disorder. *Clinical Neurophysiology*, *130*(11), 2096–2104. https://doi.org/10.1016/j.clinph.2019.08.009

Yeo, B. T. T., Krienen, F. M., Sepulcre, J., Sabuncu, M. R., Lashkari, D., Hollinshead, M., Roffman, J. L., Smoller, J. W., Zöllei, L., Polimeni, J. R., Fischl, B., Liu, H., & Buckner, R. L. (2011). The organization of the human cerebral cortex estimated by intrinsic functional connectivity. *Journal of Neurophysiology*, *106*(3), 1125–1165. https://doi.org/10.1152/jn.00338.2011

Yeo, I., & Johnson, R. A. (2000). A new family of power transformations to improve normality or symmetry. *Biometrika*, *87*(4), 954–959. https://doi.org/10.1093/biomet/87.4.954

Yu, Q., Tang, H., Tan, K. C., & Yu, H. (2014). A brain-inspired spiking neural network model with temporal encoding and learning. *Neurocomputing*, *138*, 3–13.

https://doi.org/10.1016/j.neucom.2013.06.052
Zamani Esfahlani, F., Bertolero, M. A., Bassett, D. S., & Betzel, R. F. (2020). Space-independent community and hub structure of functional brain networks. *NeuroImage*, *211*, 116612. https://doi.org/10.1016/j.neuroimage.2020.116612
Zhang, J., Kucyi, A., Raya, J., Nielsen, A. N., Nomi, J. S., Damoiseaux, J. S., Greene, D. J., Horovitz, S. G., Uddin, L. Q., & Whitfield-Gabrieli, S. (2021). What have we really learned from functional connectivity in clinical populations? *NeuroImage*, *242*, 118466. https://doi.org/10.1016/j.neuroimage.2021.118466
Zhang, S., Larsen, B., Sydnor, V. J., Zeng, T., An, L., Yan, X., Kong, R., Kong, X., Gur, R. C., Gur, R. E., Moore, T. M., Wolf, D. H., Holmes, A. J., Xie, Y., Zhou, J. H., Fortier, M. V., Tan, A. P., Gluckman, P., Chong, Y. S., … Yeo, B. T. T. (2024). In vivo whole-cortex marker of excitation-inhibition ratio indexes cortical maturation and cognitive ability in youth. *Proceedings of the National Academy of Sciences*, *121*(23), e2318641121. https://doi.org/10.1073/pnas.2318641121
Zhang, X., Braun, U., Harneit, A., Zang, Z., Geiger, L. S., Betzel, R. F., Chen, J., Schweiger, J. I., Schwarz, K., Reinwald, J. R., Fritze, S., Witt, S., Rietschel, M., Nöthen, M. M., Degenhardt, F., Schwarz, E., Hirjak, D., Meyer-Lindenberg, A., Bassett, D. S., & Tost, H. (2021). Generative network models of altered structural brain connectivity in schizophrenia. *NeuroImage*, *225*, 117510. https://doi.org/10.1016/j.neuroimage.2020.117510
Zhi, D., Calhoun, V. D., Lv, L., Ma, X., Ke, Q., Fu, Z., Du, Y., Yang, Y., Yang, X., Pan, M., Qi, S., Jiang, R., Yu, Q., & Sui, J. (2018). Aberrant Dynamic Functional Network Connectivity and Graph Properties in Major Depressive Disorder. *Frontiers in Psychiatry*, *9*. https://doi.org/10.3389/fpsyt.2018.00339
Zhou, H.-X., Chen, X., Shen, Y.-Q., Li, L., Chen, N.-X., Zhu, Z.-C., Castellanos, F. X., & Yan, C.-G. (2020). Rumination and the default mode network: Meta-analysis of brain imaging studies and implications for depression. *NeuroImage*, *206*, 116287. https://doi.org/10.1016/j.neuroimage.2019.116287
Zhou, Y., Zhou, B., Pache, L., Chang, M., Khodabakhshi, A. H., Tanaseichuk, O., Benner, C., & Chanda, S. K. (2019). Metascape provides a biologist-oriented resource for the analysis of systems-level datasets. *Nature Communications*, *10*(1), 1523. https://doi.org/10.1038/s41467-019-09234-6
Zimmermann, J., Perry, A., Breakspear, M., Schirner, M., Sachdev, P., Wen, W., Kochan, N. A., Mapstone, M., Ritter, P., McIntosh, A. R., & Solodkin, A. (2018). Differentiation of Alzheimer's disease based on local and global parameters in personalized Virtual Brain models. *NeuroImage: Clinical*, *19*, 240–251. https://doi.org/10.1016/j.nicl.2018.04.017

9. Appendix

Supplementary Tables

		State 1	State 2	State 3	State 4	State 5
HC	raw	0.027 (0.050)	0.127 (0.174)	0.155 (0.170)	0.180 (0.163)	0.504 (0.239)
	adjusted	0.031 (1.016)	-0.112 (1.037)	0.516 (1.033)	-0.171 (1.018)	-0.052 (1.056)
CHR	raw	0.022 (0.042)	0.148 (0.183)	0.104 (0.121)	0.225 (0.197)	0.496 (0.206)
	adjusted	-0.105 (0.916)	0.077 (0.896)	0.257 (0.920)	0.006 (0.975)	-0.068 (0.882)
ROP	raw	0.061 (0.133)	0.129 (0.187)	0.011 (0.023)	0.291 (0.214)	0.502 (0.236)
	adjusted	0.301 (1.033)	-0.089 (0.896)	-0.592 (0.486)	0.342 (0.938)	-0.137 (0.889)
ROD	raw	0.018 (0.047)	0.184 (0.201)	0.018 (0.027)	0.193 (0.142)	0.580 (0.211)
	adjusted	-0.276 (0.835)	0.234 (0.865)	-0.612 (0.504)	-0.037 (0.769)	0.310 (0.861)
Group differences						
HC v CHR	χ^2	17789	14700	19551	15063	17041
	p-value	0.434	0.031	0.014	0.071	0.943
HC v ROP	χ^2	15347	17702	29251	13057	19532
	p-value	0.003	0.393	< 0.001	< 0.001	0.438
HC v ROD	χ^2	20400	13740	28332	15811	13974
	p-value	0.015	< 0.001	< 0.001	0.074	0.001
CHR v ROP	χ^2	7124	10201	14340	7463	9702
	p-value	0.001	0.165	< 0.001	0.005	0.533
CHR v ROD	χ^2	9760	7936	13739	9044	6620

	p-value	0.143	0.150	< 0.001	0.746	< 0.001
ROP v ROD	χ^2	13029	7698	10301	12074	6937
	p-value	< 0.001	0.003	0.392	< 0.001	< 0.001
Confounds						
Age	χ^2	-1.416	1.303	-1.031	-0.910	0.338
	p-value	0.157	0.192	0.303	0.363	0.735
Sex	χ^2	-0.692	-0.746	1.099	-0.317	0.454
	p-value	0.489	0.455	0.272	0.751	0.650
Motion	χ^2	2.373	6.489	-0.811	-4.420	-4.084
	p-value	0.018	< 0.001	0.417	< 0.001	< 0.001
Site						
Cologne	χ^2	-1.207	-0.736	-0.836	-0.407	2.239
	p-value	0.228	0.462	0.403	0.684	0.025
Basel	χ^2	-1.323	-1.064	-0.194	0.928	-0.004
	p-value	0.186	0.287	0.846	0.354	0.997
Udine	χ^2	-1.173	-0.918	1.566	0.168	-0.512
	p-value	0.241	0.358	0.117	0.866	0.609
Milan	χ^2	-2.844	-0.989	-2.654	-4.016	4.284
	p-value	0.004	0.322	0.008	< 0.001	< 0.001
Birmingham	χ^2	-1.110	0.899	1.615	-0.925	0.022
	p-value	0.267	0.369	0.106	0.355	0.982
Turku	χ^2	-2.071	-1.043	-1.318	1.740	0.698
	p-value	0.038	0.297	0.188	0.082	0.485

Supplementary Table 1: Group differences in state frequencies and confound effects.

Mann-Whitney U-tests were used to compare corrected values across groups. Green cells indicate significant differences after Bonferroni correction ($p < 0.0016$). Effect sizes of confound effects on raw values were calculated relative to the Munich sample using a generalised linear model. Red cells indicate significant effects after Bonferroni correction ($p < 0.05/0.0011$).

		State 1	State 2	State 3	State 4	State 5
HC	raw	1.250 (1.920)	5.992 (6.624)	6.687 (6.045)	6.055 (4.352)	19.303 (26.318)
	adjusted	-0.007 (0.989)	-0.125 (1.035)	0.477 (0.957)	-0.266 (0.971)	-0.061 (1.084)
CHR	raw	1.114 (1.696)	7.519 (7.133)	4.902 (4.734)	8.249 (5.442)	15.753 (11.907)
	adjusted	-0.044 (0.928)	0.136 (0.946)	0.257 (0.859)	0.114 (1.026)	0.030 (0.788)
ROP	raw	3.286 (7.371)	5.803 (6.670)	0.864 (1.444)	9.293 (5.839)	18.480 (25.310)
	adjusted	0.299 (1.036)	-0.094 (0.910)	-0.582 (0.659)	0.306 (0.986)	-0.154 (0.938)
ROD	raw	0.935 (1.799)	7.943 (6.629)	1.464 (2.045)	7.633 (4.276)	19.095 (16.786)
	adjusted	-0.259 (0.885)	0.209 (0.825)	-0.549 (0.738)	0.080 (0.782)	0.250 (0.801)
Group differences						
HC v CHR	χ^2	17513	14167	20099	13059	15443
	p-value	0.603	0.008	0.003	< 0.001	0.148
HC v ROP	χ^2	14745	17819	29627	12531	19081
	p-value	< 0.001	0.453	< 0.001	< 0.001	0.709
HC v ROD	χ^2	20048	14300	28384	13740	13742
	p-value	0.034	0.001	< 0.001	< 0.001	< 0.001
CHR v ROP	χ^2	7067	10523	14271	8380	10495
	p-value	0.001	0.060	< 0.001	0.160	0.066
CHR v ROD	χ^2	9850	8639	13465	9220	7388
	p-value	0.107	0.749	< 0.001	0.545	0.021
ROP v ROD	χ^2	12937	7966	9932	11155	6983
	p-value	< 0.001	0.009	0.758	0.034	< 0.001
Confounds						
Age	χ^2	-0.963	1.311	-0.881	-0.582	0.853
	p-value	0.336	0.190	0.379	0.561	0.393
Sex	χ^2	-1.315	-0.286	1.052	-1.239	0.322
	p-value	0.188	0.775	0.293	0.215	0.748
Motion	χ^2	2.533	6.057	-0.713	-3.881	-4.406
	p-value	0.011	< 0.001	0.476	< 0.001	< 0.001
Site						
Cologne	χ^2	-1.043	-1.110	-0.645	-0.734	1.931
	p-value	0.297	0.267	0.519	0.463	0.053

Basel	χ^2	-1.439	-1.290	-0.846	0.289	0.551
	p-value	0.150	0.197	0.398	0.772	0.581
Udine	χ^2	-1.133	-0.636	1.800	0.499	0.515
	p-value	0.257	0.525	0.072	0.618	0.607
Milan	χ^2	-3.238	-0.750	-3.042	-3.568	5.562
	p-value	0.001	0.454	0.002	< 0.001	< 0.001
Birmingham	χ^2	-1.374	1.171	1.713	-0.758	0.327
	p-value	0.169	0.242	0.087	0.448	0.743
Turku	χ^2	-1.523	-0.749	-1.234	0.560	-0.002
	p-value	0.128	0.454	0.217	0.576	0.998

Supplementary Table 2: Group differences in state lifetimes and confound effects.

Mann-Whitney U-tests were used to compare corrected values across groups. Green cells indicate significant differences after Bonferroni correction ($p < 0.0016$). Effect sizes of confound effects on raw values were calculated relative to the Munich sample using a generalised linear model. Red cells indicate significant effects after Bonferroni correction ($p < 0.05/0.0011$).

		State 1	**State 2**	**State 3**	**State 4**	**State 5**
HC	raw	1.414 (2.173)	1.996 (1.976)	2.724 (2.246)	3.789 (2.653)	5.433 (2.282)
	adjusted	0.037 (1.049)	-0.072 (1.057)	0.395 (0.967)	-0.011 (1.115)	0.014 (1.058)
CHR	raw	1.185 (1.892)	2.038 (1.771)	2.492 (2.186)	3.523 (2.422)	5.269 (1.871)
	adjusted	-0.002 (0.985)	0.023 (0.863)	0.298 (0.903)	-0.123 (0.903)	-0.085 (0.848)
ROP	raw	1.322 (1.734)	1.860 (1.930)	0.713 (1.154)	4.280 (2.401)	5.545 (2.229)
	adjusted	0.184 (0.922)	-0.124 (0.915)	-0.554 (0.744)	0.205 (0.840)	0.075 (0.910)
ROD	raw	0.772 (1.554)	2.625 (2.094)	0.934 (1.224)	3.522 (2.174)	5.360 (2.068)
	adjusted	-0.263 (0.880)	0.247 (0.874)	-0.461 (0.809)	-0.077 (0.815)	-0.024 (0.935)
Group differences						
HC v CHR	χ^2	17417	15898	18357	18070	18116
	p-value	0.668	0.311	0.186	0.294	0.274
HC v ROP	χ^2	16617	18836	28634	16517	18263
	p-value	0.069	0.877	< 0.001	0.056	0.723

HC v ROD	χ^2	20319	14486	26633	18578	18653
	p-value	0.018	0.003	< 0.001	0.445	0.404
CHR v ROP	χ^2	7982	10159	13974	7262	8377
	p-value	0.044	0.185	<0.001	0.002	0.159
CHR v ROD	χ^2	10033	7633	12877	8657	8693
	p-value	0.057	0.054	< 0.001	0.771	0.815
ROP v ROD	χ^2	12684	7554	9355	11766	10525
	p-value	< 0.001	0.001	0.584	0.002	0.235
Confounds						
Age	χ^2	-0.347	0.679	-1.153	-0.783	-1.120
	p-value	0.729	0.497	0.249	0.434	0.263
Sex	χ^2	-0.870	-0.708	1.119	0.197	-0.080
	p-value	0.385	0.479	0.263	0.844	0.936
Motion	χ^2	2.038	5.636	-0.691	-3.138	-0.156
	p-value	0.042	< 0.001	0.490	0.002	0.876
Site						
Cologne	χ^2	-0.385	-0.442	-1.759	-0.102	0.107
	p-value	0.700	0.658	0.079	0.918	0.915
Basel	χ^2	-1.143	-1.490	-0.829	0.528	-0.876
	p-value	0.253	0.136	0.407	0.597	0.381
Udine	χ^2	-0.584	-1.215	0.707	-0.624	-2.282
	p-value	0.559	0.224	0.480	0.533	0.023
Milan	χ^2	-3.074	-1.621	-4.579	-4.655	-5.835
	p-value	0.002	0.105	< 0.001	< 0.001	< 0.001
Birmingham	χ^2	-0.402	1.044	-0.414	-1.155	0.132
	p-value	0.688	0.296	0.679	0.248	0.895
Turku	χ^2	-1.191	-1.394	-1.804	1.775	1.720
	p-value	0.234	0.163	0.071	0.076	0.085

Supplementary Table 3: Group differences in state in-degrees and confound effects.

Means and standard deviations of state in-degrees are presented after confound removal. Mann-Whitney U-tests were used to compare corrected values across groups. Green cells

indicate significant differences after Bonferroni correction (p < 0.0016). Effect sizes of confound effects on raw values were calculated relative to the Munich sample using a generalised linear model. Red cells indicate significant effects after Bonferroni correction (p < 0.05/0.0011).

Feature name	**Definition**
DN_HistogramMode_5	Mode of *z*-scored distribution (5-bin histogram)
DN_HistogramMode_10	Mode of *z*-scored distribution (10-bin histogram)
SB_BinaryStats_mean_longstretch1	Longest period of consecutive values above the mean
DN_OutlierInclude_p_001_mdrmd	Time intervals between successive extreme events above the mean
DN_OutlierInclude_n_001_mdrmd	Time intervals between successive extreme events below the mean
CO_f1ecac	First 1 / *e* crossing of autocorrelation function
CO_FirstMin_ac	First minimum of autocorrelation function
SP_Summaries_welch_rect_area_5_1	Total power in lowest fifth of frequencies in the Fourier power spectrum
SP_Summaries_welch_rect_centroid	Centroid of the Fourier power spectrum
FC_LocalSimple_mean3_stderr	Mean error from a rolling 3-sample mean forecasting
CO_trev_1_num	Time-reversibility statistic, $\langle (x_{t+1} - x_t)^3 \rangle_t$
CO_HistogramAMI_even_2_5	Automutual information, m = 2, τ = 5
IN_AutoMutualInfoStats_40_gaussian_fmmi	First minimum of the automutual information function
MD_hrv_classic_pnn40	Proportion of successive differences exceeding 0.04 σ (Mietus et al., 2002)
SB_BinaryStats_diff_longstretch0	Longest period of successive incremental decreases
SB_MotifThree_quantile_hh	Shannon entropy of two successive letters in equiprobable 3-letter symbolization
FC_LocalSimple_mean1_tauresrat	Change in correlation length after iterative differencing
CO_Embed2_Dist_tau_d_expfit_meandiff	Exponential fit to successive distances in 2-d embedding space
SC_FluctAnal_2_dfa_50_1_2_logi_prop_r1	Proportion of slower timescale fluctuations that scale with DFA (50% sampling)

Feature name	Definition
SC_FluctAnal_2_rsrangefit_50_1_logi_prop_r1	Proportion of slower timescale fluctuations that scale with linearly rescaled range fits
SB_TransitionMatrix_3ac_sumdiagcov	Trace of covariance of transition matrix between symbols in 3-letter alphabet
PD_PeriodicityWang_th0_01	Periodicity measure of (X. Wang et al., 2007)

Supplementary Table 4: 24 dynamic parameters of regional time courses (Lubba et al., 2019) considered in the correlation analysis and perturbation enrichment analysis.

Feature	Definition
MMSE_Score	Mini Mental Status Exam Total Score
PSQI_Score	Sleep (Pittsburgh Sleep Questionnaire) Total Score
PSQI_Comp1	Sleep (Pittsburgh Sleep Questionnaire) Component 1 Score
PSQI_Comp2	Sleep (Pittsburgh Sleep Questionnaire) Component 2 Score
PSQI_Comp3	Sleep (Pittsburgh Sleep Questionnaire) Component 3 Score
PSQI_Comp4	Sleep (Pittsburgh Sleep Questionnaire) Component 4 Score
PSQI_Comp5	Sleep (Pittsburgh Sleep Questionnaire) Component 5 Score
PSQI_Comp6	Sleep (Pittsburgh Sleep Questionnaire) Component 6 Score
PSQI_Comp7	Sleep (Pittsburgh Sleep Questionnaire) Component 7 Score
PicSeq_AgeAdj	NIH Toolbox Picture Sequence Memory Test: Age-Adjusted Scale Score
CardSort_AgeAdj	NIH Toolbox Dimensional Change Card Sort Test: Age-Adjusted Scale Score
Flanker_AgeAdj	NIH Toolbox Flanker Inhibitory Control and Attention Test: Age-Adjusted Scale Score
PMAT24_A_CR	Penn Matrix Test (PMAT): Number of Correct Responses
PMAT24_A_SI	Penn Matrix Test (PMAT): Total Skipped Items
PMAT24_A_RTCR	Penn Matrix Test (PMAT): Median Reaction Time (RT) for Correct Responses
ReadEng_AgeAdj	NIH Toolbox Oral Reading Recognition Test: Age-Adjusted Scale Score
PicVocab_AgeAdj	NIH Toolbox Picture Vocabulary Test: Age-Adjusted Scale Score
ProcSpeed_AgeAdj	NIH Toolbox Pattern Comparison Processing Speed Test: Age-Adjusted Scale Score
DDisc_AUC_200	Delay Discounting: Area Under the Curve (AUC) for Discounting of $200
DDisc_AUC_40K	Delay Discounting: Area Under the Curve (AUC) for Discounting of $40,000
VSPLOT_TC	Penn Line Orientation: Total Number Correct

Feature	Definition
VSPLOT_CRTE	Penn Line Orientation: Median Reaction Time Divided by Expected Number of Clicks for Correct Trials
VSPLOT_OFF	Penn Line Orientation: Total Positions Off for All Trials
SCPT_TP	Short Penn Continuous Performance Test True Positives = Sum of CPN_TP and CPL_TP
SCPT_TN	Short Penn Continuous Performance Test True Negatives = Sum of CPN_TN and CPL_TPN
SCPT_FP	Short Penn Continuous Performance Test False Positives = Sum of CPN_FP and CPL_FP
SCPT_FN	Short Penn Continuous Performance Test False Negatives = Sum of CPN_FN and CPL_FN
SCPT_TPRT	Short Penn Continuous Performance Test Median Response Time for True Positive Responses
SCPT_SEN	Short Penn Continuous Performance Test Sensitivity = SCPT_TP/(SCPT_TP + SCPT_FN)
SCPT_SPEC	Short Penn Continuous Performance Test Specificity = SCPT_TN/(SCPT_TN + SCPT_FP)
SCPT_LRNR	Short Penn Continuous Performance Test Longest Run of Non-Responses
IWRD_TOT	Penn Word Memory Test: Total Number of Correct Responses
IWRD_RTC	Penn Word Memory Test: Median Reaction Time for Correct Responses
ListSort_AgeAdj	NIH Toolbox List Sorting Working Memory Test: Age-Adjusted Scale Score
CogFluidComp_AgeAdj	NIH Toolbox Cognition Fluid Composite: Age Adjusted Scale Score
CogEarlyComp_AgeAdj	NIH Toolbox Cognition Early Childhood Composite: Age Adjusted Scale Score
CogTotalComp_AgeAdj	NIH Toolbox Cognition Total Composite: Age Adjusted Scale Score
CogCrystalComp_AgeAdj	NIH Toolbox Cognition Crystallized Composite: Age Adjusted Scale Score
ER40_CR	Penn Emotion Recognition Test: Number of Correct Responses
ER40_CRT	Penn Emotion Recognition Test: Correct Responses Median Response Time (ms)
ER40ANG	Penn Emotion Recognition Test: Number of Correct Anger Identifications
ER40FEAR	Penn Emotion Recognition Test: Number of Correct Fear Identifications
ER40HAP	Penn Emotion Recognition Test: Number of Correct Happy Identifications
ER40NOE	Penn Emotion Recognition Test: Number of Correct Neutral Identifications
ER40SAD	Penn Emotion Recognition Test: Number of Correct Sad Identifications
AngAffect_Unadj	NIH Toolbox Anger-Affect Survey: Unadjusted Scale Score
AngHostil_Unadj	NIH Toolbox Anger-Hostility Survey: Unadjusted Scale Score
AngAggr_Unadj	NIH Toolbox Anger-Physical Aggression Survey: Unadjusted Scale Score

Feature	Definition
FearAffect_Unadj	NIH Toolbox Fear-Affect Survey: Unadjusted Scale Score
FearSomat_Unadj	NIH Toolbox Fear-Somatic Arousal Survey: Unadjusted Scale Score
Sadness_Unadj	NIH Toolbox Sadness Survey: Unadjusted Scale Score
LifeSatisf_Unadj	NIH Toolbox General Life Satisfaction Survey: Unadjusted Scale Score
MeanPurp_Unadj	NIH Toolbox Meaning and Purpose Survey: Unadjusted Scale Score
PosAffect_Unadj	NIH Toolbox Positive Affect Survey: Unadjusted Scale Score
Friendship_Unadj	NIH Toolbox Friendship Survey: Unadjusted Scale Score
Loneliness_Unadj	NIH Toolbox Loneliness Survey: Unadjusted Scale Score
PercHostil_Unadj	NIH Toolbox Perceived Hostility Survey: Unadjusted Scale Score
PercReject_Unadj	NIH Toolbox Perceived Rejection Survey: Unadjusted Scale Score
EmotSupp_Unadj	NIH Toolbox Emotional Support Survey: Unadjusted Scale Score
InstruSupp_Unadj	NIH Toolbox Instrumental Support Survey: Unadjusted Scale Score
PercStress_Unadj	NIH Toolbox Perceived Stress Survey: Unadjusted Scale Score
SelfEff_Unadj	NIH Toolbox Self-Efficacy Survey: Unadjusted Scale Score
Emotion_Task_Acc	OVERALL Emotion Task accuracy
Emotion_Task_Median_RT	OVERALL Emotion Task Reaction Time
Gambling_Task_Perc_Larger	Gambling Task Overall Percentage 'Larger'
Gambling_Task_Perc_Smaller	Gambling Task Overall Percentage 'Smaller'
Gambling_Task_Median_RT_Larger	Gambling Task Overall Reaction Time 'Larger'
Gambling_Task_Median_RT_Smaller	Gambling Task Overall Reaction Time 'Smaller'
Language_Task_Acc	Language Task OVERALL accuracy
Language_Task_Median_RT	Language Task OVERALL median Reaction Time
Relational_Task_Acc	Relational Task OVERALL accuracy
Relational_Task_Median_RT	Relational Task OVERALL Reaction Time
Social_Task_Perc_Random	Social Task Overall Percentage 'Random'
Social_Task_Perc_TOM	Social Task Overall Percentage 'TOM'
Social_Task_Perc_Unsure	Social Task Overall Percentage 'Unsure'
Social_Task_Median_RT_Random	Social Task Overall Reaction Time 'Random'

Feature	Definition
Social_Task_Median_RT_TOM	Social Task Overall Reaction Time 'TOM'
WM_Task_Acc	Working Memory Task Overall Accuracy
WM_Task_Median_RT	Working Memory Task Overall Reaction Time
Endurance_AgeAdj	NIH Toolbox 2-minute Walk Endurance Test : Age-Adjusted Scale Score
GaitSpeed_Comp	NIH Toolbox 4-Meter Walk Gait Speed Test: Computed Score
Dexterity_AgeAdj	NIH Toolbox 9-hole Pegboard Dexterity Test : Age-Adjusted Scale Score
Strength_AgeAdj	NIH Toolbox Grip Strength Test: Age-Adjusted-Adjusted Scale Score
NEOFAC_A	NEO-FFI Agreeableness
NEOFAC_O	NEO-FFI Openness to Experience
NEOFAC_C	NEO-FFI Conscientiousness
NEOFAC_N	NEO-FFI Neuroticism
NEOFAC_E	NEO-FFI Extraversion
Noise_Comp	NIH Toolbox Words-In-Noise Age 6+: Computed Score
Odor_AgeAdj	NIH Toolbox Odor Identification Age 3+ Age-Adjusted Scale Score
PainIntens_RawScore	NIH Toolbox Pain Intensity Survey Age 18+: Raw score
PainInterf_Tscore	NIH Toolbox Pain Interference Survey Age 18+: T-score
Taste_AgeAdj	NIH Toolbox Regional Taste Intensity Age 12+ Age-Adjusted Scale Score
Mars_Log_Score	Mars Contrast Sensitivity Score
Mars_Errs	Errors on Mars
Mars_Final	Mars Final Contrast Sensitivity Score

Supplementary Table 5: 98 behavioural measures considered in the correlation analysis.

10. Erklärung

Hiermit versichere ich an Eides statt, dass ich die vorliegende Dissertationsschrift selbstständig und ohne die Benutzung anderer als der angegebenen Hilfsmittel angefertigt habe. Alle Stellen - einschließlich Tabellen, Karten und Abbildungen -, die wörtlich oder sinngemäß aus veröffentlichten und nicht veröffentlichten anderen Werken im Wortlaut oder dem Sinn nach entnommen sind, sind in jedem Einzelfall als Entlehnung kenntlich gemacht. Ich versichere an Eides statt, dass diese Dissertationsschrift noch keiner anderen Fakultät oder Universität zur Prüfung vorgelegen hat; dass sie - abgesehen von unten angegebenen Teilpublikationen - noch nicht veröffentlicht worden ist sowie, dass ich eine solche Veröffentlichung vor Abschluss der Promotion nicht ohne Genehmigung der / des Vorsitzenden des IPHS-Promotionsausschusses vornehmen werde. Die Bestimmungen dieser Ordnung sind mir bekannt. Die von mir vorgelegte Dissertation ist von Prof. Dr. med. Joseph Kambeitz betreut worden.

Darüber hinaus erkläre ich hiermit, dass ich die Ordnung zur Sicherung guter wissenschaftlicher Praxis und zum Umgang mit wissenschaftlichem Fehlverhalten der Universität zu Köln gelesen und sie bei der Durchführung der Dissertation beachtet habe und verpflichte mich hiermit, die dort genannten Vorgaben bei allen wissenschaftlichen Tätigkeiten zu beachten und umzusetzen.

Übersicht der Publikationen (bei Bedarf Seite anfügen):

Linnea Hoheisel, Lana Kambeitz-Ilankovic, Julian Wenzel, Shalaila S. Haas, Linda A. Antonucci, Anne Ruef, Nora Penzel, Frauke Schultze-Lutter, Theresa Lichtenstein, Marlene Rosen, Dominic B. Dwyer, Raimo K.R. Salokangas, Rebekka Lencer, Paolo Brambilla, Stephan Borgwardt, Stephen J. Wood, Rachel Upthegrove, Alessandro Bertolino, Stephan Ruhrmann, Eva Meisenzahl, Nikolaos Koutsouleris, Gereon R. Fink, Silvia Daun, Joseph Kambeitz, and the PRONIA Consortium (2024). **Alterations of Functional Connectivity Dynamics in Affective and Psychotic Disorders,** Biological Psychiatry: Cognitive Neuroscience and Neuroimaging, 9 (8), 765-776, doi: 10.1016/j.bpsc.2024.02.013.

Linnea Hoheisel, Hannah Hacker, Gereon R Fink, Silvia Daun, Joseph Kambeitz (2024). **Computational modelling reveals neurobiological contributions to static and dynamic functional connectivity patterns**, bioRxiv 2024.10.01.614888; doi: https://doi.org/10.1101/2024.10.01.614888

Ich versichere, dass ich alle Angaben wahrheitsgemäß nach bestem Wissen und Gewissen gemacht habe und verpflichte mich, jedmögliche, die obigen Angaben betreffenden Veränderungen, dem IPHS-Promotionsausschuss unverzüglich mitzuteilen.

Datum: 09.04.2025